This is to certify that the
dissertation entitled

ACTIVATED ESCAPE
IN PERIODICALLY MODULATED SYSTEMS

presented by

DMITRI RYVKINE

has been accepted towards fulfillment
of the requirements for the

Ph.D. degree in Physics

M. Dykman
Major Professor's Signature

07/06/2006
Date

DATE DUE	DATE DUE	DATE DUE

ACTIVATED ESCAPE IN PERIODICALLY MODULATED SYSTEMS

By

Dmitri Ryvkine

DISSERTATION

Submitted to
Michigan State University
in partial fulfillment of the requirements
for the degree of

DOCTOR OF PHILOSOPHY

Department of Physics and Astronomy

2006

ABSTRACT

ACTIVATED ESCAPE IN PERIODICALLY MODULATED SYSTEMS

By

Dmitri Ryvkine

Noise-induced escape from a metastable state is studied for an overdamped periodically modulated system. We develop an asymptotic technique that gives both the instantaneous and period-average escape rates for an arbitrary modulation frequency ω_F and amplitude A. Using this technique, we reveal new system independent features of escape in the periodically modulated systems.

The period-average escape rate has the form $\overline{W} = \nu \exp(-R/D)$, where ν is the prefactor, R is the activation energy, and D is the noise intensity. Near a bifurcation point the system experiences critical slowing down. This leads to scaling behavior of fluctuations. We find that, in contrast to previously studied stationary systems, a periodically driven system may display three scaling regimes and scaling crossovers near a saddle-node bifurcation point where a metastable state disappears.

The activation energy scales with the driving field amplitude A as $R \propto (A_c - A)^{\xi}$, where A_c is the bifurcational value of A. With increasing field frequency the critical exponent ξ changes from $\xi = 3/2$ for stationary systems to a dynamical value $\xi = 2$ and then again to $\xi = 3/2$.

The prefactor ν depends on A nonmonotonically. Near the bifurcation amplitude A_c it scales as $\nu \propto (A_c - A)^{\zeta}$, with crossovers $\zeta = 1/4$ to -1, and to $1/2$.

We find the parameter range where escape is strongly synchronized by the modulation and the instantaneous escape rate $W(t)$ displays sharp periodic peaks. The peaks' shape varies from Gaussian to strongly asymmetric with increasing modulation frequency or amplitude.

The trajectories followed in escape form periodically repeated in time diffusion broadened tubes. We show that these tubes can be directly observed and find their shape. Quantitatively, the tubes are characterized by the distribution of trajectories that, after escape, pass through a given point in phase space for a given modulation phase. This distribution may display several peaks shifted by the modulation period.

All analytical results are in good agreement with numerical simulations for a model system.

Acknowledgments

Most of all, I would like to thank my advisor and teacher Mark Dykman. The high standards he set for himself as a person and researcher will always be a source of admiration to me.

Brage Golding exposed me, as much as he could, to the experimental view of physics.

My other Dissertation Committee members, Bhanu Mahanti, Scott Pratt, and C.-P. Yuan, have been enthusiastic about my work and helpful with their comments.

The staff of the Department of Physics and Astronomy have been very responsive to routine needs of an international graduate student.

I should also mention Christian Hicke, with whom I was lucky to share office 4252 for two years. We discussed everything: business, politics, history, religion, and even physics.

Special thanks go to my wife, Anastasia Semykina, my parents and friends in my home town, Ekaterinburg, and my "second home" town, Prague, for all the beautiful moments in between.

TABLE OF CONTENTS

List of Figures

Chapter 1

Introduction

Noise-activated processes are at root of many physical, chemical, biological and, arguably, social phenomena: nucleation, diffusion in solids, chemical reactions, protein folding, and epidemics are examples. One of the most important activated processes is *escape*, in which a noise-driven system leaves the basin of attraction to its metastable state. It is important to understand how activated escape occurs, particularly in systems away from thermal equilibrium. Full understanding would include a description of the underlying system dynamics and escape probability. Owing to its exponential sensitivity to the system parameters, the escape probability provides an important means of characterizing a system. In particular, it determines the lifetime of the metastable state.

The notion of escape is meaningful when it refers to a *rare* event: the lifetime of a metastable state should be large compared to all other characteristic times in the system, such as its relaxation time or a period of external modulation. In this case, the system spends most of the time fluctuating around its metastable state, and only occasionally there occurs an unusually large fluctuation leading to escape.

The goal of the present thesis is to reveal and study universal features of

fluctuation-induced escape in nonequilibrium systems. In contrast to equilibrium systems, where fluctuation probabilities are known at least in principle [1], no general principles have been established for nonequilibrium systems. Therefore it is especially important to find system-independent properties of fluctuation phenomena far from equilibrium.

Fluctuation phenomena in nonequilibrium systems have been attracting much attention in recent years, particularly because fluctuations become more important with reduction of the system size. Of special interest in this respect are systems with coexisting stable states. Examples include modulated Josephson junctions [2, 3, 4, 5, 6, 7] (see Fig. 1.1), current-driven nanomagnets [8, 9, 10], semiconductor lasers [11, 12, 13], tunneling systems and nanowires [14, 15, 16, 17, 18, 19], nanoelectromechanical systems [20, 21, 22, 23] and optically trapped colloidal particles [24, 25, 26, 27] (see also Fig. 1.2). Fluctuations in such systems lead to switching between coexisting states, and therefore even where they are weak on average, they largely determine the system behavior.

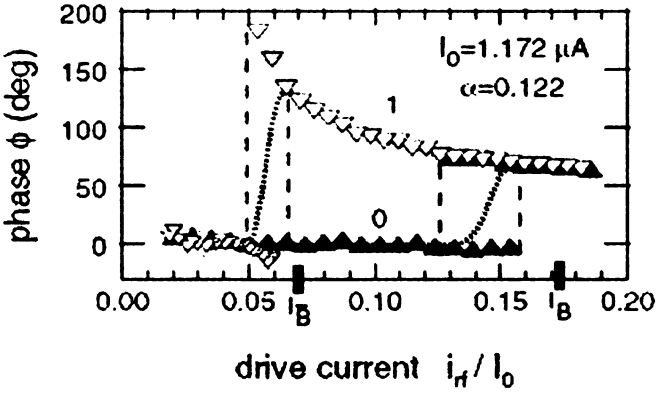

Figure 1.1: (Reproduced from Ref. [7]) The phase of the reflected signal from a driven Josephson junction exhibits hysteresis as a function of the drive current. The two coexisting metastable states correspond to the superconducting and dissipative states of the junction.

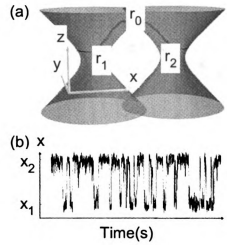

Figure 1.2: (Reproduced from Ref. [24]) (a) A three-dimensional double-well optical trap created by two laser beams. (b) A time series of the x-coordinate of a small silica particle in the trap clearly shows switching between the two metastable states. See also Ref. [134] for details.

The rate of activated escape $W \propto \exp(-\Delta U/k_B T)$ has been studied in depth for systems in thermal equilibrium, starting with Kramers' work [29]. The activation energy ΔU displays a universal behavior near bifurcation, or critical, points where the number of stable states of the system changes. An example is a saddle-node bifurcation where, for a critical value η_c of the control parameter η, a stable state and an unstable stationary state of the system merge together in phase space. For a Brownian particle this occurs where a minimum and a saddle point of the confining potential $U(\mathbf{r})$ coalesce. Such bifurcation is an analog of a spinodal point in the mean field theory. Here, for small $|\eta - \eta_c|$ the activation energy scales as $|\eta - \eta_c|^\xi$ with critical exponent $\xi = 3/2$ [30, 31, 32, 33]. This characteristic behavior of thermal activation has been carefully studied in superconducting tunnel systems [34, 35, 36, 37, 38] and nanomagnets [39, 40, 41, 42, 43] (see also Fig. 1.3), among other systems.

For nonequilibrium systems escape rates can be obtained from the analysis of the

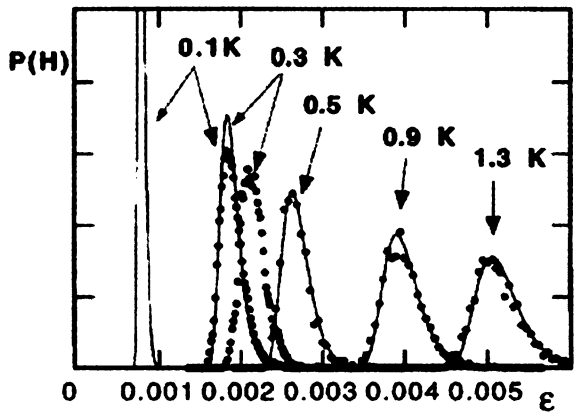

Figure 1.3: (Reproduced from Ref. [40]) For $T = 0$, magnetization of a single-domain magnet switches when the applied field reaches certain value $H_{\rm sw}^0$; for $T > 0$ the switching field $H_{\rm sw}$ is random, with a distribution around a value, which is generally different from $H_{\rm sw}^0$. The figure shows experimentally measured distributions of switching fields as a function of $\epsilon = 1 - H_{\rm sw}/H_{\rm sw}^0$ for several temperatures.

system kinetics. They are also often described by an activation-type law, where the role of temperature is played by the intensity of the external Gaussian noise D or the total number of reacting particles [14, 44, 45, 46, 47, 48, 49, 50, 51, 52, 53, 54, 55, 56]. The form of the activation barrier R depends on the details of the kinetics. However, it was predicted that where the system is stationary (or stationary in the rotating frame, for high-frequency modulation), close to the bifurcational value η_c of the control parameter η, the activation barrier should still display a power-law dependence [56, 57, 58, 59, 61, 62, 63]. The nonequilibrium $\xi = 3/2$ scaling near a saddle-node bifurcation has been observed recently in resonantly driven Josephson junctions [64] and micromechanical resonators [65] (see also Fig. 1.4). The supercritical scaling $\xi = 2$ has been observed for atoms in a parametrically driven magneto-optical trap [66].

The scaling behavior is far richer for nonequilibrium systems than for equilibrium

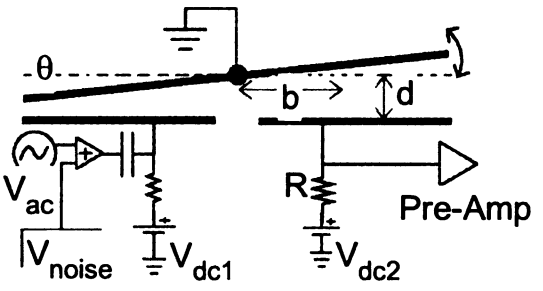

Figure 1.4: (Reproduced from Ref. [65]) A cross-sectional schematic of the micromechanical torsional oscillator with electrical connections and measurement circuitry (not to scale). When driving is weak, the system response is linear; for stronger driving there emerge two coexisting metastable states [106] (circles).

ones. For periodically modulated systems, we identify new scaling regimes close to a saddle-node bifurcation point, with crossovers between different values of the scaling exponent. We also find a complete solution of the time-dependent problem and calculate the instantaneous escape rate $W(t)$.

A basic physical feature of activated escape is that the trajectories followed in escape form a narrow tube centered at a certain path $\mathbf{q}_{\rm opt}(t)$ in the phase space of the system (different components of the vector $\mathbf{q}$ are coordinates and momenta of the system), which is the most probable escape path (MPEP) [45, 47, 49, 52, 55, 67]. In a general case where fluctuations are induced by Gaussian noise this path goes from the initially occupied metastable state $\mathbf{q}_a$ to an unstable stationary (or periodic) state $\mathbf{q}_b$ on the boundary of the basin of attraction to the metastable state [51]. In particular, for a Brownian particle in a one-dimensional potential well the optimal path goes from the minimum of the well to the barrier top. There is a qualitative difference between MPEPs in equilibrium and nonequilibrium systems. In equilibrium systems the MPEP is simply related to the dynamical trajectory of the system that goes from $\mathbf{q}_b$ to $\mathbf{q}_a$ in the absence of fluctuations [68]: the equations for these paths differ just

by the sign of the friction force. This property holds not only for the MPEP, but for most probable trajectories $\mathbf{q}_{\rm opt}(t|\mathbf{q})$ for fluctuations from $\mathbf{q}_a$ to any state $\mathbf{q}$ in its attraction basin [69].

A generic feature of nonequilibrium systems is lack of detailed balance. As a consequence, there is no simple relation between $\mathbf{q}_{\rm opt}(t|\mathbf{q})$ and the dynamical trajectory from $\mathbf{q}$ to $\mathbf{q}_a$. This limits [70] the applicability of fluctuation theorems [71, 72, 73, 74, 75]. Moreover, the pattern of optimal paths has observable and hidden singularities [76] related to nonintegrability of the equations of motion for the optimal paths [47, 52, 77, 78, 79].

Optimal fluctuational paths can be observed in experiment. This can be done by accumulating paths along which the system arrives to a vicinity of a given state $\mathbf{q}$ and studying the distribution of these paths backward in time from the instant of arrival, the prehistory probability distribution (PPD) [80]. It should peak at $\mathbf{q}_{\rm opt}(t|\mathbf{q})$. For a one-dimensional system in equilibrium – a semiconductor laser – such a peak has indeed been observed [81].

A different situation happens if the system is modulated in time with period of order of its relaxation time $t_{\rm r}$. As we show, in this case the PPD peak is narrow not only in phase space, but also in time. Moreover, as a consequence of nonequilibrium modulation, the PPD may display several peaks inside the attraction basin.

The thesis is organized as follows. In Chapter 2 we discuss scaling of the activation energy of a periodically modulated system close to a saddle-node bifurcation point. In Chapter 3 we present a complete solution of the Kramers' problem for periodically modulated systems. In Chapter 4 we explore the dynamics of escape trajectories and find the prehistory probability density for such systems. Chapter 5 concludes.

Chapter 2

Scaling and crossovers in activated escape near a bifurcation point

2.1 Introduction

The barrier for escape from a metastable state is reduced when the system is close to a bifurcation (critical, or spinodal) point where the state disappears. For systems that display hysteresis such a bifurcation point corresponds to the switching point on the hysteresis loop. The idea of bringing the system close to the bifurcation point [30] has been used in studying activated switching in Josephson junctions [34, 35, 36, 37], where it has become a standard technique for determining the critical current. This idea is also used in studies of activated magnetization reversals in nanomagnets [39, 41, 82].

Experiments on nanomagnets and Josephson junctions are often performed by ramping the control parameter (magnetic field or current) and measuring time distribution of escape events [30]. In interpreting the data it is usually assumed that, for sufficiently slow ramp rates, the system remains quasistationary. In this approxi-

mation the barrier height, i.e., the activation energy of a transition R, usually scales with the control parameter η, measured from its critical (bifurcational) value $\eta_c = 0$, as $\eta^{3/2}$. The $\eta^{3/2}$ behavior near a termination point $\eta_c = 0$ of a metastable state describes the vanishing of the meanfield free-energy barrier with the control parameter η [83].

Scaling of R near a bifurcation point is related to slowing down of one of the motions [84], i.e., the onset of a "soft mode". The relaxation time of the system t_r diverges as the control parameter $\eta \to 0$. Therefore if η depends on time, even where this dependence is slow the assumption of quasistationary may become inapplicable for small η.

In this Chapter (see also Refs. [62, 85]) a theory of activated transitions is developed for periodically modulated systems. In such systems the notion of a stable state is well-defined irrespective of the modulation rate, and the applicability of the quasistationary approximation can be carefully studied. It turns out that, unexpectedly, near a critical point this approximation breaks down even where the relaxation time t_r is still much smaller than the driving period $\tau_F = 2\pi/\omega_F$.

We show that an interplay between the critical slowing down and the slowness of time-dependent modulation leads to a rich scaling behavior of the transition rate and to crossovers between different scaling regions. This behavior near a bifurcation point is system-independent and has no counterparts in stationary systems. We find three regions in which the activation energy scales as $R \propto \eta^{\xi}$. As the parameters change, for example with the increase of the modulation frequency ω_F, the critical exponent ξ varies from 3/2 to 2 and then again to 3/2. Numerical calculations and Monte Carlo simulations for a model system agree with our predictions.

Activated transitions in periodically driven systems were investigated earlier in

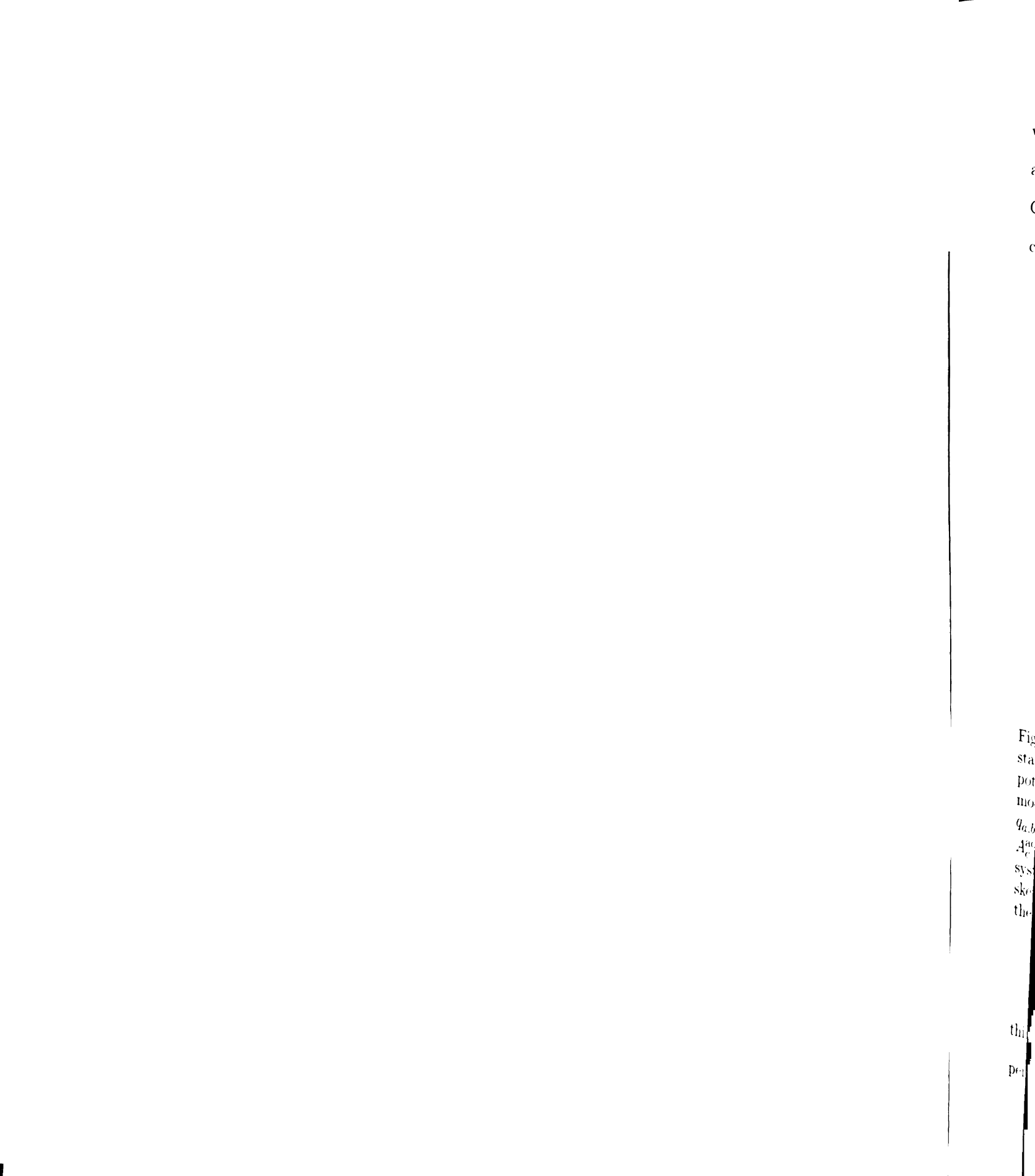

various contexts [2, 6, 54, 86, 87, 88, 89, 90, 91, 92, 93, 94, 95, 96], stochastic resonance and diffusion in modulated ratchets being recent examples [97, 98, 99, 100]. In this Chapter we study the previously unexplored region of driving amplitudes close to critical and reveal the universality that emerges.

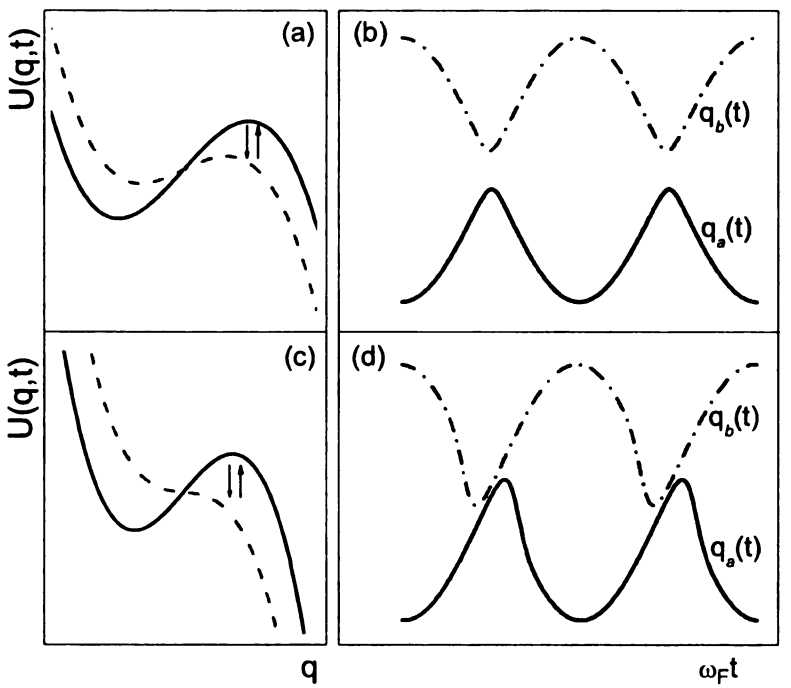

Figure 2.1: (a) An oscillating potential barrier. In the limit of slow modulation, the stable and unstable periodic states q_a and q_b are the instantaneous positions of the potential minimum and barrier top, respectively. (b) For slow modulation, when the modulation amplitude A is close to its adiabatic bifurcational value $A_c^{\rm ad}$, the states $q_{a,b}(t)$ come close to each other once per period. (c) As A further increases beyond $A_c^{\rm ad}$, the barrier of U disappears for a portion of the modulation period, but the system may still have coexisting periodic states $q_{a,b}(t)$. As seen in (d), they become skewed compared to the adiabatic picture, to avoid crossing. In the critical range, the form of $q_{a,b}(t)$ is model-independent.

A qualitative picture of motion near a bifurcation point can be obtained if one thinks of the system as a particle in a potential $U(q,t)$ that oscillates in time with period τ_F, see Fig. 2.1 (a). Such particle has periodic stable and unstable states,

$q_a(t)$ and $q_b(t)$. In the adiabatic limit $\omega_F \to 0$ they lie at the minimum and local maximum of the potential in Fig. 2.1 (a). As the modulation amplitude A increases, the states become close to each other for a portion of the period τ_F, see Fig. 2.1 (b). The barrier height reaches its minimum during this time, and this is when the system is most likely to escape from the potential well. The driving amplitude $A_c^{\rm ad}$ for which the barrier disappears in the limit $\omega_F \to 0$ determines the adiabatic bifurcation point.

However, for nonzero ω_F, as A approaches $A_c^{\rm ad}$ the periodic states $q_{a,b}(t)$ become distorted to avoid crossing and may coexist even where the barrier has completely disappeared for a portion of a period, see Fig. 2.1 (c,d). The adiabatic approximation becomes inapplicable for such modulation.

The parameter range where adiabaticity is broken can be estimated by noticing that the adiabatic relaxation time $t_{\rm r}$ (i) is a function of the instantaneous modulation phase $\phi = \omega_F t$, and (ii) sharply increases near the bifurcation point. As a consequence, $t_{\rm r}$ sharply increases when ϕ approaches the value where $q_{a,b}$ are at their closest, because this corresponds to approaching the bifurcation point. The quasistationary (adiabatic) approximation requires that $|\partial t_{\rm r}/\partial t| \ll 1$. It is this condition that limits the range of adiabaticity, rather than a much less restrictive condition $t_{\rm r}\omega_F \ll 1$.

In the nonadiabatic region, a sufficiently large fluctuation is still required to move the system away from the stable periodic state. For $A \gtrsim A_c^{\rm ad}$, there emerges the new scaling of the activation energy R. The control parameter is now $\eta \propto A_c - A$, where A_c is the "true" bifurcation value of the modulation amplitude where the states $q_a(t)$ and $q_b(t)$ coalesce.

In the limit $\omega_F t_{\rm r} \gg 1$ the behavior near a bifurcation point is in some sense simpler. In this case $q_a(t)$ and $q_b(t)$ come close to each other everywhere on the

cycle, not just for a part of the period. The motion of the system in the vicinity of $q_{a,b}(t)$ is oscillations with a slowly varying amplitude. The amplitude change can be described by averaging the complete dynamics over the period. It is then mapped onto motion in an effectively stationary potential. Not surprisingly, the scaling of the escape activation energy R with the distance to the bifurcation point is the same as for stationary systems.

In Sec. 2.2 and Appendix A we provide a general formulation of the problem of activated escape in periodically modulated systems driven by Gaussian noise. In Sec. 2.3.1 and Appendix B we discuss the dynamics near a bifurcation point in the adiabatic limit $\omega_F t_r \to 0$. In Sec. 2.3.2 we consider the strongly nonadiabatic dynamics that emerges where still $\omega_F t_r \ll 1$. In Sec. 2.3.3 and Appendix C the dynamics near a bifurcation point is described in the parameter range where the field becomes effectively fast-oscillating, i.e. $\omega_F t_r \gg 1$, even though the relaxation time in the absence of modulation $t_r^{(0)}$ may be $\lesssim 1/\omega_F$. The connection between the nonadiabatic local theory of Sec. 2.3.2 and the theory of Sec. 2.3.3 is discussed in Sec. 2.3.4. In Sec. 2.4 the activation energy is explicitly evaluated in the three regions discussed in Sec. 2.3, and the scaling laws for the activation energy $R \propto (A_c - A)^\xi$ in these regions are obtained. The scaling crossovers are discussed. We also find nonadiabatic corrections to the escape rate in the adiabatic region. In Sec. 2.5 we consider a periodically modulated Brownian particle. Numerical results for the activation energy are compared to the results of Monte Carlo simulations and to the predictions of Sec. 2.4. Sec. 2.6 contains concluding remarks.

2.2 Activated escape: general formulation

We will adopt a phenomenological approach in which a multidimensional system with dynamical variables $\mathbf{q}(t)$ is described by the Langevin equation

$$\dot{\mathbf{q}} = \mathbf{K}(\mathbf{q}; A, t) + \mathbf{f}(t), \quad \mathbf{K}(\mathbf{q}; A, t + \tau_F) = \mathbf{K}(\mathbf{q}; A, t). \tag{2.1}$$

The function $\mathbf{K}$ is periodic in time, with the modulation period $\tau_F = 2\pi/\omega_F$; A is a control parameter that characterizes the modulation strength. For example, in the case of an overdamped particle in a potential $U_0(\mathbf{q})$ modulated by an additive periodic force $\mathbf{F}(t)$, the vector $\mathbf{K}$ becomes

$$\mathbf{K}(\mathbf{q}; A, t) = -\boldsymbol{\nabla} U_0(\mathbf{q}) + \mathbf{F}(t). \tag{2.2}$$

(here and below, $\boldsymbol{\nabla} \equiv \partial/\partial\mathbf{q}$). In this case $A = \max|\mathbf{F}|$ is the modulation amplitude (note that the force $\mathbf{F}(t) = \mathbf{F}(t + \tau_F)$ does not have to be sinusoidal).

The function $\mathbf{f}(t)$ in Eq. (2.1) is zero-mean Gaussian noise with correlation matrix

$$\varphi_{ij}(t - t') = \langle f_i(t) f_j(t') \rangle. \tag{2.3}$$

The characteristic noise intensity D can be defined as the maximal value of the power spectrum,

$$D = \max \Phi_{nn}(\omega), \quad \Phi_{nm}(\omega) = \int dt e^{i\omega t} \varphi_{nm}(t). \tag{2.4}$$

For noise from thermal source D is $\propto k_B T$. The noise intensity D is the smallest parameter of the theory. Smallness of D leads to the rate of noise-induced escape W being much smaller than t_r^{-1} and ω_F.

In the absence of noise, Eq. (2.1) may have different periodic solutions $\mathbf{q}_{\rm per}$, which can be stable (attractors), unstable (repellers), or hyperbolic (saddles). We are interested in the parameter range where one of the stable periodic solutions

$\mathbf{q}_a(t) = \mathbf{q}_a(t+\tau_F)$ comes close to a saddle-type periodic solution $\mathbf{q}_b(t)$ with the same period (period 1, for concreteness). For slow modulation, these states are sketched in Fig. 2.1. They merge together at the saddle-node bifurcation point $A = A_c$. In what follows we will assume that A is close to the critical value A_c.

Escape from a metastable state $\mathbf{q}_a(t)$ occurs as a result of a large fluctuation. The fluctuational force $\mathbf{f}(t)$ has to overcome the restoring force $\mathbf{K}$ and drive the system away from the basin of attraction to $\mathbf{q}_a(t)$ [e.g., away from the potential well in Fig. 2.1 (a)]. We will assume that the required force $\mathbf{f}(t)$ is much larger than the typical noise amplitude $\propto D^{1/2}$.

The motion of the system during escape is random. However, different trajectories have exponentially different probabilities. The system is most likely to move along a particular trajectory called the optimal path $\mathbf{q}_{\rm opt}(t)$ [68]. It is determined by the most probable noise realization $\mathbf{f}_{\rm opt}(t)$. In the case of a periodically modulated 1D system driven by stationary Gaussian noise, a way to find the optimal paths was discussed earlier [94]. We now briefly outline a generalization of the formulation to multidimensional systems, following the arguments in Ref. [51] (more details are provided in Appendix A).

For a stationary Gaussian noise, the probability density of realizations of $\mathbf{f}(t)$ is given by the functional (cf. Ref. [101])

$$\mathcal{P}[\mathbf{f}(t)] = \exp(-\mathcal{R}_0[\mathbf{f}(t)]/D), \tag{2.5}$$

where $\mathcal{R}_0$ is quadratic in $\mathbf{f}$,

$$\mathcal{R}_0[\mathbf{f}] = \frac{1}{2}\iint dt dt' f_i(t)\mathcal{F}_{ij}(t-t')f_j(t'). \tag{2.6}$$

The matrix $\mathcal{F}$ is the inverse of $\varphi_{ij}(t-t')/D$,

$$\int dt' \mathcal{F}_{ij}(t-t')\varphi_{jk}(t'-t'') = D\delta_{ik}\delta(t-t''). \tag{2.7}$$

We are interested in noise realizations that lead to escape, and therefore $\mathbf{f}(t)$ largely exceeds its root-mean-square value. From Eq. (2.5), the probabilities of such noise realizations are exponentially small and exponentially strongly depend on the form of $\mathbf{f}(t)$. As a consequence, escape trajectories should form a narrow "tube" centered at an optimal path $\mathbf{f}_{\rm opt}(t)$ that maximizes $\mathcal{P}[\mathbf{f}(t)]$, i.e., minimizes $\mathcal{R}_0[\mathbf{f}(t)]$. The minimum of $\mathcal{R}_0$ should be found with the constraints that (i) the system and noise trajectories, $\mathbf{q}_{\rm opt}(t)$ and $\mathbf{f}_{\rm opt}(t)$, are interrelated by the equation of motion (2.1), (ii) the path $\mathbf{q}_{\rm opt}(t)$ starts in the vicinity of the stable state $\mathbf{q}_a(t)$ and ends behind or on the boundary of the basin of attraction to $\mathbf{q}_a(t)$, and (iii) the force $\mathbf{f}_{\rm opt}(t)$ is equal to zero before the escape event happens and becomes equal to zero once the system has escaped, so that, as $\mathbf{f}_{\rm opt}(t)$ decays, it does not drag the system back to the basin of attraction to $\mathbf{q}_a$.

As explained in Appendix A, these conditions lead to boundary conditions for optimal paths of the form

$$\mathbf{q}_{\rm opt}(t) \to \begin{cases} \mathbf{q}_a(t) \text{ for } t \to -\infty, \\ \mathbf{q}_b(t) \text{ for } t \to \infty, \end{cases}$$
$$\mathbf{f}_{\rm opt}(t) \to \mathbf{0} \text{ for } t \to \pm\infty. \tag{2.8}$$

[Note that $\mathbf{q}_{\rm opt}(t)$ ends on the basin boundary, not on another attractor.]

The variational problem for optimal paths is reduced to minimizing the functional

$$\mathcal{R}[\mathbf{q},\mathbf{f}] \;= \mathcal{R}_0[\mathbf{f}] + \int dt' \boldsymbol{\lambda}(t') \cdot [\dot{\mathbf{q}}(t') - \mathbf{K}(\mathbf{q}; A, t') - \mathbf{f}(t')] \tag{2.9}$$

with boundary conditions (2.8). The function $\boldsymbol{\lambda}(t)$ is a Lagrange multiplier. The boundary condition for it is $\boldsymbol{\lambda}(t) \to \mathbf{0}$ for $t \to \pm\infty$.

It follows from Eqs. (2.8), (2.9) and from the results of Appendix A that the optimal trajectories $\mathbf{q}_{\rm opt}(t), \mathbf{f}_{\rm opt}(t)$ are instanton-like [102, 103]. The typical duration

of motion is given by the relaxation time of the system t_r and the noise correlation time t_{corr}. In stationary systems instantons are translationally invariant with respect to time, i.e., if $\mathbf{q}_{opt}(t), \mathbf{f}_{opt}(t)$ is a solution, then $\mathbf{q}_{opt}(t+\tau), \mathbf{f}_{opt}(t+\tau)$ is also a solution, for an arbitrary τ. In contrast, in periodically modulated systems this is true only for $\tau = \tau_F$. The instantons are synchronized by the modulation: generally there is one instanton per period that would provide a global minimum to $\mathcal{R}$.

From Eq. (2.5), we obtain for the escape probability

$$W \propto \exp(-R/D), \quad R = \min \mathcal{R}[\mathbf{q}, \mathbf{f}]. \tag{2.10}$$

The activation energy R is equal to the value of the functional $\mathcal{R}_0[\mathbf{f}_{opt}]$ calculated for the optimal noise trajectory for escape.

For small noise intensity, the escape rate $W \ll \omega_F$. It periodically depends on time. However, in the small-D limit this dependence is seen only in the prefactor [92, 93, 54]. Here we are interested in the exponent, which gives the period-averaged escape rate $\overline{W}$. It is equal to the probability of escape over the time τ_F divided by τ_F

In the general case, the variational problem for the activation energy can be solved only numerically. Therefore it is particularly important to find model-independent properties of R. So far they have been found for comparatively weak modulation, where it was shown that R has a term linear in the modulation amplitude [94]. In this Chapter we analyze the activation energy R in a previously unexplored region near a bifurcation point and show that R displays a nontrivial scaling behavior in this region.

2.3 Dynamics near a bifurcation point

The dynamics near a saddle-node bifurcation point has universal features related to the occurrence of a slow variable, or a "soft mode" [84]. For periodically modulated systems, closeness to the bifurcation point in the parameter space usually implies that the merging states are close to each other in phase space throughout the modulation period.

If the modulation frequency ω_F is small compared to the reciprocal relaxation time in the absence of modulation $1/t_r^{(0)}$, there emerges a situation where the stable and unstable states come close to each other only for a portion of a period. During this time, the system behaves as if it were close to a bifurcation point. Then it is possible to single out a slow variable that controls the system dynamics. Escape from a metastable state is most probable when $\mathbf{q}_a(t)$ and $\mathbf{q}_b(t)$ are closest to each other.

On the other hand, if the modulation frequency $\omega_F \gtrsim 1/t_r^{(0)}$, near the bifurcation point the states $\mathbf{q}_a(t)$ and $\mathbf{q}_b(t)$ are close to each other throughout the modulation period. Then escape can happen with nearly same probability at any modulation phase, i.e., synchronization of escape by the modulation is essentially lost.

Because the dynamics near a bifurcation point is slow, the system filters out high-frequency components of the noise. As a result, the noise becomes effectively δ-correlated (we will not consider here the situation where the noise power spectrum has singular features at high frequencies). The reduction to one slow variable driven by white noise can be done directly in the equations of motion. For slow modulation ($\omega_F t_r^{(0)} \ll 1$), this reduction is local in time (see Appendix B), otherwise it has to be done globally over the cycle (see Appendix C). Alternatively, the dimensionality reduction can be done directly in the variational problem for the optimal escape path (see Appendix A).

2.3.1 The adiabatic approximation

In the limit of slow modulation, where the period of the field τ_F is large compared to the system relaxation time $t_{\rm r}^{(0)}$, a convenient starting point of the analysis is the adiabatic approximation. The adiabatic periodic states of the system $\mathbf{q}_{\rm per}^{\rm ad}$ are given by the equation

$$\mathbf{K}(\mathbf{q}_{\rm per}^{\rm ad}; A, t) = \mathbf{0}, \tag{2.11}$$

which is obtained by disregarding $\dot{\mathbf{q}}$ and the noise $\mathbf{f}$ in the equation of motion (2.1).

The adiabatic stable state (attractor) $\mathbf{q}_a^{\rm ad} \equiv \mathbf{q}_a^{\rm ad}(t)$ is the solution $\mathbf{q}_{\rm per}^{\rm ad}$ for which the real parts of the eigenvalues of the matrix $\hat{\mu}$,

$$\mu_{ij} = \left(\partial K_i/\partial q_j\right),$$

are all negative. These eigenvalues give the "instantaneous" relaxation rates, for a given phase of the modulation $\phi = \omega_F t$. For the periodic adiabatic saddle-type state $\mathbf{q}_b^{\rm ad}(t)$ one of the eigenvalues of $\hat{\mu}$ has a positive real part.

In the adiabatic approximation, the saddle-node bifurcation occurs in the following way. At the critical value of the control parameter $A = A_c^{\rm ad}$, the periodic trajectories $\mathbf{q}_a^{\rm ad}(t)$ and $\mathbf{q}_b^{\rm ad}(t)$ given by (2.11) merge, but it happens only once per period. One can picture it by looking at Fig. 2.1 (b) and imagining that the states $\mathbf{q}_a(t)$ and $\mathbf{q}_b(t)$ touch each other. We set the corresponding instant of time equal to $t = 0$ (or $t = n\tau_F$), i.e., we assume that $\mathbf{q}_a^{\rm ad}(0) = \mathbf{q}_b^{\rm ad}(0)$ for $A = A_c^{\rm ad}$. Additionally, we set $\mathbf{q}_a^{\rm ad}(0) = \mathbf{q}_b^{\rm ad}(0) = \mathbf{0}$.

At the adiabatic bifurcation point $A = A_c^{\rm ad}, t = 0$ one of the eigenvalues μ_1 of the matrix $\hat{\mu}$ is equal to zero, whereas all other eigenvalues $\mu_{i>1}$ have *negative* real parts. The adiabatic approximation means that -Re $\mu_{i>1} \gg \omega_F$, or equivalently, that the

relaxation time max $\left[|\mathrm{Re}\,\mu_{i>1}|^{-1}\right]$ is small compared to τ_F. This relaxation time is typically of the order of $t_{\mathrm{r}}^{(0)}$.

We now write the dynamical variables $\mathbf{q}$ in the basis of the right eigenvectors of the matrix $\hat{\mu}$ at the bifurcation point and expand $\mathbf{K}$ in the equation of motion (2.1) in a series in $\mathbf{q}, t$, and $A - A_c^{\mathrm{ad}}$. As shown in Appendix B, the motion described by the variable q_1 is much slower than the motion described by the variables $q_{i>1}$. Over the time $\sim t_{\mathrm{r}}^{(0)}$ they "adjust" to the value of q_1, i.e., they follow q_1 adiabatically. The variable q_1 is the soft mode. It satisfies the equation of motion

$$\dot{q}_1 = K(q_1; A, t) + f_1(t), \tag{2.12}$$
$$K = \alpha q_1^2 + \beta\,\delta A^{\mathrm{ad}} - \alpha\gamma^2(\omega_F t)^2.$$

Here $\delta A^{\mathrm{ad}} = A - A_c^{\mathrm{ad}}$; the parameters α, β, γ are expressed in terms of the derivatives of $\mathbf{K}$ at the adiabatic bifurcation point and are given by Eqs. (B.3), (B.4).

The stable and unstable adiabatic periodic states in the absence of noise exist for $\alpha\beta\,\delta A^{\mathrm{ad}} < 0$. For concreteness and without loss of generality we set $\alpha > 0$. For small $|\omega_F t|$ the adiabatic states can be found by setting $K((q_1)_{a,b}^{\mathrm{ad}}; A, t) = 0$. This gives

$$(q_1)_{a,b}^{\mathrm{ad}} = \mp(2\alpha t_{\mathrm{r}}^{\mathrm{ad}})^{-1},$$

where $t_{\mathrm{r}}^{\mathrm{ad}}$ is the instantaneous adiabatic relaxation time. It is given by $|\partial K/\partial q_1|^{-1}$ evaluated for $q_1 = (q_1)_a^{\mathrm{ad}}$,

$$t_{\mathrm{r}}^{\mathrm{ad}} = \frac{1}{2}\left[-\alpha\beta\delta A^{\mathrm{ad}} + (\alpha\gamma\omega_F t)^2\right]^{-1/2} \tag{2.13}$$

[the explicit expression for $(q_1)_{a,b}^{\mathrm{ad}}(t)$ is given by Eq. (B.5)].

Validity of the adiabatic approximation

The applicability of the adiabatic approximation requires not only that $\omega_F t_{\mathrm{r}}^{\mathrm{ad}} \ll 1$, but also $|\partial t_{\mathrm{r}}^{\mathrm{ad}}/\partial t| \ll 1$. If this latter condition is not met, the system cannot follow

the modulation without delay, its state depends on how the parameters were varying in time. From Eq. (2.13), near the bifurcation point the time dependence of $t_{\rm r}^{\rm ad}$ is pronounced, so that

$$\max |\partial t_{\rm r}^{\rm ad}/\partial t| = 3^{-3/2}\gamma\omega_F/|\beta\delta A^{\rm ad}| \gg \omega_F t_{\rm r}^{\rm ad}.$$

Therefore the inequality $|\partial t_{\rm r}^{\rm ad}/\partial t| \ll 1$ is much stronger than $\omega_F t_{\rm r}^{\rm ad} \ll 1$. It holds if

$$t_{\rm r}^{\rm ad} \ll t_l, \qquad t_l = (\alpha\gamma\omega_F)^{-1/2}, \tag{2.14}$$

i.e., $\omega_F \ll |\beta\delta A^{\rm ad}|/\gamma$.

The inequality (2.14) restricts the range of validity of the adiabatic approximation. It is the time t_l rather than $1/\omega_F$ that imposes an upper bound on the adiabatic relaxation time of a periodically driven system where this approximation still applies. This time sets a new dynamical time scale. It fully characterizes the dynamics beyond the adiabatic limit in the range $\omega_F t_{\rm r} \ll 1$, as discussed in Sec. 2.3.2.

2.3.2 Locally nonadiabatic regime

As A approaches $A_c^{\rm ad}$, the criterion (2.14) is violated. The periodic stable and unstable states are pressed against each other. Since they cannot cross, they become distorted, as shown in Fig. 2.1 (d). Ultimately they merge, but along a line rather than at a point. From Eq. (2.12) one can see that this is just a straight line, which is described by the equation

$$q_{1c}(t) = \gamma\omega_F t. \tag{2.15}$$

Eqs. (2.12), (2.15) define the new nonadiabatic bifurcational value of the modulation amplitude for slow driving,

$$A_c^{\rm sl} = A_c^{\rm ad} + \beta^{-1}\gamma\omega_F. \tag{2.16}$$

The corrections to $A_c^{\rm sl}$ of higher order in ω_F are discussed in Sec. 2.3.4.

The change of the bifurcation amplitude described by Eq. (2.16) is somewhat similar to the effect of bifurcation delay [104, 105], which occurs when the bifurcation parameter is ramped through the bifurcation point. Here, however, we consider a periodically driven system; the bifurcation is not delayed in time, rather it is the bifurcational modulation amplitude that is changed compared to the adiabatic limit.

It is convenient to change in Eq. (2.12) to dimensionless variables $Q = \alpha t_l q_1$ and $\tau = t/t_l$, and to introduce the control parameter

$$\eta = \beta(\gamma\omega_F)^{-1}(A_c^{\rm sl} - A). \tag{2.17}$$

We note that η is the only parameter of a slowly driven system in the critical region. It describes both adiabatic and nonadiabatic behavior and gives the reduced distance to the bifurcation point. Interestingly, the distance along the modulation-amplitude axis $A_c^{\rm sl} - A$ is scaled by the modulation frequency ω_F; both these quantities are supposed to be small, but their ratio η can be arbitrary.

The equation of motion for the reduced variable takes the form

$$\frac{dQ}{d\tau} = G(Q, \eta, \tau) + \tilde{f}(\tau),\ G = Q^2 - \tau^2 + 1 - \eta. \tag{2.18}$$

The function $\tilde{f}(\tau) = (\gamma\omega_F)^{-1} f_1(t_l\tau)$ in Eq. (2.18) describes reduced noise. It is effectively δ-correlated on the slow-time scale, $\langle \tilde{f}(\tau)\tilde{f}(\tau')\rangle = 2\tilde{D}\delta(\tau - \tau')$, as explained in Appendix B. The noise intensity $\tilde{D}$ is given by Eq. (B.7).

The stable and unstable states $Q_{a,b}(\tau)$ are given by the equation $dQ/d\tau = G$. In the absence of noise this equation has symmetry $Q \to -Q, \tau \to -\tau$. As a consequence, the stable and unstable states are antisymmetric, $Q_b(\tau) = -Q_a(-\tau)$. Therefore it suffices to find only $Q_a(\tau)$.

We start with the adiabatic approximation. It applies for $\eta \gg 1$. The adiabatic stable and unstable states in the reduced variables are given by the equation $G = 0$ and have the form

$$Q_{a,b}^{\rm ad} = \mp \left[\tau^2 + (\eta - 1)^2\right]^{1/2}. \tag{2.19}$$

Each of these states is symmetric with respect to $\tau = 0$, where they are closest to each other. The adiabatic bifurcation point is $\eta = 1$, which corresponds to $A = A_c^{\rm ad}$.

The region $\eta \lesssim 1$ is nonadiabatic, and $\eta = 0$ (or $A = A_c^{\rm sl}$) is the nonadiabatic bifurcation point for slow driving. At this point $Q_{a,b}(\tau)$ merge into the straight line $Q_c(\tau) = \tau$.

Close to the nonadiabatic bifurcation point, where $\eta \ll 1$, one can find $Q_{a,b}(\tau)$ by perturbation theory in the whole range $-\infty < \tau < |\ln \eta|^{1/2}/2$. The linearized equation for the difference $\delta Q(\tau) = Q_a(\tau) - \tau$ has a form $\frac{d\delta Q}{d\tau} = 2\tau\, \delta Q + \eta$. By solving it we obtain

$$Q_a(\tau) = -Q_b(-\tau) \approx \tau - \eta \int_{-\infty}^{\tau} d\tau_1\, e^{\tau^2 - \tau_1^2}. \tag{2.20}$$

In the region of large negative τ the function $Q_a(\tau) = -Q_b(-\tau)$ has a simple form $Q_a(\tau) \approx -\tau - \eta(2\tau)^{-1}$. The states Q_a and Q_b are closest to each other, with separation $\sim \eta$, in the range $|\tau| < |\ln \eta|^{1/2}/2$. The interstate separation decreases as η approaches the bifurcational value $\eta = 0$. At the same time, the range of τ where $Q_a(\tau)$ and $Q_b(\tau)$ stay close to each other increases with decreasing η.

As τ increases beyond $\approx |\ln \eta|^{1/2}/2$, there occurs a sharp crossover from the nearly linear in τ solution for $Q_a(\tau)$ (2.20) to the adiabatic solution (2.19) $Q_a \propto -\tau$. The functions $Q_{a,b}(\tau)$ for a specific value of η are shown in Fig. 2.2.

The interval of the real time $|t| \lesssim t_{\rm r} = t_l |\ln \eta|^{1/2}$, where the states $Q_{a,b}$ are nearly linear in t, should be much smaller than $1/\omega_F$ in order for Eq. (2.12) to apply. This

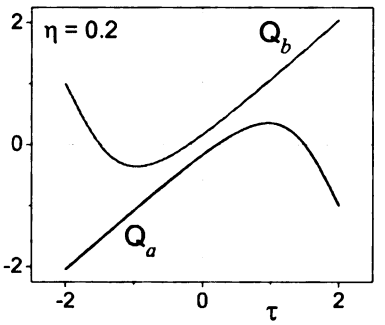

Figure 2.2: Nonadiabatic stable and unstable states $Q_a(\tau)$ and $Q_b(\tau) = -Q_a(-\tau)$ for slow modulation as given by the equation $dQ/d\tau = G(Q, \eta, \tau)$ for $\eta = 0.2$. The functions $Q_{a,b}(\tau)$ are strongly asymmetric, in contrast to the adiabatic states (2.19) which are even functions of τ.

imposes a restriction on η,

$$\eta \gg \exp(-C|\alpha|\gamma/\omega_F), \quad C \sim 1. \tag{2.21}$$

For smaller $\eta \propto |A_c^{\rm sl} - A|$ the local approximation, where the coefficients are expanded about the adiabatic bifurcation point, no longer applies. The relaxation time $t_{\rm r}$ becomes comparable to the modulation period, and the behavior of the system during the whole cycle becomes important. It follows from Eq. (2.21), however, that for low frequencies the local approximation is extremely good.

On the whole, the locally nonadiabatic regime is limited in η by the condition $\eta \lesssim 1$ and by Eq. (2.21). The width of the amplitude range $A_c^{\rm sl} - A$ imposed by the first condition linearly increases with the field frequency, in the approximation (2.16). Therefore locally-nonadiabatic critical behavior is more pronounced for higher frequencies. However, the appropriate frequency range is limited from above by the condition (2.21). For higher ω_F there should occur a crossover to a fully nonlocal picture, which is discussed in the next section.

2.3.3 Fast-oscillating field

Sufficiently close to the "true" critical value of the modulation amplitude A_c, the relaxation time of the system becomes large compared to the modulation period even if $\omega_F t_r^{(0)} \lesssim 1$ far from the bifurcation point. The inequality $\omega_F t_r \gg 1$ defines the third region, in addition to the adiabatic and locally nonadiabatic, where we could analyze the dynamics near a bifurcation point. The analysis of this region is simplified by the fact that here the modulating field is effectively fast-oscillating.

For $\omega_F t_r \gg 1$, near the bifurcation point the periodic stable and unstable states $\mathbf{q}_a(t)$ and $\mathbf{q}_b(t)$ stay close to each other throughout the cycle, see Fig. 2.3. For $A = A_c$, they coalesce into a periodic critical cycle $\mathbf{q}_c(t) = \mathbf{q}_c(t + \tau_F)$. When A is close to A_c and $\mathbf{q}$ is close to $\mathbf{q}_c$, we can simplify the equations of motion (2.1) by expanding the function $\mathbf{K}$ in $\delta\mathbf{q} = \mathbf{q} - \mathbf{q}_c$ and $\delta A = A - A_c$ (cf. Ref. [84]),

$$\delta\dot{\mathbf{q}} = \hat{\mu}\delta\mathbf{q} + \frac{1}{2}(\delta\mathbf{q}\cdot\boldsymbol{\nabla})^2\mathbf{K} + \delta A\frac{\partial}{\partial A}\mathbf{K} + \mathbf{f}(t). \tag{2.22}$$

Here, as before, $\mu_{ij} \equiv \mu_{ij}(t) = \partial K_i/\partial q_j$, but all derivatives of $\mathbf{K}$ are now evaluated for $A = A_c$ and $\mathbf{q} = \mathbf{q}_c(t)$. Therefore all coefficients in Eq. (2.22) are periodic functions of time.

If initially the system is close to $\mathbf{q}_c(t)$, its distance from $\mathbf{q}_c(t)$ will oscillate with frequency ω_F and with an amplitude that slowly varies over the period τ_F. This amplitude is a slow variable, $Q^{\rm sm}(t)$. The equation for $Q^{\rm sm}(t)$ can be obtained by an appropriate averaging method explained in Appendix C. After rescaling to dimensionless coordinate $Q \propto Q^{\rm sm}$ and time $\tau \propto t$, see Eq. (C.11), this equation takes a form which is similar to Eq. (2.18),

$$\frac{dQ}{d\tau} = G(Q,\eta) + \tilde{f}(\tau), \tag{2.23}$$
$$G = Q^2 - \eta, \qquad \eta = \beta'(A_c - A)$$

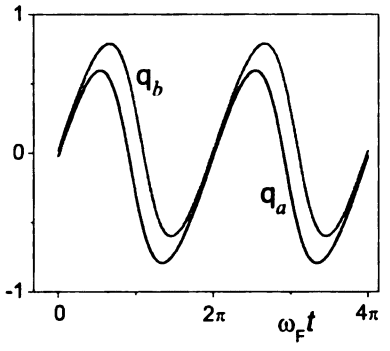

Figure 2.3: The stable and unstable states, $\mathbf{q}_a(t)$ and $\mathbf{q}_b(t)$, close to the bifurcation point. For $\omega_F t_r \gg 1$ the states are close to each other throughout the modulation period. The figure refers to a one-dimensional overdamped particle in a potential $U(q,t) = \frac{1}{4}q - \frac{1}{3}q^3 - Aq\cos(\omega_F t)$ for $(A_c - A)/A_c \approx 0.01$. The modulation is comparatively slow, $\omega_F t_r^{(0)} = 1$, but for chosen A the relaxation time becomes long, $\omega_F t_r \approx 9.8$.

[in contrast to Eq. (2.18), the function G here is independent of time]. The coefficient β' is given by Eq. (C.7).

The parameter η in Eq. (2.23) is the scaled distance to the bifurcation point. The stationary states $Q_{a,b} = \mp\eta^{1/2}$ exist for $\eta > 0$. They merge for $\eta = 0$. The noise $\tilde{f}(\tau)$ is effectively white on the time scale that largely exceeds ω_F^{-1} and the noise correlation time $t_{\rm corr}$. Its intensity $\tilde{D}$ is given by Eq. (C.12).

The results of this Section and Appendix C refer to the case $\omega_F t_r \gg 1$, but arbitrary $\omega_F t_r^{(0)}$. Therefore the problem is different from the standard problem of slow motion in a fast-oscillating field [106], where of interest is the smooth term in the oscillating coordinate. In contrast, here we are interested in the slowly varying oscillation amplitude. If $\omega_F t_r^{(0)} \gg 1$, a transition to slow and fast variables can be made already in the original equation of motion (2.1), by separating $\mathbf{q}$ into slow and fast oscillating parts. The equation for the slow part near the bifurcation point will

again have the form (2.23), but the expressions (C.7) for α', β' will be simplified; in particular, the factor κ_{11} in Eq. (C.7) will be equal to one.

2.3.4 Connection to the locally nonadiabatic regime

Eq. (2.22) allows us to look from a different perspective at the locally nonadiabatic regime that emerges for $\omega_F t_r \ll 1$. In contrast to the approach of Sec. 2.3.2, where the starting point was the adiabatic approximation, here we will assume that A is close to the true bifurcational value of the amplitude A_c and that $\mathbf{q}(t)$ is close to the critical cycle $\mathbf{q}_c(t)$, at least for a part of the period τ_F.

For $\omega_F t_r \ll 1$, one can think of a local in time description of the dynamics near the cycle $\mathbf{q}_c(t)$. From Eq. (2.22), this dynamics is determined by the eigenvalues $\mu_\nu(t)$ of the matrix $\hat{\mu}(t)$. In contrast to the analysis of Sec. 2.3.1, we consider here the matrix $\hat{\mu}$ calculated for the critical cycle $\mathbf{q}_c(t)$ rather than the two similar matrices calculated separately for the adiabatic stable and unstable states.

For much of the driving period the real parts of $\mu_\nu(t)$ are all large, $|\mathrm{Re}\ \mu_\nu| \sim 1/t_r^{(0)} \gg \omega_F$. Then, when the system is in the stable state, it follows the field adiabatically. The adiabaticity is broken where one of the eigenvalues, say $\mu_1(t)$, goes through zero. As we will see, at this time the stable and unstable states are most close to each other. We set the time when it happens equal to zero, i.e., $\mu_1(0) = 0$.

For small $|t| \ll \tau_F$ the analysis of the system dynamics is in many respects similar to that in Sec. 2.3.2 and Appendix C. First, $\delta\mathbf{q}(t)$ in Eq. (2.22) is written as $\sum_\nu \delta q_\nu \mathbf{e}_\nu(0)$, where $\mathbf{e}_\nu(0)$ are the right eigenvectors of the matrix $\hat{\mu}(0)$. The component δq_1 of $\delta\mathbf{q}$ along the eigenvector $\mathbf{e}_1(0)$ of $\hat{\mu}(0)$ will be the slow variable, or the soft mode.

The matrix $\hat{\mu}(t)$ can be expanded about $t = 0$ for small $|t|$,

$$\hat{\mu}(t) \approx \hat{\mu}(0) + \dot{\hat{\mu}}(0)t, \tag{2.24}$$

where the time derivative is taken for $t = 0$. This derivative is small, its matrix elements on the eigenvectors $\bar{\mathbf{e}}_\nu(0), \mathbf{e}_{\nu'}(0)$ are $|\dot{\mu}_{\nu\nu'}| \sim \omega_F / t_{\rm r}^{(0)} \ll \left(t_{\rm r}^{(0)}\right)^{-2}$ [here, $\bar{\mathbf{e}}_\nu(0)$ are the left eigenvectors of the matrix $\hat{\mu}(0)$].

With (2.24), Eq. (2.22) can be solved for the "fast" components $\delta q_{\nu>1}$. Over a short time $\sim t_{\rm r}^{(0)}$ they approach their quasistationary values for given δq_1. Those are small, of order $\delta q_1^2, \delta A, \delta q_1 \omega_F t$, and follow δq_1 adiabatically. Noise-induced fluctuations of $\delta q_{\nu>1}$ about the quasistationary values are also small for small noise intensity. Therefore the effect of $\delta q_{\nu>1}$ on the dynamics of δq_1 can be disregarded.

The equation of motion for δq_1 has a form of the Riccati equation with a random force,

$$\begin{aligned} \delta\dot{q}_1 &= \dot{\mu}_1 t \delta q_1 + \alpha \delta q_1^2 + \beta \delta A + f_1(t), \\ f_1(t) &= \bar{\mathbf{e}}_1(0) \cdot \mathbf{f}(t), \qquad \dot{\mu}_1 = \bar{\mathbf{e}}_1(0) \cdot \dot{\hat{\mu}}(0) \mathbf{e}_1(0). \end{aligned} \tag{2.25}$$

Here, $\alpha = (1/2)\big(\mathbf{e}_1(0) \cdot \boldsymbol{\nabla}\big)^2 K_1$, $\beta = \partial K_1 / \partial A$, with $K_1 = \bar{\mathbf{e}}_1(0) \cdot \mathbf{K}$ being now the component of $\mathbf{K}$ in the direction $\mathbf{e}_1(0)$. All derivatives of $\mathbf{K}$ are calculated on the critical cycle $\mathbf{q}_c(t)$ for $t = 0$. Because $|\dot{\mu}_1|$ is small, relaxation of δq_1 is slow compared to relaxation of $\delta q_{\nu>1}$, for typical $|t| \ll \tau_F$.

Eq. (2.25) describes the stable and unstable states of the original equation of motion (2.1) in the region $|t| \ll \tau_F$. It is seen that these states, $(\delta q_1)_a$ and $(\delta q_1)_b$, exist provided

$$\dot{\mu}_1 > 0, \quad \alpha\beta\,\delta A < 0. \tag{2.26}$$

In this range Eq. (2.25) is equivalent to Eq. (2.18). This can be seen if, on the one hand, Eq. (2.18) is written for the deviation $\delta Q = Q - \tau$ of Q from its value on the

critical cycle $Q_c = \tau$, and on the other hand, in Eq. (2.25) one changes to scaled variables $\delta Q = \alpha(2/\dot{\mu}_1)^{1/2}\delta q_1$ and $\tau = (\dot{\mu}_1/2)^{1/2}t$. The control parameter η in (2.18) becomes

$$\eta = -2\alpha\beta\dot{\mu}_1^{-1}\delta A. \tag{2.27}$$

The analysis of Eq. (2.18) then applies to Eq. (2.25). In particular, the statement in the beginning of this subsection that the stable and unstable states are at their closest for $t = 0$ is an immediate consequence of the explicit expression for these states (2.20).

There is an important difference between this approach and the approach of Sec. 2.3.2. Because here we do not start from the adiabatic approximation, we formally have not specified how small is the difference between the critical amplitude A_c and its adiabatic value $A_c^{\rm ad}$. In Eq. (2.16) we only obtained the linear in $\omega_F t_{\rm r}^{(0)}$ term in $A_c - A_c^{\rm ad}$. In general, $A_c - A_c^{\rm ad}$ has also higher-order terms. They can be obtained by taking into account the dependence of the coefficients α, β, γ in Eq. (B.3) on A, which was previously disregarded. This is illustrated for a particular model in Sec. 2.5. It is for the renormalized critical amplitude, i.e., for the control parameter given by Eq. (2.27), that there holds the exponential limit (2.21) on the range where the local nonadiabatic approximation applies. The inequality (2.21) indicates that, for small frequency, the critical amplitude found from the local theory is exponentially close to the exact A_c. This is confirmed by numerical calculations for a model discussed in Sec. 2.5.

2.4 Activation energy of escape

It follows from the results of Sec. 2.3 that, near a bifurcation point, a periodically driven system has a soft mode Q, and the noise that drives this mode is effectively white. The equation of motion is of the form $dQ/d\tau = G + f(\tau)$ (2.18), where the function G is given by $G = Q^2 + 1 - \eta - \tau^2$ for $\omega_F t_r \ll 1$ [cf. Eq. (2.18)] and $G = Q^2 - \eta$ for $\omega_F t_r \gg 1$ [cf. Eq. (2.23)]. The intensity $\tilde{D}$ of the noise $f(\tau)$ has the form (B.7) and (C.12) in these two cases.

For a white-noise driven system, the variational problem (2.9), (2.10) of calculating the period-averaged rate of activated escape $\overline{W}$ can be written in the form

$$\overline{W} = \text{const} \times \exp(-\tilde{R}/\tilde{D}), \quad \tilde{R} = \min \tilde{\mathcal{R}}[Q], \tag{2.28}$$
$$\tilde{\mathcal{R}} = \int d\tau\, L\left(Q, \frac{dQ}{d\tau}, \tau\right), \quad L = \frac{1}{4}\left(\frac{dQ}{d\tau} - G\right)^2.$$

(cf. Appendix A). In contrast to the standard formulation [55], the function G here may depend on time τ and is not time-periodic, in the actual range of τ. The minimization is carried out over the paths $Q(\tau)$ that start at the stable state $Q_a(\tau)$ for $\tau \to -\infty$ and end at the unstable state $Q_b(\tau)$ for $\tau \to +\infty$. The non-stationarity emerges for slow modulation, where $\omega_F t_r \ll 1$, and is related to the assumptions that (i) escape is most likely to occur during a portion of the period where the states $Q_{a,b}$ are close, and (ii) the duration of motion along the optimal escape path $Q_{\text{opt}}(\tau)$ is much less than the modulation period.

We have solved the variational problem using the Hamilton equations of motion for Q and $P = \partial L/\partial(dQ/d\tau)$,

$$\frac{\partial Q}{\partial \tau} = 2P + G, \qquad \frac{\partial P}{\partial \tau} = -P\frac{\partial G}{\partial Q}. \tag{2.29}$$

We then verified the assumptions made in obtaining Eqs. (2.28), (2.29).

Equations (2.29) were solved both analytically and numerically. In numerical calculations, we chose the initial conditions on the optimal path close to $Q_a(\tau)$ with large but finite negative τ. In this range Eqs. (2.29) can be linearized in $Q - Q_a(\tau)$. On the solution that goes away from Q_a the momentum P is linear in $Q - Q_a$,

$$P \approx [Q - Q_a(\tau)]/\sigma_a^2(\tau) \tag{2.30}$$
$$\sigma_a^2(\tau) = 2\int_{-\infty}^{\tau} d\tau' \exp\left[4\int_{\tau'}^{\tau} d\tau'' Q_a(\tau'')\right]$$

We used the shooting method: we sought such initial $Q - Q_a(\tau)$ for given τ that the trajectory approaches $Q_b(\tau)$ for large τ, cf. Ref. [94].

Numerical results for the activation energy in the whole range of slow driving, where $\omega_F t_r \ll 1$, are shown below in Figs. 2.4, 2.5 on linear and logarithmic scales, respectively. Note that the activation energy is a function of a single control parameter $\eta \propto A_c - A$, and in this sense the results are universal, i.e. system-independent. In the rest of this Section we discuss analytical results and compare them with the numerical results.

2.4.1 Activation energy in the adiabatic approximation

The adiabatic regime applies when the driving is slow, $\omega_F t_r \ll 1$, and the system is sufficiently far from the bifurcation point, so that $t_r \ll t_l$ [cf. Eq. (2.14)] or equivalently $|\delta A^{ad}| \equiv |A_c^{ad} - A| \gg \omega_F|\gamma/\beta|$. Respectively, the dimensionless control parameter $\eta \propto A_c - A$ is large, $\eta - 1 \gg 1$, [cf. Eq. (2.17); we note that the actual parameter in the adiabatic range is not η but $\eta - 1$]. In this case we expect that escape occurs when the adiabatic states (2.19) are closest to each other, i.e., for $\tau = 0$. Then, in the first approximation, the term τ^2 in the function G in Eq. (2.18)

can be disregarded, and G becomes

$$G^{\rm ad} = Q^2 + 1 - \eta. \tag{2.31}$$

The solution of Eq. (2.29) with G of the form (2.31) and with boundary conditions $Q(\tau) \to \mp(\eta-1)^{1/2}$ for $\tau \to \mp\infty$ is well known. It is an instanton (kink)

$$Q^{\rm ad}_{\rm opt}(\tau, \tau_0) = (\eta-1)^{1/2} \tanh[(\eta-1)^{1/2}(\tau-\tau_0)]$$

centered at an arbitrary τ_0.

The characteristic duration of motion along the path $Q^{\rm ad}_{\rm opt}(\tau)$ in dimensionless time is $\Delta\tau \sim (\eta-1)^{-1/2}$, which corresponds to $\Delta t \sim t_{\rm r}$ in real time. Since $\Delta\tau \ll (\eta-1)^{1/2}$, the term τ^2 in the function G [Eq. (2.18)] can be disregarded compared to $\eta-1$, which justifies replacing G with $G^{\rm ad}$ as long as $|\tau_0| \ll (\eta-1)^{1/2}$.

The activation energy (2.28) calculated along the path $Q^{\rm ad}_{\rm opt}$ is

$$\tilde{R}^{\rm ad} = \frac{4}{3}(\eta-1)^{3/2} \propto (A^{\rm ad}_c - A)^{3/2}. \tag{2.32}$$

This equation shows that the activation energy of escape scales with the distance to the bifurcation point as $(A_c - A)^\xi$ with $\xi = 3/2$ in the adiabatic region.

2.4.2 Nonadiabatic correction to the activation energy

We now consider the lowest-order correction to the adiabatic activation energy. Two factors have to be taken into account. First is that, because of the nonzero duration of motion along the escape path $\Delta\tau$, the equilibrium states $Q^{\rm ad}_{a,b}(\tau)$ change, which was disregarded in the analysis of Sec. 2.4.1. However, the corresponding correction to $\tilde{R}$ is exponentially small. Indeed, if we consider $\tilde{\mathcal{R}}$ as a function of the end point Q on the optimal path, we have $|\partial\tilde{\mathcal{R}}/\partial Q| = |P|$, where P is the momentum on the optimal

path. For an instantonic solution, the momentum goes to zero as $Q_{\rm opt} \to Q_{a,b}$, see Eq. (2.30). Therefore a small change of $Q_{a,b}$ affects the activation energy very weakly.

The major nonadiabatic correction to $\tilde{R}$ comes from the time-dependent term in $G = G^{\rm ad} - \tau^2$ [cf. Eq. (2.18)]. This term lifts the time invariance of the instanton $Q_{\rm opt}(\tau, \tau_0)$ with respect to τ_0,

To first order in τ^2, i.e., to lowest order in $(\eta - 1)^{-1}$, the correction $\delta\tilde{R}$ can be found from Eq. (2.28) by integrating the term τ^2 along the zeroth order trajectory $Q^{\rm ad}_{\rm opt}(\tau, \tau_0)$,

$$\delta\tilde{R} = \min_{\tau_0} \int d\tau' \, \frac{dQ^{\rm ad}_{\rm opt}(\tau', \tau_0)}{d\tau'} \, \tau'^2. \tag{2.33}$$

(we used that $dQ^{\rm ad}_{\rm opt}/d\tau = -G^{\rm ad}$). Minimization here is done over τ_0, the center of the instanton. It is necessary because $\tilde{R}$ is the absolute minimum of the functional $\tilde{\mathcal{R}}$.

A direct calculation shows that the minimum of $\delta\tilde{R}$ is reached for $\tau_0 = 0$, and

$$\delta\tilde{R} = \frac{\pi^2}{6}(\eta - 1)^{-1/2}. \tag{2.34}$$

The correction $\delta\tilde{R}$ rapidly falls off with increasing $\eta - 1$. On the other hand, as η decreases and becomes ≈ 1, the term $\delta\tilde{R}$ increases very fast, which indicates a breakdown of the adiabatic theory in this region.

The analytical results in the adiabatic region are compared with the numerical solution for the activation energy $\tilde{R}$ in Fig. 2.4. The corrected adiabatic theory works well in the whole range where the control parameter $\eta \gtrsim 3$, but for smaller η nonadiabatic effects are significant and have to be taken into account in a nonperturbative way.

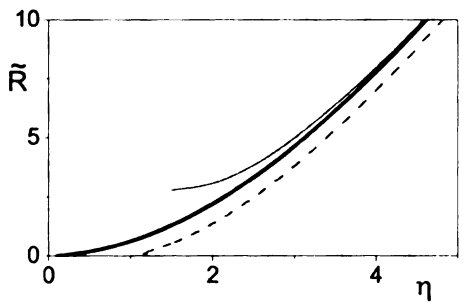

Figure 2.4: The activation energy $\tilde{R}$ vs. $\eta \propto A_c - A$ for slow driving, $\omega_F t_r \ll 1$. The thick solid line shows the numerical solution of Eq. (2.28). The dashed line is the adiabatic activation energy (2.32), $\tilde{R}^{\rm ad} \propto (\eta - 1)^{3/2}$. The thin solid line shows the corrected adiabatic activation energy $\tilde{R}^{\rm ad} + \delta\tilde{R}$. It is close to the numerical result for $\eta \gtrsim 3$. The correction $\delta\tilde{R}$ diverges at the adiabatic bifurcation point $\eta = 1$.

2.4.3 Activation energy in the locally nonadiabatic region

Standard techniques do not allow to solve equations (2.29) for the optimal path analytically in the general case $\eta \sim 1$. This is because the function G in Eq. (2.29) explicitly depends on time τ. However, a solution can be obtained close to the bifurcation point, where $\eta \propto A_c - A$ is small, but not exponentially small, cf. Eq. (2.21).

Unusually for an instanton-type problem, and because of the strong time dependence of G, the optimal path can be found by *linearizing* the equations of motion (2.29) about the critical state $Q_c = \tau$. This gives

$$\delta\dot{Q} = 2\tau\delta Q - \eta + 2P, \quad \dot{P} = -2P\tau, \tag{2.35}$$

where $\delta Q \equiv Q - \tau$. The solution of these equations with boundary conditions $Q(\tau) \to Q_{a,b}(\tau)$ for $\tau \to \mp\infty$ is

$$\begin{aligned} Q_{\rm opt}(\tau) &= \tau - \eta \int_0^\tau d\tau' [1 - \sqrt{2}\, e^{-\tau'^2}] e^{\tau^2 - \tau'^2}, \\ P_{\rm opt}(\tau) &= \eta e^{-\tau^2}/\sqrt{2}, \end{aligned} \tag{2.36}$$

where we took into account the explicit form of $Q_{a,b}(t)$ (2.20).

It is seen from Eq. (2.36) that the momentum on the optimal path $P_{\rm opt}$ has a shape of a Gaussian pulse centered at $\tau = 0$, with width ~ 1. The coordinate $Q_{\rm opt}(\tau)$ over the dimensionless time $\tau \sim 1$ switches between the equilibrium states $Q_{a,b}$. The typical duration of motion in real time is t_l.

From Eqs. (2.36), the nonadiabatic activation energy of escape for $\omega_F t_{\rm r} \ll 1$ is

$$\tilde{R}^{\rm nonad} = (\pi/8)^{1/2}\eta^2 \propto (A_c - A)^2. \tag{2.37}$$

Here, the critical amplitude A_c is given by Eq. (2.16), to first order in ω_F.

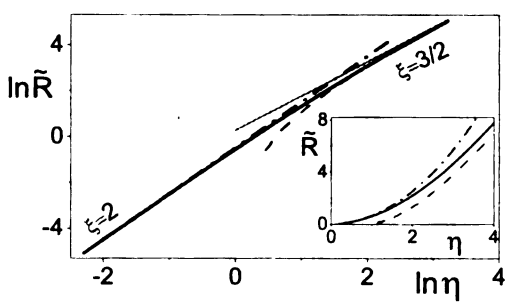

Figure 2.5: The activation energy $\tilde{R} = -\tilde{D}\ln\overline{W}$ on a logarithmic and linear scale (inset) vs. $\eta \propto A_c - A$ for slow modulation, $\omega_F t_{\rm r} \ll 1$. Thick solid lines show the numerical solution of the variational problem (2.28). It describes the crossover between different scaling regions. The thin solid line shows the adiabatic scaling for large η, $\tilde{R} \propto \eta^{\xi}$ with $\xi = 3/2$. The full result of the adiabatic approximation is shown by the dashed line. The dash-dot line shows the nonadiabatic result (2.37) that applies for $\eta \ll 1$; here $\tilde{R} \propto \eta^{\xi}$ with $\xi = 2$.

It is seen from Eq. (2.37) that, in the locally nonadiabatic region, the activation energy again displays scaling behavior, $\tilde{R} \propto (A_c - A)^{\xi}$. But the scaling exponent is $\xi = 2$, it differs from the adiabatic exponent $\xi = 3/2$ (2.32) that has been known for stationary systems. This is a result of the complicated nonadiabatic dynamics associated with avoided crossing of the stable and unstable states, cf. Fig. 2.1. The

onset of this scaling behavior is the central result of this Chapter.

The predicted $\xi = 2$ scaling is compared with the result of the numerical calculation in Fig. 2.5. The analytical and numerical results are in quantitative agreement in the whole range $\eta \lesssim 2$.

2.4.4 Activation energy for $\omega_F t_r \gg 1$

It was shown in Sec. 2.3.3 that, sufficiently close to a bifurcation point, there holds a condition $\omega_F t_r \gg 1$, even where the modulation frequency is less than the relaxation rate far away from the bifurcation point, $\omega_F t_r^{(0)} \lesssim 1$. Finding the activation energy of escape $\tilde{R} \equiv \tilde{R}^{\rm fast}$ for $\omega_F t_r \gg 1$ is formally similar to that in the adiabatic approximation. The only difference is that $\eta - 1$ in Eq. (2.31) should be now replaced by η. This gives

$$\tilde{R}^{\rm fast} = (4/3)\eta^{3/2} \propto (A_c - A)^{3/2}. \tag{2.38}$$

Both the coefficient β' that relates η to $A_c - A$ [see Eqs. (2.23) and (C.7)] and the noise intensity $\tilde{D}$ (C.12) depend on the arbitrary initial time t_i. It enters the weighting factor $\kappa_{11}(t, t_i)$ which was used in obtaining the equation of motion for the slow variable (2.23). A straightforward analysis shows that t_i drops out from the ratio $\beta'^{3/2}/\tilde{D}$, which gives the escape rate $\overline{W} \propto \exp(-\tilde{R}^{\rm fast}/\tilde{D})$.

Eq. (2.38) shows that the activation energy displays scaling behavior with the distance to the bifurcation point in the range $\omega_F t_r \gg 1$. The scaling exponent is $\xi = 3/2$, as in the adiabatic case.

2.4.5 Scaling crossovers near a critical point

Eqs. (2.32), (2.37), and (2.38) show the onset of three regions where the activation energy of escape displays scaling dependence on the modulation amplitude, $R \propto \tilde{R} \propto (A_c - A)^{\xi}$. The adiabatic and locally nonadiabatic regions emerge only if the modulation frequency is slow compared to the relaxation rate far from the bifurcation point, $\omega_F t_r^{(0)} \ll 1$. In this case, as seen from Fig. 2.5, as the bifurcation point is approached, the system displays first the adiabatic scaling $\xi = 3/2$, which for smaller $A_c - A$ goes over into the scaling $\xi = 2$. As the bifurcation point A_c is approached even closer, there emerges the fast-oscillating regime where $\xi = 3/2$ again.

The widths of the regions of different scaling strongly depend on the modulation frequency. For small $\omega_F t_r^{(0)} \ll 1$ the range of amplitudes where motion is effectively fast oscillating, $\omega_F t_r \gg 1$, is exponentially narrow. However this range increases very rapidly with increasing ω_F. The particular way in which the widths of different scaling regions vary with ω_F depends on the system dynamics, as illustrated in Sec. 2.5. Ultimately, for $\omega_F t_r^{(0)} \gtrsim 1$, the regime of effectively fast oscillations becomes the only observable regime near a bifurcation point.

2.5 Scaling crossovers for a model system

To test the occurrence of three scaling regions and the scaling crossovers, we have studied activated escape for a model system, an overdamped Brownian particle in a modulated potential well. It is described by the Langevin equation

$$\dot{q} = -\frac{\partial U(q,t)}{\partial q} + f(t), \quad \langle f(t) f(t') \rangle = 2D\delta(t - t'),$$
$$U(q,t) = -\frac{1}{3}q^3 + \frac{1}{4}q - Aq\cos\omega_F t. \tag{2.39}$$

The shape of the potential $U(q,t)$ is shown schematically in Fig. 2.1 (a). In the absence of modulation, $A = 0$, the system has a metastable state at the bottom of the potential well, $q_a = -1/2$, and an unstable equilibrium at the barrier top, $q_b = 1/2$. The relaxation time is $t_r^{(0)} = 1/U''(q_a) = 1$. In the presence of modulation, the states $q_{a,b}$ oscillate in time. As the modulation amplitude A increases to the critical value A_c (the saddle-node bifurcation), the states merge, and then, for $A > A_c$, disappear.

The frequency dependence of the critical amplitude A_c is shown in Fig. 2.6. In the limit $\omega_F = 0$ we have $A_c \equiv A_c^{\rm ad} = 1/4$. The linear in ω_F correction to A_c can be obtained from Eq. (2.16) by noticing that the adiabatic bifurcational value of the coordinate is $q_c^{\rm ad} = 0$, and the adiabatic bifurcation occurs for $t = 0$ (or equivalently, $t = n\tau_F$). Near the adiabatic bifurcation point we have

$$\dot{q} = q^2 + \delta A^{\rm ad} - \frac{1}{2} A\omega_F^2 t^2 + f(t), \tag{2.40}$$

with $\delta A^{\rm ad} = A - A_c^{\rm ad}$. This equation will have the same form as Eq. (2.12) if we replace the factor A in $A\omega_F^2 t^2$ with $A_c^{\rm ad} = 1/4$ [as it was done in Eq. (2.12)].

From Eq. (2.40) it follows that, for the model under consideration, the parameters in Eq. (2.12) are $\alpha = \beta = 1, \gamma = (A_c^{\rm ad}/2)^{1/2} = 2^{-3/2}$. Therefore, from Eq. (2.16), to first order in ω_F the critical amplitude is $A_c^{\rm sl} = 1/4 + 2^{-3/2}\omega_F$. It is shown in the main part of Fig. 2.6 with the dashed line.

As discussed in Sec. 2.3.4, the local nonadiabatic theory allows us to find higher-order terms in the critical amplitude. This is done by noticing that the critical state $q_c(t)$ into which the stable and unstable states merge at the bifurcation point is linear in t for small t, i.e., $q_c(t) - q_c^{\rm ad} \propto t$. By substituting this solution into Eq. (2.40) (without noise) we obtain

$$A_c \approx \left[1 + \omega_F^2 + \omega_F \left(\omega_F^2 + 2\right)^{1/2}\right]/4, \ \omega_F t_r \ll 1. \tag{2.41}$$

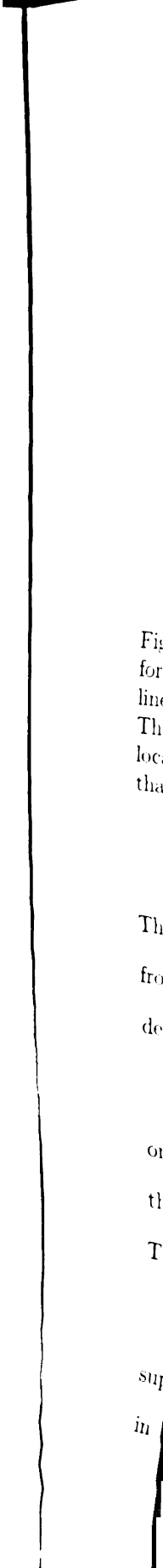

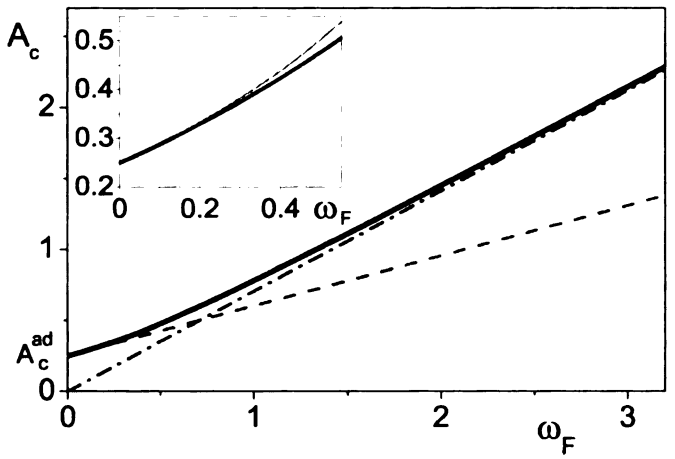

Figure 2.6: The critical amplitude A_c as a function of the modulation frequency ω_F for the system (2.39). Numerical results are shown by thick solid lines. The dashed line shows the linear in ω_F nonadiabatic correction to A_c described by Eq. (2.16). The thin solid line in the inset describes a correction obtained from the self-consistent local analysis, Eq. (2.41). The dash-dot line describes the high-frequency asymptotic that follows from Eq. (2.42).

This equation is in good agreement with the numerical data for $\omega_F t_r^{(0)} \lesssim 0.4$, as seen from the inset in Fig. 2.6. The difference between the numerical and analytical A_c decreases exponentially fast with decreasing ω_F.

We also evaluated for slow driving the time derivative of the eigenvalue $\mu_1 = 2q_c(t)$ on the critical cycle $q_c(t)$. For the model (2.40) the stable and unstable states are at their closest for $t = 0$. Eqs. (2.17), (2.27) show that, at this time, $\dot{\mu}_1 = (2A_c)^{1/2}\omega_F$. This value agrees with the numerical values of $\dot{\mu}_1$ to better than 10% for $\omega_F < 0.5$.

In the high frequency limit, $\omega_F t_r^{(0)} \gg 1$, the motion of the system (2.39) is a superposition of slow motion and fast oscillations at frequency ω_F. To lowest order in ω_F^{-1} we have $q \approx Q + (A/\omega_F)\sin\omega_F t$. The equation for the slow variable Q

becomes

$$\dot{Q} = Q^2 - \frac{1}{4} + \frac{A^2}{2\omega_F^2} + f(t). \tag{2.42}$$

It shows that, for large ω_F, we have $A_c \approx \omega_F/\sqrt{2}$. This is in good agreement with numerical data in Fig. 2.6 for $\omega_F \gtrsim 2$.

In the intermediate range, $\omega_F t_{\rm r}^{(0)} \lesssim 1$, the motion may not be separated into slow and fast-oscillating for weak modulation, but the separation becomes possible near a critical point, $\omega_F t_{\rm r} \gg 1$. Here, the coefficients in the equation of motion for the slow variable and the effective noise intensity (C.7), (C.12) are nonlocal and had to be evaluated numerically as functions of ω_F.

2.5.1 Activation energy

For a periodically modulated overdamped Brownian particle described by Eq. (2.39), the activation energy of escape R can be found from the variational problem (2.9), (2.10) or, equivalently, (2.28) [94]. The variables Q, P, τ, and the function G in the Lagrangian L (2.28) and the Hamilton equations (2.29) should be changed to q, p, t, and $-\partial U(q,t)/\partial q$, respectively. As explained in Sec. 2.2, there is one optimal path per modulation period. The initial condition for the momentum p on the optimal path is given by Eq. (2.30), with $Q_a(\tau)$ replaced by $q_a(t)$ [the expression for σ_a^2 can be further simplified taking into account the periodicity of $q_a(t)$]. Then Eqs. (2.29) can be solved numerically.

The obtained activation energy R as function of the modulation amplitude for four characteristic values of ω_F is shown in Fig. 2.7. The solid lines on this plot correspond to the results of the numerical solution of the variational problem. The dashed lines in the panels for $\omega_F = 0.1, 0.25$ (we remind that $t_{\rm r}^{(0)} = 1$) show the

adiabatic approximation,

$$R^{\rm ad} = \min\left[U\big(q_b(t)\big) - U\big(q_a(t)\big)\right] = \frac{4}{3}\left(\frac{1}{4} - A\right)^{3/2}.$$

The dash-dot lines on all panels show the locally nonadiabatic approximation near the bifurcation point, which gives

$$R^{\rm nonad} = \left(\frac{\pi}{8}\right)^{1/2}\left(\frac{2}{\dot{\mu}_1}\right)^{1/2}(A_c - A)^2.$$

In plotting this expression we used the values of A_c and $\dot{\mu}_1$ found numerically (they were very close to the analytical expressions given above).

Finally, the dashed lines in Fig. 2.7 in the panels for $\omega_F = 0.5, 1$ show scaling for the effectively fast-oscillating regime near the bifurcation point, with

$$R^{\rm fast} = \frac{4}{3}\beta'^{3/2}\frac{D}{\tilde{D}}\,(A_c - A)^{3/2}.$$

The coefficients β' and $\tilde{D}$ as given by Eqs. (C.7), (C.12) were obtained numerically.

It is seen from Fig. 2.7 that, for small ω_F, the adiabatic approximation applies over a broad region of driving amplitudes. Near the bifurcation point it gives scaling $R \propto (A_c - A)^\xi$ with $\xi = 3/2$ (cf. the panel for $\omega_F = 0.1$). However, close to the bifurcation point this scaling does not work. Instead there emerges the nonadiabatic dynamic scaling with $\xi = 2$. For $\omega_F = 0.1$ the range of the nonadiabatic scaling is comparatively narrow.

As the frequency increases, the amplitude range characterized by the $\xi = 2$-scaling dramatically increases. For $\omega_F = 0.25$ this is practically the only scaling seen near the bifurcation point.

With further increase of ω_F, close to the bifurcation point there emerges a region of the fast-oscillation scaling $R \propto (A_c - A)^\xi$ where again $\xi = 3/2$. The panel for $\omega_F = 0.5$ shows a crossover from the scaling $\xi = 3/2$ very close to the bifurcation

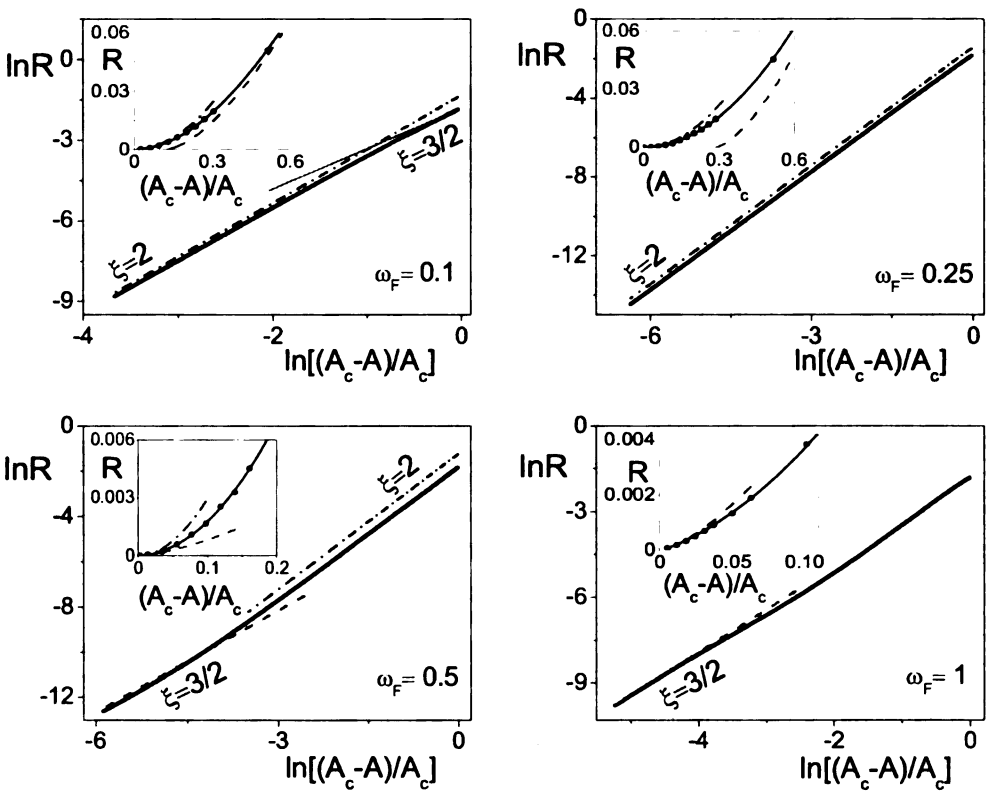

Figure 2.7: The activation energy of escape R vs. modulation amplitude A on the logarithmic and linear (inset) scales for a Brownian particle in a modulated potential (2.39). The values of ω_F are indicated on each panel. The thick solid lines show the results of the numerical solution of the variational problem for R. The dashed lines for $\omega_F = 0.1, 0.25$ show the adiabatic approximation, whereas for $\omega_F = 0.5, 1.0$ they show the approximation of effectively fast oscillations: in both cases the scaling exponent is $\xi = 3/2$ (for $\omega_F = 0.1$ this asymptotic scaling is shown by the thin solid line). The dash-dot lines show the $\xi = 2$ scaling (2.37). The dots show the results of numerical simulations of Eq. (2.39).

point to the scaling $\xi = 2$ further away from A_c. Note that the frequency $\omega_F = 0.5$ is neither small nor large, and therefore there is a noticeable difference in the coefficients at $(A_c - A)^2$ obtained from the full variational problem for R and from the locally nonadiabatic theory near the bifurcation point.

When $\omega_F t_r^{0)} \gtrsim 1$ we do not expect to see scaling for either adiabatic or locally nonadiabatic regime. The only scaling to be expected near the bifurcation point is the fast-oscillation one, with $\xi = 3/2$. This is indeed seen in the panel for $\omega_F = 1$ in Fig. 2.7. We note that the global fast-oscillation approximation (2.42) does not apply for $\omega_F t_r^{0)} = 1$.

2.5.2 Simulations

An additional test of the results can be obtained by directly simulating the Brownian dynamics described by Eq. (2.39). We conducted such simulations using the second order integration scheme of stochastic differential equations developed in Ref. [107]. As a result of the simulations we obtained the probability distribution of the dwell time in the metastable state $p_{\rm dw}(t)$. It gives the probability density (over time) for a system prepared at $t = 0$ close to the attractor to stay in the basin of attraction until time t and leave at that time.

In practice we calculated $p_{\rm dw}(t)$ by detecting the system at time t at a point q that lied well beyond, but not too far from, the oscillating boundary $q_b(t)$. It is simply related to the time-dependent escape probability $W(t)$, which gives the probability current from the attraction basin at time t if the system was in the stable state at $t = 0$ [92],

$$p_{\rm dw}(t) = W(t) \exp\left[-\int_0^t dt' \, W(t')\right]. \tag{2.43}$$

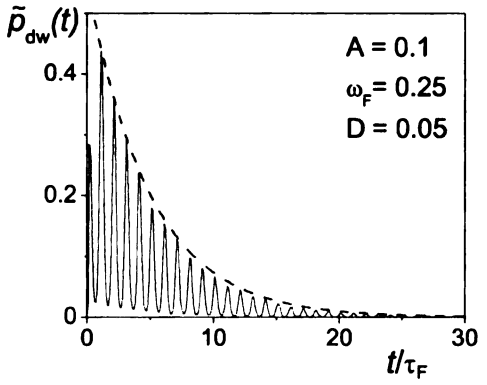

Figure 2.8: The scaled probability density of the dwell time $\tilde{p}_{\rm dw}(t) = p_{\rm dw}(t)\tau_F$ obtained by numerical simulations of a Brownian particle in a modulated potential, Eq. (2.39). The parameters are $A = 0.1, D = 0.05, \omega_F = 0.25$ (solid line). The dashed line shows the exponential fit of the envelope with decrement $\overline{W}\tau_F = 0.008$.

The average escape rate is given by the mean dwell time,

$$\overline{W} = \left[\int_0^\infty dt\, t\, p_{\rm dw}(t)\right]^{-1}. \tag{2.44}$$

We studied small noise intensities so that $\overline{W} \ll \omega_F$; then $\overline{W}$ was independent of the position of the "observation" point q.

In most simulations the system was prepared initially at the stable state $q_a(t)$; we found that $\overline{W}$ was independent of the initial state provided it was close to $q_a(t)$.

The dwell-time distribution for a particular set of parameter values in Eq. (2.39) is shown in Fig. 2.8. The data refer to modulation at a comparatively low frequency and with comparatively small amplitude. The function $p_{\rm dw}(t)$ is strongly modulated in time, with period τ_F. This means that escape events are strongly synchronized by the modulation, in agreement with the analytical results for $W(t)$ obtained for the same model in Ref. [92].

The average escape rate $\overline{W}$ was found from the data of the type shown in Fig. 2.8

by calculating the mean dwell time (2.44) and also from an exponential fit of the envelope of $p_{\rm dw}(t)$. These two approaches gave the same result. For each set of A, ω_F, D we observed $\sim 10^5$ escape events. Then D was changed. The activation energy of escape was found from $\ln \overline{W}$ for 2-4 values of D. We tested that it was independent of D in the range $R/D \gtrsim 6$.

The data of simulations are shown in Fig. 2.7 by dots. For all parameter values they are in excellent agreement with the results of the numerical solution of the variational problem (2.9).

2.6 Conclusions

In conclusion, we have identified three regions near a bifurcation point where the activation energy of escape displays scaling behavior as a function of the amplitude of periodic modulation. The main results refer to slow modulation, where $\omega_F t_{\rm r} \ll 1$. We show the emergence of nonadiabatic behavior in this region. The nonadiabaticity leads to a crossover from the scaling with exponent $\xi = 3/2$, previously found for stationary systems, to a new dynamical scaling with $\xi = 2$. The $\xi = 2$ region first emerges near the bifurcation point and then expands with increasing modulation frequency. With further increase of ω_F the crossover $\xi = 2$ to $\xi = 3/2$ can be observed. Again, the effectively fast-oscillating region with $\xi = 3/2$-scaling emerges first near the bifurcation point. Even though the widths of the regions of different scaling depend on the parameters of a system, the phenomenon of scaling crossovers should be universal.

The onset of the $\xi = 2$-scaling is a consequence of the slowing down of motion near a bifurcation point. The adiabatic relaxation time of the system $t_{\rm r}$ strongly depends

on the distance to the bifurcation point, $t_r \propto (A_c - A)^{-1/2}$. The nonadiabatic scaling emerges where t_r becomes $\sim [\tau_F t_r^{(0)}]^{1/2}$. For smaller $|A_c - A|$ the dependence of t_r on $A_c - A$ becomes weak, while t_r still largely exceeds the modulation period τ_F. This is associated with avoided crossing of the stable and unstable states, which occurs with decreasing $A_c - A$ as these states are pressed against each other when the system approaches the adiabatic bifurcation point, see Fig. 2.2.

Both in the adiabatic regime and the nonadiabatic regime for $\omega_F t_r \ll 1$ escape is most likely to occur while the equilibrium states are close to each other. The escape rate is therefore determined by the behavior of the system for a small portion of the modulation period, i.e., locally in time.

The regime of effectively fast oscillations near the bifurcation point emerges for $\omega_F t_r \gg 1$. It can arise even where the modulation period τ_F exceeds the relaxation time far from the bifurcation point. In this regime the motion is controlled by a slow variable, but the dynamics of this variable is no longer determined by local (in time) characteristics. The relevant characteristics are obtained by averaging the appropriate parameters along the critical periodic trajectory of the system into which the stable and unstable periodic cycles merge at the bifurcation point.

We have developed a general formulation of escape of periodically modulated systems driven by colored Gaussian noise. Near a bifurcation point slow motion of the system effectively filters out high-frequency components of the noise spectrum and makes the noise effectively white. From the theoretical point of view it is interesting that, in the locally-nonadiabatic regime of $\xi = 2$ scaling, the instanton-like optimal escape path can be found from *linear* equations of motion.

We expect that the new $\xi = 2$ scaling and the scaling crossovers can be seen in various systems. Examples are modulated Josephson junctions, nanomagnets, and

optically trapped Brownian particles, where escape in the presence of modulation has been already studied experimentally, albeit in different regimes.

Chapter 3

Noise-induced escape of periodically modulated systems: From weak to strong modulation

3.1 Introduction

The most frequently used types of nonequilibrium modulation are ramping of a control parameter and periodic modulation. Ramping is usually done slowly, and it is assumed that the system remains quasistationary [30]. Periodic modulation is conceptually simpler as periodic metastable states are well-defined irrespective of the modulation frequency. However, a theory of the escape rate is more complicated, because the system is away from thermal equilibrium [95]. Recently significant attention was attracted also to escape over a randomly fluctuating barrier [108, 109].

In the present Chapter (see also Refs. [110, 111]) we study periodically modulated systems and extend to them the analysis of the escape rate done by Kramers for

systems in thermal equilibrium [29]. Our approach gives the full time-dependent escape rate $W(t)$ as well as the period-average rate $\overline{W} = \nu \exp(-R/D)$, where R is the activation energy of escape and D is the noise intensity, $D = k_B T$ for thermal noise. We find $W(t)$ for an arbitrary modulation amplitude A and an arbitrary interrelation between the modulation frequency ω_F and the relaxation time of the system t_r. We show that the prefactor ν depends on A strongly and nonmonotonically. It displays scaling behavior near the bifurcational modulation amplitude A_c where the metastable state of the system disappears.

In the absence of modulation escape can happen at any time with the same probability density. For systems in thermal equilibrium, the activation energy equals the free energy barrier height. The prefactor ν is given by the generalized attempt frequency and does not depend on D for not too small damping [29].

Even a comparatively weak driving can exponentially strongly modulate the escape rate leading to strong escape synchronization for small D [94]. This is easy to see for a Brownian particle in a slowly modulated potential well, see Fig. 3.1(a): it is most likely to escape once per modulation period when the barrier is at its lowest. The "time window" for escape is diffusion-broadened. Therefore the period-average escape rate is $\overline{W} \propto D^{1/2}$ [92].

For an overdamped Brownian particle a transition, with increasing modulation amplitude A, from the D-independent prefactor in the absence of modulation [29] to $\nu \propto D^{1/2}$ was discussed in Ref. [92]. However, the results were limited to comparatively weak modulation, region I in Fig. 3.1(b). The range of intermediate modulation, region II, was discussed in Refs. [54, 93, 112]. However, the obtained prefactor in the period-average rate diverges for $A \to 0$. The approach of Ref. [93, 112] is inapplicable for slow modulation compared to the relaxation time of the system. In contrast, the

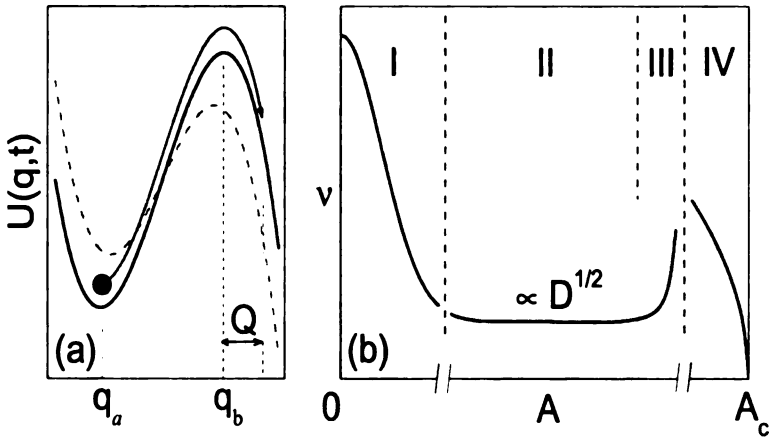

Figure 3.1: (a) An oscillating potential barrier. In the limit of slow modulation, the stable and unstable periodic states q_a and q_b are the instantaneous positions of the potential minimum and barrier top, respectively. The instantaneous escape rate is characterized by the current at an "observation point" located at a sufficiently large distance Q from q_b. (b) The dependence of the prefactor ν in the period-average escape rate $\overline{W} = \nu \exp(-R/D)$ on the modulation amplitude A (schematically). For $A \to 0$, ν is given by the Kramers theory. In regions II and III escape is synchronized and $\nu \propto D^{1/2}$, where D is the noise intensity. In region III, close to the critical point A_c where the metastable state disappears, the prefactor scales as $\nu \propto (A_c - A)^{-1}$. In region IV $\nu \propto (A_c - A)^{1/2}$ is independent of D.

technique developed in this Chapter is free from these limitations. The scaling regions III and IV and the strongly nonmonotonic behavior of the prefactor have not been previously identified.

To find the instantaneous escape rate $W(t)$ we relate it, in the spirit of Kramers' approach, to the current *well behind* the boundary $q_b(t)$ of the basin of attraction to the initially occupied metastable state (q is the system coordinate). We call the current away from the attraction basin the escape current. In stationary systems and for the time $t \ll W^{-1}$ the escape current is independent of the coordinate and is the same on the basin boundary and behind it. In periodically modulated systems this is no longer the case. A particle that crossed the boundary at one time may cross

it back at a later time, because the boundary itself is moving. In experiments the position of the instantaneous basin boundary is not necessarily known. The current is usually detected well behind the boundary, for example, close to another metastable state. The functional form of this current is qualitatively different from that at $q_b(t)$ calculated in Refs. [54, 93, 112].

The escape current can be obtained by relating the probability distributions of the system $\rho(q,t)$ behind the boundary $q_b(t)$ and close to the attractor $q_a(t)$ from which the system escapes. We do this in two steps. First, we find the general form of the current-carrying distribution $\rho(q,t)$ in the boundary layer about $q_b(t)$, where the equation of motion of the system can be linearized. Then we match it to the distribution inside the attraction basin but well outside the diffusion layer around $q_b(t)$. This distribution can be obtained in the eikonal approximation for small D. It has singular features [47, 77, 113]. The matching is performed using these singular features.

In Sec. 3.2 we describe the model and give the general form of the boundary-layer distribution. In Sec. 3.3 this distribution is used to obtain general expressions for the instantaneous and period-average escape rate. Matching of the intrawell and boundary-layer distributions is discussed in Sec. 3.4. In Sec. 3.5 we study the pulse shape of synchronized escape current in different regimes. Section 3.6 provides a brief discussion of the period-average escape rate in the regions I and II in Fig. 3.1(b). In Sec. 3.7 we identify three different types of the scaling behavior of the prefactor ν close to the bifurcation point and find the critical exponents. In Sec. 3.8 the general results are compared with Monte Carlo simulations for a specific system. In Sec. 3.9 we summarize the results and sketch a surprisingly rich map of different types of escape behavior in the plane of modulation parameters.

3.2 The model and the boundary layer distribution

Escape from a metastable state of a periodically modulated system is well characterized if the noise is weak, so that the escape rate $W \ll t_{\mathrm{r}}^{-1}, \omega_F$. In this case, over the relaxation time t_{r} the periodically modulated system will most likely approach its periodic metastable state (attractor) with the coordinate $q_a(t) = q_a(t+\tau_F)$ ($\tau_F = 2\pi/\omega_F$ is the modulation period). Then most likely, it will be performing small fluctuations about q_a and will "forget" the initial state $q(0)$. Eventually there will occur a large fluctuation in which the system will go over the boundary $q_b(t)$ and leave the basin of attraction, i.e. escape.

The instantaneous escape rate $W(t)$ is characterized by the current $\langle \dot{q}(t) \rangle$ away from the metastable state. The current has to be measured well behind the boundary $q_b(t)$, so that the system practically does not return to the metastable state.

The probability distribution $\rho(q,t)$ of a periodically modulated overdamped Brownian particle is given by the Fokker-Planck equation (FPE)

$$\partial_t \rho = -\partial_q \left[K(q,t)\rho \right] + D\partial_q^2 \rho. \tag{3.1}$$

Here, $K(q,t)$ is the periodic force driving the particle, $K(q,t) = K(q,t+\tau_F) \equiv -\partial_q U(q,t)$, where $\tau_F = 2\pi/\omega_F$ is the modulation period and $U(q,t)$ is the instantaneous potential.

The equation of motion of the particle in the absence of noise is $\dot{q} = K(q,t)$. The metastable state $q_a(t)$, from the vicinity of which the system escapes due to noise, and the basin boundary $q_b(t)$ are the stable and unstable periodic solutions of this equation, respectively.

We will assume that the noise intensity D is small. Then in a broad time range

$t_r \ll t \ll 1/\overline{W}$ the distribution $\rho(q,t)$ is nearly periodic in the basin of attraction to $q_a(t)$. The current away from this basin, and thus the escape rate $W(t)$, are also periodic.

3.2.1 Motion near periodic states

The distribution ρ is maximal at the metastable state $q_a(t)$ and falls off exponentially away from it. In the presence of periodic driving it acquires singular features as $D \to 0$ [47, 77, 113], some of which have counterparts in wave fields [114], with D playing the role of the wavelength. The singularities accumulate near $q_b(t)$. In order to find $W(t)$ one has to understand how they are smeared by diffusion.

In the absence of noise the motion of the system close to the periodic states $q_i(t)$ $(i = a, b)$ is described by the equation $\dot{q} = K$ with K linearized in $\delta q = q - q_i(t)$:

$$\delta\dot{q} = \mu_i(t)\delta q, \quad \mu_i(t) = \mu_i(t + \tau_F) \equiv [\partial_q K]_{q_i(t)}. \tag{3.2}$$

The evolution of $\delta q(t)$ is given by $\delta q(t) = \kappa_i(t, t')\delta q(t')$, where

$$\kappa_i(t, t') = \exp\left[\int_{t'}^{t} d\tau\, \mu_i(\tau)\right] \quad (i = a, b). \tag{3.3}$$

Over the period τ_F the distance δq decreases (for $i = a$) or increases (for $i = b$) by the Floquet multiplier

$$M_i = \kappa_i(t + \tau_F, t) = \exp\left(\bar{\mu}_i \tau_F\right), \qquad i = a, b, \tag{3.4}$$

where $\bar{\mu}_i$ is the period-average value of $\mu_i(t)$, with $\bar{\mu}_a < 0, \bar{\mu}_b > 0$.

For weak noise the linearized force K can be used to find $\rho(q,t)$ near $q_{a,b}(t)$. Near the metastable state q_a, the distribution ρ is Gaussian [115],

$$\rho(q,t) = \frac{1}{\sqrt{2\pi D\sigma_a^2(t)}} \exp\left\{-\frac{[q - q_a(t)]^2}{2D\sigma_a^2(t)}\right\}. \tag{3.5}$$

The time-periodic variance is

$$\sigma_i^2(t) = 2\left|M_i^{-2} - 1\right|^{-1} \int_0^{\tau_F} dt_1 \kappa_i^{-2}(t + t_1, t) \tag{3.6}$$

with $i = a$; in the absence of modulation $\sigma_a^2 = 1/|\mu_a|$.

3.2.2 Distribution near the unstable state

The periodic distribution near the unstable state $q_b(t)$, i.e., the boundary-layer distribution, is substantially non-Gaussian. It corresponds to a periodic current away from the attraction basin. The distribution can be found from Eq. (3.1) using the Laplace transform, similar to the weak-driving limit [92]:

$$\rho(q,t) = \int_0^\infty dp\, e^{-pQ/D}\, \tilde{\rho}(p,t),\ Q = q - q_b(t). \tag{3.7}$$

We assume that Q is small, $|Q| \ll \min_t |q_b(t) - q_a(t)|$. Using the expansion $K = \dot{q}_b(t) + \mu_b(t)Q$, we obtain from the FPE (3.1) a first-order equation for the Laplace transform $\tilde{\rho}(p,t)$

$$\partial_t \tilde{\rho} = \mu_b(t) p \partial_p \tilde{\rho} + (p^2/D)\tilde{\rho}. \tag{3.8}$$

This equation can be solved by the method of characteristics, giving

$$\tilde{\rho}(p,t) = \mathcal{E} D^{-1/2} \exp\left\{-\left[s(\phi) + p^2\sigma_b^2(t)/2\right]/D\right\}. \tag{3.9}$$

In Eq. (3.9), $\mathcal{E}$ is a constant and $s(\phi)$ is an arbitrary zero-mean periodic function, $s(\phi + 2\pi) = s(\phi)$. They have to be found by matching $\rho(q,t)$ (3.7) to the distribution inside the attraction basin. The function $\sigma_b^2(t)$ in Eq. (3.9) is given by Eq. (3.6) with $i = b$, and the factor $D^{-1/2}$ is singled out for convenience.

The phase of the function s is $\phi \equiv \phi(p,t)$,

$$\phi(p,t) = \Omega_F \ln[p\, \kappa_b(t,t')/\bar{\mu}_b l_D]. \tag{3.10}$$

Here,

$$\Omega_F = \omega_F/\bar{\mu}_b \equiv 2\pi/\ln M_b$$

is the reduced field frequency, $l_D = (2D/\bar{\mu}_b)^{1/2}$ is the typical diffusion length, and t' determines the initial value of ϕ. From Eq. (3.10), $\phi(p, t + \tau_F) = \phi(p, t) + 2\pi$.

3.3 Instantaneous and period-average escape rate

3.3.1 General expression for the escape rate

The experimentally accessible instantaneous rate of escape from the metastable state is characterized by the current $j(q,t)$ from its attraction basin. We assume that this basin lies for $q < q_b(t)$, i.e., $q_a(t) < q_b(t)$. Then the escape current is the rate of change of the population in the region $(-\infty, q]$, with q lying behind the basin boundary $q_b(t)$. As explained in the Introduction, of interest is $j(q,t)$ for such q that $Q = q - q_b(t) \gg l_D$. Eq. (3.7) is advantageous as it immediately gives such a current.

We consider first $j(q,t)$ not for a fixed q, but for a fixed distance $Q = q - q_b(t)$ from the boundary,

$$\begin{aligned} j(q,t) &= -\frac{\partial}{\partial t}\int_{-\infty}^{q_b(t)+Q} dq\rho(q,t) \\ &\approx \mu_b(t)\rho(q_b(t)+Q,t)Q. \end{aligned} \tag{3.11}$$

Here we have used the FPE (3.1) and linearized $K(q_b(t) + Q, t)$ in Q; we have also disregarded the diffusion current, which is a good approximation for $Q \gg l_D$.

The distribution $\rho(q_b(t) + Q, t)$ in the expression for the current (3.11) is given by Eqs. (3.7), (3.9). For $Q \gg l_D$ the term $\propto p^2/D$ in Eq. (3.9) can be neglected

compared to pQ/D. Changing in Eq. (3.7) to integration over $x = pQ/D$ we obtain

$$\begin{aligned} j(q,t) &= \mu_b(t)\mathcal{E}D^{1/2}\int_0^\infty dx\, e^{-x}\,\exp[-s(\phi_d)/D], \\ \phi_d &= \phi(xD/Q,t) = \Omega_F \ln[x\,\kappa_b(t_d,t')]. \end{aligned} \tag{3.12}$$

Here $t_d \equiv t_d(Q,t)$ is given by the equation $\kappa_b(t_d,t) = l_D/2Q$.

It follows from Eq, (3.12) that in the whole harmonic region j depends on the observation point Q only in terms of the delay time t_d. This time shows how long it takes the system to roll down to the point Q, $\partial_Q t_d = -1/[\mu_b(t_d)Q]$. We note that $\mu_b(t)$ can be negative for a part of the period, leading to reversals of the instantaneous current.

The escape rate $\overline{W}$ is given by the period-average $j(q,t)$. The averaging can be done for a given q or a given Q behind the boundary. The result will be the same, since the period-average value of $\partial_q j$ is equal to zero, and therefore the period-average current is independent of coordinate. It is convenient to do time averaging in Eq. (3.12) by changing from integration over time to integration over ϕ_d with account taken of the relation $d\phi_d/dt = \Omega_F\mu_b(t)$. The result is independent of Q, as expected, and reads

$$\overline{W} = \frac{\bar{\mu}_b}{2\pi}\mathcal{E}D^{1/2}\int_0^{2\pi} d\phi\,\exp[-s(\phi)/D]. \tag{3.13}$$

Eqs. (3.12) and (3.13) provide a complete solution of the Kramers problem of escape of a modulated system and reduce it to finding the function s. It is seen from Eqs. (3.9), (3.13) that this function has the meaning of the zero-mean periodic part of the activation energy of escape. Eqs. (3.12) and (3.13) are similar in form to the expressions for the instantaneous and average escape rates for comparatively weak modulation obtained in Ref. [92]. For such modulation $|s| \ll R$, which allowed finding s explicitly (see Appendix D).

3.3.2 Synchronization of escape

Periodic modulation may lead to an exponentially strong time dependence of the escape probability within a period, that is, to *synchronization* of escape events. This effect is determined by the parameter $|s_{\rm m}|/D$. Here $s_{\rm m} \equiv \min_\phi s(\phi)$ is the minimal value of s reached for a certain phase $\phi = \phi_{\rm m}$. By construction, $s_{\rm m} < 0$. We will be interested in *strong* synchronization, when the escape current displays sharp narrow periodic peaks as function of time.

Strong synchronization of escape requires that $|s_{\rm m}| \gg D$ (a more precise criterion will be discussed below). In this case the factor $\exp[-s(\phi_d)/D]$ in Eq. (3.12) for $j(q,t)$ is a sharp function of ϕ_d. The major contribution to the integral over x comes from the range where s is close to $s_{\rm m}$ and, respectively, the phase ϕ_d is close to $\phi_{\rm m}$. The time dependence of $j(q,t)$ can be found by changing in Eq. (3.12) from integration over x to integration over ϕ_d. Because $|s_{\rm m}| \gg D$, the integrand $(dx/d\phi_d)\exp[-x-(s/D)]$ is maximal for $\phi_d = \phi_{\rm m} - 2\pi k$ with $k = 0, \pm 1, \ldots$. For such ϕ_d and for a given k the integrand is equal to

$$g_k(t) = \Omega_F^{-1} x_k \exp\left[-x_k - (s_{\rm m}/D)\right],$$

where

$$x_k(t) = \kappa_b^{-1}(t_d, t') \exp[(\phi_{\rm m} + 2\pi k)/\Omega_F]. \tag{3.14}$$

The whole integral (3.12) is determined by the sum of g_k.

As a function of time, g_k is maximal for $x_k = 1$. Within any period of time from t to $t + \tau_F$ the condition $x_k = 1$ is met only for one k, and only for one instant of time t_k. For all other k the function $x_k \exp(-x_k)$ is much smaller provided $\Omega_F \lesssim 1$. We note that, if $x_k = 1$ for a given t_k, then it follows from Eqs. (3.3), (3.14) that $x_{k+1} = 1$ for $t_{k+1} = t_k + \tau_F$. This means that, as a function of time, the escape

rate displays sharp periodic peaks with period τ_F. The shape of the peaks will be discussed below.

When $|s_{\rm m}| \ll D$, there is no exponential synchronization, and the escape current smoothly depends on time. It happens in particular when modulation is weak or the modulation frequency is large, $\Omega_F \gg 1$.

3.4 Matching the intrawell and boundary-layer distributions

3.4.1 Intrawell distribution near the basin boundary

To find $j(q,t)$ we match the boundary-layer distribution (3.7) to the tail of the intrawell distribution. The matching has to be done close to the basin boundary $q_b(t)$, where Eq. (3.7) applies, but it is convenient to do it well inside the attraction basin, $-[q-q_b(t)] \gg l_D$, that is, outside the diffusion layer around $q_b(t)$. Of primary interest is the case of strong modulation, $|s_{\rm m}| \gg D$, since the case of weak to moderately strong modulation was considered earlier [92].

The intrawell distribution in the region $-Q \gg l_D$ $[Q = q-q_b(t)]$ can be found, for example, by solving the FPE (3.1) in the eikonal approximation, with the diffusion coefficient D being a small parameter,

$$\rho(q,t) = e^{-S(q,t)/D}, \quad S = S_0 + DS_1 + \ldots \tag{3.15}$$

(here, in contrast to Ref. [110] we single out the factor D in S_1 explicitly).

To zeroth order in D, the equation for $S_0 \equiv S_0(q,t)$ can be written as

$$\partial_t S_0 = -H\left(\partial_q S_0, q; t\right). \tag{3.16}$$

Eq. (3.16) has the form of a Hamilton-Jacobi equation for the action S_0 of an auxiliary conservative system with Hamiltonian [55]

$$H(p,q;t) = p^2 + pK(q,t),\ p = \partial_q S_0. \tag{3.17}$$

The auxiliary system is non-autonomous, its Hamiltonian is a periodic function of time. Since we are interested in the periodic distribution $\rho(q,t)$, we need to find a periodic solution of Eq. (3.16). This can be done using the method of characteristics, i.e., by studying Hamiltonian trajectories $(q(t),p(t))$ of the auxiliary system,

$$\dot{q} = K + 2p, \quad \dot{p} = -p\partial_q K. \tag{3.18}$$

Eqs. (3.18) have two hyperbolic periodic states, $(q_a(t),0)$ and $(q_b(t),0)$, where $q_a(t)$ and $q_b(t)$ are the metastable state and the basin boundary of the original dissipative system. We are interested in Hamiltonian trajectories $(q(t),p(t))$ that belong to the *unstable* manifold of the periodic state $(q_a(t),0)$. For such trajectories, action $S_0(q,t)$ is minimal for $q = q_a(t)$, and $\rho(q,t)$ is maximal, respectively. Indeed, a straightforward calculation based on Eq. (3.18) shows that, for q close to $q_a(t)$, the momentum on the unstable manifold is $p = [q-q_a(t)]/\sigma_a^2(t)$, where σ_a^2 is given by Eq. (3.6). Respectively, $S_0 = [q-q_a(t)]^2/2\sigma_a^2(t)$, in agreement with Eqs. (3.5), (3.15) for $\rho(q,t)$.

To logarithmic accuracy, the escape rate is determined by the probability to reach the basin boundary $q_b(t)$, i.e., by the action $S_0\big(q_b(t),t\big)$ [94]. The Hamiltonian trajectories of the auxiliary system that form this action belong to the *stable* manifold of the periodic state $(q_b(t),0)$. The trajectory $(q_{\rm opt}(t),p_{\rm opt}(t))$, which minimizes $S_0\big(q_b(t),t\big)$, approaches $q_b(t)$ asymptotically as $t \to \infty$. This is a heteroclinic trajectory of the auxiliary system, an intersection of the unstable and stable manifolds of the states $(q_a(t),0)$ and $(q_b(t),0)$, respectively [47, 77, 113].

In the case of dissipative systems with detailed balance, including systems in thermal equilibrium, the corresponding manifolds coincide with each other. However, in nonequilibrium systems this is no longer true. In periodically modulated systems there is only one heteroclinic trajectory with minimal S_0 per period. The coordinate $q_{\rm opt}(t)$ on this trajectory is the most probable escape path (MPEP). This is the trajectory that the original system is most likely to follow in escape. It is physically observable and has been seen both in experiments and simulations [94].

Close to $q_b(t)$, the Hamiltonian equations (3.18) for $q(t), p(t)$ can be linearized and solved. On the MPEP

$$p_{\rm opt}(t) = -Q_{\rm opt}(t)/\sigma_b^2(t) = \kappa_b^{-1}(t,t')p_{\rm opt}(t'), \tag{3.19}$$
$$S_0\big(q_{\rm opt}(t),t\big) = R - Q_{\rm opt}^2(t)/2\sigma_b^2(t),$$

where $Q_{\rm opt}(t) = q_{\rm opt}(t) - q_b(t)$. The quantity $R = S_0\big(q_{\rm opt}(t),t\big)_{t\to\infty}$ is the activation energy of escape.

Eqs. (3.19) apply to an arbitrary trajectory on the stable manifold of the state $(q_b(t),0)$ close to this state. The MPEP is just one such trajectory. It is determined by the condition that it starts at $(q_a(t),0)$ for $t \to -\infty$. This condition synchronizes the trajectory and determines $p_{\rm opt}(t)$ for a given t. It is important that the optimal paths are periodically repeated in time with period τ_F. The values of $p_{\rm opt}(t)$ form an infinite series. For neighboring paths they differ by the factor M_b^{-1}. They can be also thought of as the values of $p_{\rm opt}(t + k\tau_F)$ for the same MPEP and different k, with $p_{\rm opt}(t + k\tau_F) \to 0$ for $k \to \infty$.

From Eqs. (3.19), everywhere on the stable manifold of $(q_b(t),0)$ the action has the form

$$S_b(q,t) = R - Q^2/2\sigma_b^2(t). \tag{3.20}$$

It is parabolic as function of Q.

Due to nonintegrability of the dynamics with Hamiltonian (3.17), the action surface $S_0(q,t)$, which gives the intrawell probability distribution (3.15), becomes flat for small $Q - Q_{\rm opt}$ [47, 77, 113]. It touches the surface $S_b(q,t)$ on the MPEP. Away from the MPEP $S_0(q,t) > S_b(q,t)$. Therefore the function

$$\rho_b(q,t) = \rho(q,t)\exp[S_b(q,t)/D] \tag{3.21}$$

is maximal on the MPEP.

The prefactor of the eikonal-approximation distribution is given by the term $\exp(-S_1)$, cf. Eq. (3.15). On the MPEP the auxiliary function $z = \exp(2S_1)$ obeys the equation [116]

$$\frac{d^2 z}{dt^2} - 2\frac{d(z\,\partial_q K)}{dt} + 2zp\partial_q^2 K = 0, \tag{3.22}$$

where $q = q_{\rm opt}(t)$, $p = p_{\rm opt}(t)$. The initial condition to this equation follows from the explicit form (3.5) of $\rho(q,t)$ near the stable state,

$$z(t) \to 2\pi D\sigma_a^2(t), \quad t \to -\infty. \tag{3.23}$$

Close to $q_b(t)$, from Eq. (3.22)

$$z(t) = D[\mathcal{Z}_1\sigma_b^2(t) + \mathcal{Z}_2 p_{\rm opt}^{-2}(t)], \tag{3.24}$$

where $\mathcal{Z}_{1,2}$ are constants [93, 112]. This solution was found in Ref. [93, 112], but the term $\propto \mathcal{Z}_1$ was disregarded.

3.4.2 Matching the exponents and prefactors

We are now in a position to match the functions $\rho_b(q,t)$ (3.21) as given by the eikonal approximation (3.15), (3.19) and (3.24), and the boundary-layer solution (3.7). In

the spirit of the eikonal approximation, matching should be done in the vicinity of the MPEP, where ρ_b is maximal.

The eikonal approximation applies when the optimal escape paths $q_{\rm opt}(t + k\tau_F)$ ($k = 0, \pm 1 \ldots$) are separated by a large distance compared to the diffusion length l_D. For small noise intensity D the corresponding range incorporates much of the harmonic region near $q_b(t)$, because the width of the latter region Δq is independent of D and $\Delta q \gg l_D$ for small D. Physically, l_D characterizes the width of the tube of paths along which the system moves in escape [94]. In the region $-Q \lesssim l_D$ the tubes of escape paths overlap and the eikonal approximation no longer applies.

In contrast, the boundary layer distribution Eq. (3.7) covers the whole harmonic region $|Q| \ll \Delta q$, including the diffusion-dominated region $|Q| \lesssim l_D$. Thus, for small noise intensity D, the two distributions should overlap in a broad range $l_D \ll -Q \ll \Delta q$ inside the harmonic region but outside the diffusion-dominated layer.

We first consider the boundary-layer expression (3.7) for $\rho_b(q,t)$ in the region $-Q \gg l_D$ and for strong modulation, $|s_{\rm m}| \gg D$. As we show, $\rho_b(q,t)$ is maximal for all times t provided q lies on an appropriate trajectory that belongs to the stable manifold of $q_b(t)$.

Eq. (3.7) is simplified for $-Q \gg l_D$, because the integral over p can be evaluated by the steepest descent method. The extremum of the integrand is given by the condition

$$p\sigma_b^2(t) + Q + \Omega_F p^{-1} \frac{ds}{d\phi} = 0.$$

The integrand is maximal if $p = -Q/\sigma_b^2(t)$ and s is minimal for this p, i.e., $\phi(p,t) = \phi_{\rm m}$ and $s = s_{\rm m}$. The relation $p = -Q/\sigma_b^2(t)$ holds for any trajectory on the stable manifold of $q_b(t)$, cf. Eq. (3.19). Moreover, since on these trajectories $p = p(t) = \kappa_b^{-1}(t,t')p(t')$, it follows from Eq. (3.10) that $\phi(p,t) = \text{const}$. Therefore if the phase

$\phi = \phi_{\rm m}$ for one instant of time, it will be equal to $\phi_{\rm m}$ for all times.

The function ρ_b (3.21) calculated in the eikonal approximation is maximal on the MPEP. Therefore ρ_b in the boundary-layer approximation should be maximal on the MPEP as well. It follows from the above arguments that it will indeed be maximal on the MPEP provided

$$\phi\big(p_{\rm opt}(t), t\big) = \phi_{\rm m}. \tag{3.25}$$

This amounts to choosing the appropriate initial phase (the value of t') in Eq. (3.10). With this choice, steepest descent integration in Eq. (3.7) gives the boundary-layer distribution near the MPEP in the form

$$\begin{aligned} \rho(q,t) &= \mathcal{E}_b(t) \exp[-S_b(q,t)/D], \\ \mathcal{E}_b(t) &= \tilde{\mathcal{E}} D^{-1/2} \left[\sigma_b^2(t) + \Omega_F^2 \, s''_{\rm m} \, p_{\rm opt}^{-2}(t)\right]^{-1/2}, \end{aligned} \tag{3.26}$$

where

$$\begin{aligned} \tilde{\mathcal{E}} &= \mathcal{E}(2\pi D)^{1/2} \exp[(R - s_{\rm m})/D], \\ s''_{\rm m} &= [d^2 s/d\phi^2]_{\phi_{\rm m}}. \end{aligned} \tag{3.27}$$

It is seen from Eqs. (3.19), (3.26) that, with the right choice of phase, the exponents of the boundary-layer and eikonal-approximation distributions coincide with each other along the MPEP. Moreover, the slopes $\partial_q S_b(q,t)$, which are determined by $p_{\rm opt}(t)$, also coincide.

For the matching of the distributions to be complete, the function $\mathcal{E}_b(t)$ of the boundary-layer distribution (3.26) should match on the MPEP the prefactor of the eikonal-approximation distribution $z^{-1/2}$ (3.24). Remarkably, they indeed have the same form, as functions of time, near $q_b(t)$. Therefore the parameters $\mathcal{Z}_1$ and $\mathcal{Z}_2$ allow one to determine $\mathcal{E}$ and $s''_{\rm m}$, and vice versa, $\mathcal{E}$ and $s''_{\rm m}$ give $\mathcal{Z}_1$ and $\mathcal{Z}_2$. With

the appropriately defined parameters, not only the exponents but also the prefactors of the boundary-layer and eikonal distributions fully match each other.

The function $p_{\rm opt}(t)$ exponentially decays with time, and therefore the term $\propto p_{\rm opt}^{-2}(t)$ in $\mathcal{E}_b$ and $z^{-1/2}$ exponentially increases as $t \to \infty$. This leads to qualitatively different forms of the prefactor for different frequencies and strengths of the modulation. For $\Omega_F^2 s_{\rm m}'' \ll l_D^2/\sigma_b^2(t)$, which corresponds to slow and not too strong modulation (see below), the term $\propto p_{\rm opt}^{-2}$ in $\mathcal{E}_b$ is small in the whole harmonic region. Then the constant $\mathcal{Z}_2$ in $z(t)$ should be small as well. In this case the prefactor is determined by the constant $\mathcal{Z}_1$. This gives

$$\tilde{\mathcal{E}} = \mathcal{Z}_1^{-1/2}. \tag{3.28}$$

In the opposite case of very strong and/or higher-frequency modulation, where $\Omega_F^2 s_{\rm m}'' \sim \Delta q^2/\sigma_b^2(t)$, the term $\propto p_{\rm opt}^{-2}$ is much larger than $\sigma_b^2(t)$ in the whole harmonic region, and the constant $\mathcal{Z}_1$ in $z(t)$ can be disregarded. In this case

$$\tilde{\mathcal{E}}/\Omega_F\sqrt{s_{\rm m}''} = \mathcal{Z}_2^{-1/2}. \tag{3.29}$$

Equation (3.26) describes also the intermediate case where the term $\propto p_{\rm opt}^{-2}$ in $\mathcal{E}_b(t)$ and $z(t)$ is small in a part of the harmonic region sufficiently far from $q_b(t)$, but becomes large closer to q_b while still outside the layer $\sim l_D$. This regime corresponds to strong synchronization for comparatively weak driving. Here, both parameters $\mathcal{Z}_1$ and $\mathcal{Z}_2$ are important and can be used for matching, giving the same result. The corresponding analysis is provided in Appendix D.

As we will show, to calculate the escape rate in the regime of strong synchronization there is no need in finding the whole function $s(\phi)$ in the boundary-layer distribution, it is sufficient to know only $s_{\rm m}''$. Eqs. (3.19), (3.26) then provide the complete solution of the problem of escape.

3.5 Time dependence of the escape rate

3.5.1 Adiabatic limit

Explicit expressions for the escape rate in the regime of strong synchronization can be obtained for comparatively weak or comparatively slow (adiabatic) modulation, where $s''_{\rm m} \sim |s_{\rm m}| \gg D$ but

$$\Omega_F^2 s''_{\rm m} \ll R. \tag{3.30}$$

The results for comparatively weak modulation, $|s_{\rm m}| \ll R$, should go over into the results [92], which were limited to this range, but included the strong-synchronization region $|s_{\rm m}| \gg D$. This is demonstrated in Appendix D. We show that $s''_{\rm m}$ found from Eqs. (3.22), (3.26) by perturbation theory in the modulation amplitude A coincides with the result of Ref. [92].

Condition (3.30) can be met for large A, where $s''_{\rm m} \sim R$, provided the modulation frequency is small compared to the reciprocal relaxation time, $\omega_F t_{\rm r} \sim \Omega_F \ll 1$. In this adiabatic regime the stable and unstable states $q_{a,b}^{\rm ad}(t)$ are the periodic solutions of the equation

$$K\big(q_{a,b}^{\rm ad}(t), t\big) = 0.$$

In the adiabatic approximation, escape happens very fast compared to the modulation period. This means that the escape trajectory can be calculated as if the force $K(q,t)$ did not depend on t explicitly. One can think then of a particle in the instantaneous potential well $U(q,t)$, cf. Fig. 3.1(a). The intrawell distribution has the form

$$\rho(q,t) = [2\pi D\sigma_a^2(t)]^{-1/2} \exp\left\{-\left[U(q,t) - U\big(q_a^{\rm ad}(t),t\big)\right]/D\right\}, \tag{3.31}$$

where $\sigma_a^{-2}(t) = \partial_q^2 U(q,t)$, with the derivative evaluated for $q = q_a^{\rm ad}(t)$

The adiabatic MPEP is given by the equation $\dot{q}_{\rm opt} = -K\big(q_{\rm opt}(t), t_{\rm m}\big)$. The time $t_{\rm m}$ (i.e., the phase of the modulation $\phi_{\rm m} = \omega_F t_{\rm m}$) is found from the condition that the adiabatic barrier height of the potential $U(q,t)$,

$$\Delta U(t) = U\big(q_b^{\rm ad}(t), t\big) - U\big(q_a^{\rm ad}(t), t\big), \tag{3.32}$$

be minimal, $d\Delta U/dt = 0$ for $t = t_{\rm m}$. The minimal barrier height gives the activation energy of escape,

$$R = \Delta U_{\rm m} \equiv \Delta U(t_{\rm m})$$

The value of $s_{\rm m}''$ can be obtained by matching the intrawell distribution (3.31) and the boundary-layer distribution (3.9). The matching is done most easily for sufficiently large $Q = q - q_b^{\rm ad}(t)$, so that $|Q| \gg l_D$ and $\mu_b(t_{\rm m})Q^2 \gg \Omega_F^2 s_{\rm m}''$, and for $\delta t = t - t_{\rm m}$ small compared to the modulation period τ_F but large compared to the typical relaxation time $\mu_b^{-1}(t_{\rm m})$. In this range, in Eq. (3.31)

$$U(q,t) - U\big(q_a^{\rm ad}(t), t\big) \approx \Delta U_{\rm m} + \frac{1}{2}\Delta\ddot{U}_{\rm m}\delta t^2 + \frac{1}{2}\mu_b Q^2,$$

where $\Delta\ddot{U}_{\rm m} = d^2\Delta U/dt^2$, with the derivative calculated for $t = t_{\rm m}$; here and below in this subsection for brevity we use μ_b for $\mu_b(t_{\rm m})$.

To find the boundary-layer distribution we note that, for the corresponding $\delta t, Q$, the integral over p in Eq. (3.7) can still be evaluated by the steepest descent method. However, in contrast to the analysis of Sec. 3.4.2, the phase ϕ that provides the extremum to the integral is not equal to the optimal phase $\phi_{\rm m}$, which corresponds to the adiabatic MPEP $q_{\rm opt}(t)$. Indeed, the MPEP goes through a given $q = Q + q_b^{\rm ad}(t_{\rm m})$ at the time $t_{\rm opt}(Q)$ that differs from $t_{\rm m}$ by the relaxation time $\sim \mu_b^{-1}$. We have chosen δt so that $|t_{\rm opt}(Q) - t_{\rm m}| \ll |\delta t|$.

A straightforward but somewhat tedious analysis shows that the major term in

the phase difference is $\phi - \phi_{\rm m} \approx \Omega_F \mu_b \, \delta t$. Then Eq. (3.7) gives

$$\rho(q,t) \approx (2\pi\mu_b)^{1/2} \mathcal{E} \exp\left\{ -\frac{1}{D}\left[s_{\rm m} + \frac{1}{2}\left(\mu_b Q^2 + \Omega_F^2 \mu_b^2 s''_{\rm m} \delta t^2 \right) \right] \right\}$$

By comparing this expression with Eq. (3.31) near $q_b, t_{\rm m}$ we obtain

$$\begin{aligned} \mathcal{E} &= \left[4\pi^2 D \mu_b / |\mu_a| \right]^{-1/2} e^{-(\Delta U_{\rm m} - s_{\rm m})/D}, \\ s''_{\rm in} &= \Delta \ddot{U}_{\rm m} / \Omega_F^2 \mu_b^2 \end{aligned} \tag{3.33}$$

[here $\mu_i \equiv \mu_i(t_{\rm in})$, for $i = a, b$].

We note that the modulation frequency ω_F drops out from the expression for $s''_{\rm in}$, because $\Omega_F \propto \omega_F$ while $\Delta \ddot{U} \propto \omega_F^2$. In Appendix E we show that the same expressions for the distribution parameters can be obtained by solving equation (3.22) for the prefactor.

Escape current

The expressions for the coefficients (3.33) allow evaluating the escape current $j(q,t)$ (3.12) in an explicit form. For $s''_{\rm m} \gg D$ the current has sharp peaks as function of time, i.e., escape is strongly synchronized. The peak shape can be found by extending the analysis of Sec. 3.3.2 used to demonstrate the very onset of synchronization.

For ϕ_d close to $\phi_{\rm in} - 2\pi k$ with integer k, the expression (3.12) for ϕ_d can be written as

$$\begin{aligned} &\phi_d \approx \phi_{\rm in} + \Omega_F \ln(x/x_k), \\ &x_k = x_0 \exp(2\pi k/\Omega_F), \quad x_0 = p_{\rm opt}(t) Q/D, \end{aligned} \tag{3.34}$$

where we used Eq. (3.25) for $p_{\rm opt}(t)$ [$x_k \equiv x_k(Q,t)$]. Expanding in Eq. (3.12) $s(\phi_d)$

near the minimum and using Eq. (3.33) we obtain

$$j(q,t) = W_{\rm m} \sum\nolimits_k J_k(Q,t), \quad W_{\rm m} = \frac{|\mu_a \mu_b|^{1/2}}{2\pi} e^{-R/D},$$
$$J_k = \int_0^\infty dx e^{-x} \exp\left\{-(\theta/2)\left[\ln\left(x/x_k\right)\right]^2\right\}, \tag{3.35}$$

where

$$\theta = \Omega_F^2 s_{\rm m}''/D \sim \Omega_F^2 |s_{\rm m}|/D. \tag{3.36}$$

The factor $W_{\rm m}$ in Eq. (3.35) is the Kramers escape rate in the stationary potential $U(q, t_{\rm m})$. Because of the modulation, escape current (3.35) is a periodic sequence of sharp peaks. To show this we note first that, for any given time, the functions $x_k(Q,t)$ with different k are exponentially different, because $\Omega_F \ll 1$. Therefore J_k are also exponentially different. Only one J_k becomes large within a given period $(t, t+\tau_F)$. This happens in a narrow time interval where the corresponding $x_k \sim 1$, see below. The periodicity of the current is a consequence of the relation $x_k(Q, t+\tau_F) = x_{k+1}(Q,t)$, which follows from Eq. (3.19).

The shape of the current peaks is determined by the parameter θ. For $\theta \ll 1$, the typical x_k that contribute to J_k in Eq. (3.35) are given by the condition $\theta \ln^2 x_k \lesssim 1$. For t close to $t_{\rm m}$ one can show from Eq. (3.18) with $K = K(q, t_{\rm m})$ that $p_{\rm opt}(t) = C\exp[-(t-t_{\rm m})\mu_b]$, with $C \sim \mu_b[q_b(t_{\rm m}) - q_a(t_{\rm m})]$. Then from Eq. (3.34)

$$x_k(t) \approx \exp[-(t-t_k)\mu_b], \qquad t_k = t_{\rm m} + k\tau_F, \tag{3.37}$$

with $k = 0, \pm 1, \ldots$ [we disregard the correction $\mu_b^{-1}\ln(QC/D)$ to t_k; it is of the order of the Suzuki time [117]]. Then the escape current near its maxima becomes

$$j(q,t) = W_{\rm m} \sum\nolimits_k e^{-(t-t_k)^2 \Delta \ddot{U}_{\rm m}/2D}, \qquad \theta \ll 1. \tag{3.38}$$

The current pulses (3.38) have Gaussian form. They are centered at $t = t_k = t_{\rm m} + k\tau_F$. The pulse width δt_w is determined by the noise intensity and the modulation

frequency, $\delta t_w \sim (D/\Delta U_{\rm m})^{1/2}\tau_F$. We note that the condition $\theta \ll 1$ means that this width is much larger than the relaxation time of the system $\sim \mu_b^{-1}$, cf. Fig. 3.2(a). Eq. (3.38) corresponds to the fully adiabatic picture, where the escape rate is given by the instantaneous barrier height $\Delta U(t)$.

For larger θ, where $\theta \sim 1$, the pulse shape is no longer Gaussian. We emphasize that this happens where the modulation is still slow, $\Omega_F \ll 1$, and one would expect the adiabatic picture to fully apply.

The pulse shape can be found explicitly in the limit $\theta \gg 1$ but $\Omega_F \ll 1$. In this case J_k can be evaluated by the steepest descent, giving

$$J_k(Q,t) \approx (2\pi/\theta)^{1/2} x_k \exp(-x_k). \tag{3.39}$$

As a function of time, J_k displays a peak where $x_k(t) = 1$. The width of the peak $\delta t_w \sim \mu_b^{-1}$ is now independent of both the noise intensity and the modulation frequency. The peak is strongly asymmetric, because x_k depends on time exponentially, cf. Eq. (3.37).

The evolution of the peak shape with varying parameter θ is demonstrated in Fig. 3.2. It is the same as for weak modulation [118], but the dependence of the parameters on the modulation amplitude is different, for strong modulation. Fig. 3.2 (b) shows that, with increasing modulation frequency, not only the height of the peaks decreases, i.e., the modulation of the escape current becomes less pronounced, but also the width of the pulses with respect to the modulation period rapidly increases.

3.5.2 Nonadiabatic regime

The shape of the escape current peaks can be analyzed also for $\Omega_F \lesssim 1$, where the adiabatic approximation does not apply. Our analysis is based on Eqs. (3.12),

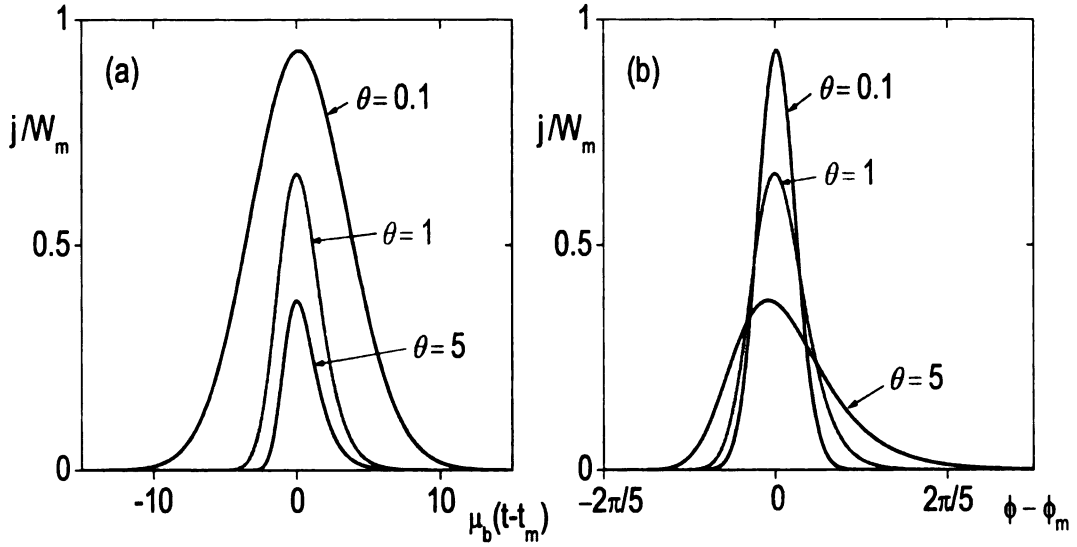

Figure 3.2: (a) Pulses of escape current in the adiabatic approximation as functions of time scaled by the relaxation time. With increasing parameter θ the pulses change from Gaussian to strongly asymmetric. (b) The same pulses as functions of time scaled by the modulation period, $\phi = \omega_F t$.

(3.26), (3.27). The function $p_{\rm opt}^{-2}(t) \propto \kappa_b^2(t,t')$ in Eq. (3.26) for $\mathcal{E}_b$ exponentially increases in time near q_b, therefore the term $\propto p_{\rm opt}^{-2}$ in $\mathcal{E}_b$ and z becomes dominating before the MPEP reaches the diffusion region $|Q| \sim l_D$, and in Eqs. (3.12), (3.26) $\mathcal{E}_b = \tilde{\mathcal{E}} D^{-1/2} \left(\Omega_F^2 s_{\rm m}'' p_{\rm opt}^{-2}(t)\right)^{-1/2}$.

Integration over x in Eq. (3.12) can be done by the steepest descent method. Using Eq. (3.25) one can write in Eq. (3.12) $\phi_d - \phi_{\rm m} = \Omega_F \ln[xD/Qp_{\rm opt}(t)]$. The major contribution to $j(q,t)$ near its maximum comes from the range $|\phi_d - \phi_{\rm m}| \lesssim (D/\Omega_F^2 s_{\rm m}'')^{1/2} \ll 1$. Expanding $s(\phi_d)$ to the second order in $\phi_d - \phi_{\rm m}$ and performing integration over x we obtain from Eqs. (3.12), (3.26)

$$j(q,t) = \frac{\mu_b(t)\tilde{\mathcal{E}} D^{1/2}}{\Omega_F \sqrt{s_{\rm m}''}} e^{-R/D} \sum_{k=-\infty}^{\infty} x_k e^{-x_k}, \qquad (3.40)$$

$$x_k = x_0 \exp(2\pi k/\Omega_F), \qquad x_0 = p_{\rm opt}(t)Q/D.$$

Note that here $p_{\rm opt}(t)$ can be smaller than $l_D/\sigma_b^2(t)$.

Eq. (3.40) describes the escape rate in the whole region $\Omega_F^2 s_{\rm m}'' \gg D$; it does not require the adiabatic approximation. The ratio $\tilde{\mathcal{E}}/\sqrt{s_{\rm m}''}$ can be obtained from Eq. (3.29) by solving Eq. (3.22). In the adiabatic limit Eq. (3.40) gives the same result as Eq. (3.39). The current peaks (3.40) are strongly asymmetric. The current is maximal, for given Q, when $x_k = 1$. The width of the current peaks is given by the reciprocal relaxation time $\sim \mu_b^{-1}$. The form of the current peaks is totally different from that of the diffusion current $-D\partial_Q \rho$ on the basin boundary $Q = 0$. This current was studied in Refs. [93, 112, 54]. It can be easily obtained from Eqs. (3.7), (3.26) with $Q = 0$. The regime $\Omega_F^2 s_{\rm m}''/D \ll 1$, where the current has the form (3.38), cannot be studied in the approximation [93, 112] at all.

With increasing Ω_F the peaks of j (3.40) are smeared out and the escape synchronization is weakened. For $\Omega_F \gg 1$ the exponentially strong synchronization disappears. Besides the fact that the width of the peaks $\bar{\mu}_b^{-1}$ becomes of the order of the interpeak distance τ_F for $\Omega_F \gtrsim 1$, $s_{\rm m}''$ rapidly decreases with ω_F for large Ω_F.

3.5.3 Nonlinear current propagation

In experiments the instantaneous escape rate can be measured as current $j(q,t)$ for a given q well behind the basin boundary $q_b(t)$, i.e. $q - q_b(t) \gg l_D$. When noise is weak, motion behind the basin boundary is practically noise-free ("deterministic"). Then the escape current is $j(q,t) = K(q,t)\rho(q,t)$. The function $\rho(q,t)$ can be related to the distribution $\rho(q_b(t)+Q,t)$ in the harmonic region where $Q \gg l_D$. The relation can be obtained from the Fokker-Planck equation in the neglect of the diffusion term, $\partial_t \rho + \partial_q[K(q,t)\rho] = 0$, and can be expressed in terms of the trajectories in the absence

of noise $q_{\rm det}(t;t_0)$. A trajectory $q_{\rm det}$ is given by the equation

$$\partial_t q_{\rm det} = K(q_{\rm det}, t), \tag{3.41}$$
$$q_{\rm det}(t;t_0) = q, \quad q_{\rm det}(t_0;t_0) = q_b(t_0) + Q.$$

The boundary conditions in Eq. (3.41) follow from the fact that $q_{\rm det}(t;t_0)$ arrives at "observation point" q at time t and starts at point $q_b(t_0)+Q$ at time t_0. Eq. (3.41) gives t_0 as a function of q,t. The distribution behind the boundary is

$$\rho(q,t) = \exp\left\{-\int_{t_0}^{t} d\tau \left[\partial_q K(q,\tau)\right]_{\rm det}\right\} \rho_0(t_0), \tag{3.42}$$

where the derivative $\partial_q K$ is calculated along the trajectory $q_{\rm det}(t;t_0)$, and $\rho_0(t_0) = \rho(q_b(t_0)+Q, t_0)$.

The current $j(q,t)$ has a simple form for adiabatic modulation, $\Omega_F \ll 1$. In this case, as long as q is not too far from $q_b(t_{\rm m})$, one can calculate the trajectory $q_{\rm det}$ for the modulation phase that corresponds to $t = t_{\rm m}$, where the current is close to maximum. This gives for $t_0 = t_0^{\rm ad}$ the expression

$$t_0^{\rm ad}(q,t) = t - \delta t_0^{\rm ad}(q), \quad \delta t_0^{\rm ad} = \int_{q_b(t_{\rm m})+Q}^{q} \frac{dq'}{K(q',t_{\rm m})}. \tag{3.43}$$

Eq. (3.43) shows that there is a simple q-dependent shift between t and $t_0^{\rm ad}$, which is equal to the duration of deterministic motion from $q_b(t_{\rm m})+Q$ to the observation point q. We assume that this shift is small compared to the modulation period τ_F.

In the adiabatic approximation Eq. (3.42) is further simplified for t close to $t_{\rm m} + k\tau_F$. In this case

$$\exp\left[-\int_{t_0}^{t} d\tau \left(\partial_q K\right)_{\rm det}\right] \approx \frac{K\left(q_b(t_{\rm m})+Q, t_{\rm m}\right)}{K(q,t_{\rm m})} \approx \mu_b(t_{\rm m})Q/K(q,t_{\rm m}),$$

where we have taken into account that $K(q_b(t_{\rm m}),t_{\rm m}) = \dot{q}_b(t_{\rm m}) \propto \omega_F$ [in the case of additive modulation, $K(q,t) = K_0(q) + F(t)$, we have $K(q_b,t_{\rm m}) = 0$]. Therefore, we

obtain for the current in the adiabatic approximation

$$j^{\rm ad}(q,t) = j(Q, t_0^{\rm ad}). \tag{3.44}$$

Thus, in the adiabatic approximation the current near the peaks does not change shape but just shifts in phase, with the phase shift described by Eq. (3.43). With increasing parameter θ (3.36) the current peaks change from Gaussian, for $\theta \ll 1$, see Eq. (3.38), to strongly asymmetric, see Eq. (3.39). The peaks are located at $t = t_k + \delta t_0^{\rm ad}$, with $t_k = t_{\rm m} + k\tau_F$, Eq. (3.37). We note that in Eq. (3.37) we disregarded a shift of t_k by the Suzuki time $\sim \mu_b^{-1} \ln(Q/l_D)$. This shift compensates the term in $\delta t^{\rm ad}$ (3.43) that logarithmically depends on Q, so that the overall position of the current peaks (3.38), (3.39), (3.44) is independent of the matching point Q.

In the nonadiabatic case the difference $t - t_0$ depends not only on the observation point q, but also on time t. In addition, the factor that relates $\rho(q,t)$ and $\rho_0(t_0)$ in Eq. (3.42) becomes t-dependent. Therefore, the overall shape of the current changes. However, the escape current has sharp peaks only where their width is small compared to the inter-peak distance. From this point of view, the case of slow modulation is most interesting for studying the shape of escape current and synchronization of escape as a whole.

3.6 Period-average escape rate

In the range $s''_{\rm m} \sim |s_{\rm m}| \gg D$, the period-average escape rate (3.13) is

$$\overline{W} = \nu \exp(-R/D), \qquad \nu = \bar{\mu}_b \tilde{\mathcal{E}} D^{1/2}/2\pi\sqrt{s''_{\rm m}}. \tag{3.45}$$

The prefactor ν can be expressed in terms of $\mathcal{Z}_2$ using Eq. (3.29), formally giving the result [93, 112] even where the theory [93, 112] does not apply.

The asymptotic technique developed in this Chapter allows obtaining the prefactor ν in several limiting cases. For comparatively weak modulation, $D \ll |s_{\rm m}| \ll R$, Eqs. (3.22), (3.45) give the same result as in Ref. [92], with the scaling $\nu \propto (s''_{\rm m})^{-1/2} \propto A^{-1/2}$. Since the theory [92] covers the whole range $|s_{\rm m}| \ll R$, a transition from the Kramers limit of no modulation to the case of arbitrarily strong modulation is now fully described.

In the whole range where the adiabatic approximation applies, $\Omega_F \ll 1$, from Eqs. (3.27), (3.33) we obtain

$$\nu = (2\pi)^{-3/2} |\mu_a \mu_b|^{1/2} D^{1/2} \omega_F (\Delta \ddot{U}_{\rm m})^{-1/2} \tag{3.46}$$

where $\mu_{a,b}$ are calculated for $t = t_{\rm m}$. Interestingly, ν (3.46) is independent of the modulation frequency.

3.7 Scaling near the bifurcation point

Close to the bifurcational value of the modulation amplitude $A = A_c$ where the metastable and unstable states $q_{a,b}(t)$ merge, the escape rate displays system-independent features. As shown in Chapter 2 (see also Refs. [62, 85]), the activation energy R of the system scales as $R \propto \eta^{\xi}$, where $\eta \propto (A_c - A)$ is the reduced distance to the bifurcation point along the amplitude axis [see Eq. (3.49) below]. Three scaling regimes have been identified for R. With increasing modulation frequency ω_F or decreasing η, the critical exponent ξ changes from $\xi = 3/2$ for stationary systems (adiabatic scaling) to $\xi = 2$ (locally nonadiabatic scaling) and then back to $\xi = 3/2$ (high-frequency scaling). Below we discuss scaling of the prefactor ν in these regimes.

3.7.1 Adiabatic scaling

Like in Chapter 2, we start the analysis with the limiting case of slow modulation, $\omega_F t_{\rm r} \ll 1$. In this case the adiabatic stable and unstable states $q^{\rm ad}_{a,b}(t)$ are given by the equation $K(q^{\rm ad}_{a,b}(t),t) = 0$ [cf. Eq. (2.11) of Chapter 2]. The adiabatic critical amplitude $A^{\rm ad}_c$ is determined by the condition that the states $q^{\rm ad}_{a,b}(t)$ touch each other. This happens once per period, and we set $t = k\tau_F$ ($k = 0, \pm 1, \ldots$) at this time. We also set $q^{\rm ad}_{a,b}(k\tau_F) = 0$ for $A = A^{\rm ad}_c$. Expanding the Langevin equation of motion around this point, we obtain

$$\dot{q} = \alpha q^2 + \beta \delta A^{\rm ad} - \alpha\gamma^2(\omega_F t)^2 + f(t), \tag{3.47}$$

This equation has the same form as Eq. (2.12) for the soft mode q_1. Here $\alpha = (1/2)\partial_q^2 K$, $\beta = \partial_A K$, $\gamma^2 = -(2\alpha\omega_F^2)^{-1}\partial_t^2 K$; all derivatives are evaluated at $q = t = 0$, $A = A^{\rm ad}_c$; γ is independent of ω_F; it is assumed, without loss of generality, that $\alpha > 0$; $\delta A^{\rm ad} = A - A^{\rm ad}_c$. The force $f(t)$ is a zero-mean white Gaussian noise, $\langle f(t)f(t')\rangle = 2D\delta(t-t')$.

The adiabatic approximation applies provided not only $t^{\rm ad}_{\rm r}\omega_F \ll 1$, but also $\partial_t t^{\rm ad}_{\rm r} \ll 1$, where $t^{\rm ad}_{\rm r}(t) = (1/2)[(\alpha\gamma\omega_F t)^2 - \alpha\beta\delta A^{\rm ad}]^{-1/2}$ is the adiabatic relaxation time, as given by Eq. (2.13) of Chapter 2. The relaxation time strongly depends on t and diverges for $A \to A^{\rm ad}_c$ and $t \to 0$. The inequality $\partial_t t^{\rm ad}_{\rm r} \ll 1$ is therefore the most restrictive condition on adiabaticity; it requires that $t^{\rm ad}_{\rm r} \ll t_l$, where $t_l = (\alpha\gamma\omega_F)^{-1/2}$ is a new dynamical time scale [62, 85]. The condition $t^{\rm ad}_{\rm r} \ll t_l$ is equivalent to $\omega_F \ll |\beta\delta A^{\rm ad}|/\gamma$.

The problem of escape is simplified in the adiabatic regime [30, 31, 56, 57, 62, 85, 109]. For a periodically modulated system, from Eq. (3.47) we obtain $|\mu_a| = \mu_b = 2|\alpha\beta\delta A^{\rm ad}|^{1/2}$, $\Delta\ddot{U}_{\rm m} = 4\omega_F^2\gamma^2|\alpha\beta\delta A^{\rm ad}|^{1/2}$. Then, from Eq. (3.46), the prefactor

scales as $\nu \propto |\delta A^{\rm ad}|^{1/4}$. We note that, in the adiabatic approximation ν decreases as A approaches the bifurcational value and, because escape is strongly synchronized, $\nu \propto D^{1/2}$.

3.7.2 Locally nonadiabatic scaling

As explained in Sec. 2.3.1 of Chapter 2, the critical slowing down of the system motion makes the adiabatic approximation inapplicable in the region $|\delta A^{\rm ad}|/A_c^{\rm ad} \lesssim \Omega_F$, where the condition $t_{\rm r}^{\rm ad} \ll t_l$ is violated. In this range we rewrite Eq. (3.47) in the form of Eq. (2.18),

$$\dot{Q} = Q^2 - \tau^2 + 1 - \eta + \tilde{f}(\tau), \tag{3.48}$$

where $Q = \alpha t_l q$, $\tau = t/t_l$, $\dot{Q} = dQ/d\tau$, $\tilde{f}(\tau) = (\gamma\omega_F)^{-1} f(t_l\tau)$. The control parameter is defined as

$$\eta = \beta(\gamma\omega_F)^{-1}(A_c - A), \qquad A_c \approx A_c^{\rm sl}. \tag{3.49}$$

Here $A_c^{\rm sl} = A_c^{\rm ad} + \gamma\omega_F/\beta$ is given by Eq. (2.16). It is, to the first order in ω_F, the "true" bifurcation point, which is shifted from $A_c^{\rm ad}$ because of the slowing down of the system and the associated with it delayed response. For small driving frequencies, $\omega_F t_{\rm r} \ll 1$, where the local expansion (3.47) applies, the shift in the bifurcational amplitude is linear in frequency. The corrections to $A_c^{\rm sl}$ of higher orders in ω_F are discussed in Sec. 2.3.4 of Chapter 2.

For $\eta \ll 1$ the activation energy scales as $R \propto \eta^2$. In this region the most probable escape path $Q_{\rm opt}(\tau), P_{\rm opt}(\tau)$ corresponding to Eq. (3.48) is given by Eq. (2.36) of Chapter 2. Using those expressions in Eq. (3.22), we obtain

$$z(\tau) = 4\pi\tilde{D}\int_{-\infty}^{\tau} d\tau_1 \exp(2\tau^2 - 2\tau_1^2). \tag{3.50}$$

Here $\tilde{D} = \alpha^{1/2}(\gamma\omega_F)^{-3/2}D$ is the intensity of the random scaled force $\tilde{f}(\tau)$. This gives

$$\nu = \nu_0 D^{1/2}|\delta A|^{-1}\omega_F^{5/4}, \qquad \delta A = A - A_c, \tag{3.51}$$

where

$$\begin{aligned}\nu_0 &= (32\pi^7)^{-1/4}|\alpha\gamma|^{1/4}\beta^{-1} \\ &= (64\pi^7\omega_F)^{-1/4}|\partial_t^2 K\, \partial_q^2 K|^{1/8}/|\partial_A K|.\end{aligned}$$

From Eq. (3.51), the prefactor $\nu \propto |\delta A|^{-1}$ sharply increases as the modulation amplitude approaches A_c. This is qualitatively different from the decrease of ν in the adiabatic approximation. The result agrees with the numerical solution of Eqs. (3.22), (3.45) for a model system shown in Fig. 3.3. The calculations in a broad range of A are also confirmed by Monte Carlo simulations, as discussed below.

3.7.3 High-frequency scaling

For high frequencies, $\Omega_F \gg 1$, escape is not synchronized by the modulation. The prefactor in the escape rate is $\nu = |\bar{\mu}_a\bar{\mu}_b|^{1/2}/2\pi$, it is independent of the noise intensity D. Near the bifurcation point it scales as in stationary systems [30, 57], where $\nu \propto |\delta A|^{1/2}$ and $R \propto |\delta A|^{3/2}$. We note that modulation is necessarily fast very close to the bifurcation point, because $|\bar{\mu}_{a,b}| \to 0$ for $A \to A_c$. Therefore the prefactor always goes to zero for $A \to A_c$. However, for small ω_F the corresponding region of δA is exponentially narrow [62, 85]. The increase of ν with decreasing $A_c - A$ in the locally nonadiabatic region does not contradict this picture because in this region $\nu \propto D^{1/2}$, whereas for effectively high-frequency modulation ν is independent of D.

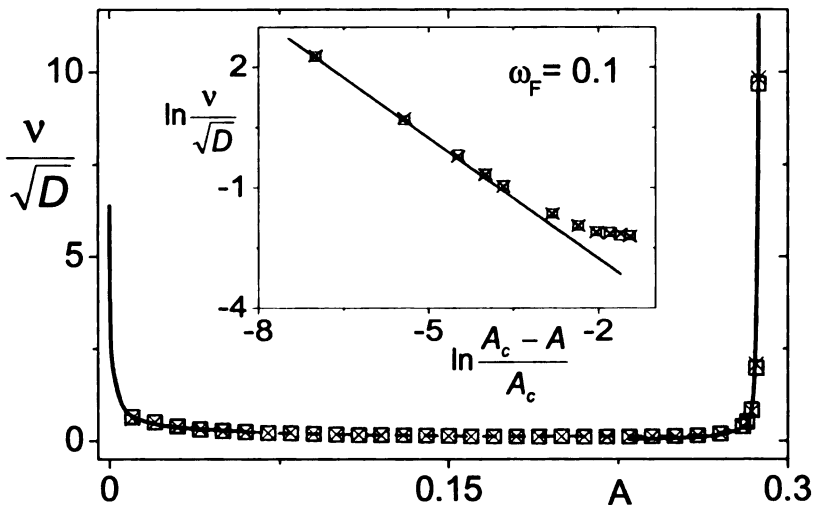

Figure 3.3: The prefactor ν in the average escape rate $\overline{W}$ (3.45). The results refer to the model (3.52) with $\omega_F = 0.1$ and describe escape in the regime of strong synchronization, where $\nu \propto D^{1/2}$. The solid line for small A shows the scaling $\nu \propto A^{-1/2}$. The solid lines for small $\delta A = A - A_c$ in the main figure and in the inset show the scaling (3.51). The dashed line shows the result of the numerical solution of Eq. (3.22). The squares and crosses show the results of Monte Carlo simulations for $R/D = 5$ and $R/D = 6$, respectively.

3.8 Results for a model system

To illustrate the findings, we consider a simple model system, a Brownian particle in a cubic potential subject to sinusoidal modulation. The Langevin equation is of the form

$$\dot{q} = K(q,t) + f(t), \quad K = q^2 - 1/4 + A\cos(\omega_F t), \tag{3.52}$$

with $f(t)$ being white Gaussian noise of intensity D.

3.8.1 The adiabatic regime

The adiabatic stable and unstable states of the system (3.52) in the absence of noise are $q_{a,b}^{\rm ad}(t) = \mp\left[1/4 - A\cos(\omega_F t)\right]^{1/2}$, and the adiabatic critical amplitude is $A_c^{\rm ad} = 1/4$. The adiabatic barrier height is $\Delta U(t) = (4/3)\left[1/4 - A\cos(\omega_F t)\right]^{3/2}$. Its minimum $\Delta U_{\rm m} = (4/3)(1/4 - A)^{3/2}$ is reached for $t_{\rm m} = k\tau_F$, with $k = 0, \pm 1, \ldots$.

The reduced curvature $\Omega_F^2 s_{\rm m}''$ of the function $s(\phi)$ in the boundary-layer distribution at $\phi_{\rm m} = \omega_F t_{\rm m}$ is given by Eq. (3.33),

$$\Omega_F^2 s_{\rm m}'' = (1/2) A \omega_F^2 (1/4 - A)^{-1/2}. \tag{3.53}$$

Therefore the condition of strong but slow modulation, $\Omega_F^2 s_{\rm m}'' \ll D$, which must hold for the pulses of the escape current to be of Gaussian shape, takes the form

$$\omega_F^2 \ll D(1/4 - A)^{1/2}/A.$$

It becomes more and more restrictive for the modulation frequency as the modulation amplitude A approaches the adiabatic bifurcational value $1/4$.

The prefactor ν of the period-average escape rate in the adiabatic limit for sufficiently strong modulation is given by Eq. (3.46). For our model it has a simple explicit form

$$\nu = (2\pi^{3/2})^{-1} D^{1/2} (1/4 - A)^{1/4} A^{-1/2}. \tag{3.54}$$

As expected, $\nu \propto A^{-1/2}$ for small amplitude, whereas close to the adiabatic bifurcation point $\nu \propto (A_c^{\rm ad} - A)^{1/4}$.

3.8.2 Locally nonadiabatic regime near the bifurcation point

As explained in Section 3.7, sufficiently close to the bifurcation point the adiabatic approximation breaks down. As a result, the bifurcation point A_c shifts away from

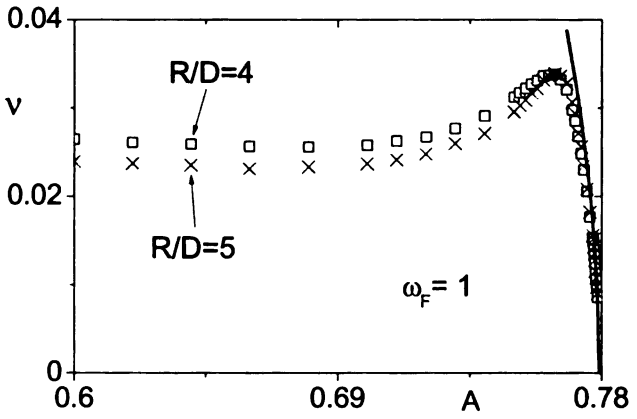

Figure 3.4: The prefactor ν in the average escape rate $\overline{W}$ (3.45) close to the bifurcation point $A = A_c$. The results refer to the model (3.52) with $\omega_F = 1$. The squares and crosses show the results of Monte Carlo simulations for $R/D = 4$ and $R/D = 5$, respectively. The solid line shows the asymptotics $\nu = |\bar{\mu}_a \bar{\mu}_b|^{1/2}/2\pi \propto (A_c - A)^{1/2}$.

$A_c^{\rm ad}$ (to higher amplitude, in our case). Close to A_c the pulses of escape current become strongly asymmetric, even though the modulation frequency is small. The scaling of the prefactor in the period-average escape rate also changes dramatically, from decreasing (as in the adiabatic approximation) to increasing for $A \to A_c$. From Eqs. (3.51), (3.52)

$$\nu = (64\sqrt{2}\pi^7)^{-1/4} D^{1/2} |\delta A|^{-1} \omega_F^{5/4}. \tag{3.55}$$

The results on the prefactor for the discussed model system in the range $\omega_F t_{\rm r}^{(0)} \ll 1$ are shown in Figure 3.3 ($t_{\rm r}^{(0)}$ is the relaxation time in the absence of modulation; for the model (3.52) $t_{\rm r}^{(0)} = 1$). They refer to the modulation frequency $\omega_F = 0.1$. The dependence of $\nu/\sqrt{D}$ on the modulation amplitude A is shown in the main part of the figure. The solid line for small A represents Eq. (3.54). The solid line close to the bifurcational amplitude $A_c \simeq 0.29$ is given by Eq. (3.55). The dashed line for intermediate values of A is given by Eq. (3.45) with $\tilde{\mathcal{E}}/\sqrt{s_{\rm m}''}$ (3.29) evaluated by

numerically integrating Eq. (3.22). It is also well described by Eq. (3.54) for $A < 0.2$. The analytical results agree with the results of simulations represented by squares and crosses. The inset shows in more detail the locally nonadiabatic scaling $\nu \propto |\delta A|^{-1}$ in the region near A_c.

The simulations have been done using the standard second-order integration scheme [107] for stochastic differential equations. The period-average escape rate was found as a reciprocal of the average dwell time of particles leaving the attraction basin. For each set of parameter values we accumulated $\sim 10^5$ escape events. The prefactor of the escape rate ν was evaluated as $\nu = \overline{W} \exp(R/D)$. The values of activation energy R were obtained independently by solving the appropriate instantonic problem. We checked previously [62, 85] that these values agree extremely well with Monte Carlo simulations. For each value of A the noise intensity D was adjusted so as to keep R/D fixed at $R/D = 5$ (squares) and $R/D = 6$ (crosses).

The results on the prefactor for higher modulation frequency are shown in Fig. 3.8.1. They were obtained in the same way as for lower frequency. It is seen from Fig. 3.8.1 that for the used model, already for $\omega_F t_r^{(0)} = 1$ the amplitude dependence of the prefactor differs very significantly from the result of the adiabatic approximation. In particular, the prefactor displays the scaling behavior $\nu \propto (A_c - A)^{1/2}$ near the bifurcation point. It is independent of the noise intensity and is well described by the expression $\nu = |\bar{\mu}_a \bar{\mu}_b|^{1/2}/2\pi$.

3.9 Conclusions

The results of this Chapter and the previous work allow us to draw a general scheme of the dependence of the rate of activated escape on the modulation parameters. This

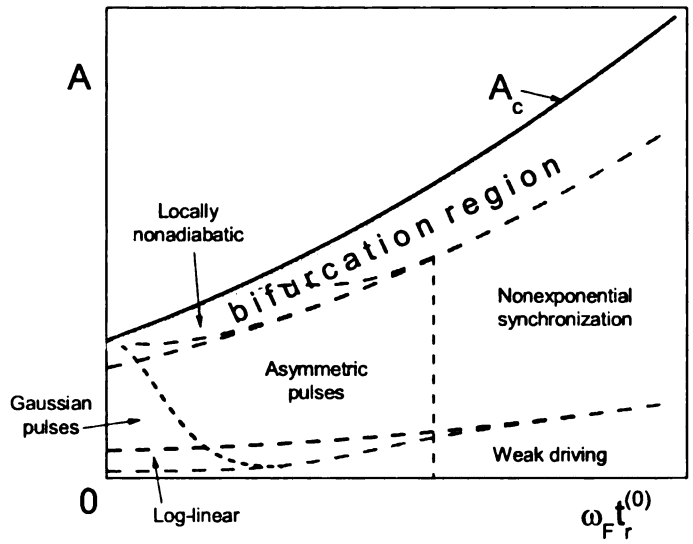

Figure 3.5: Different regions of escape behavior in modulated overdamped systems depending on the modulation frequency ω_F and amplitude A; $t_r^{(0)}$ is the relaxation time in the absence of modulation. The smeared boundaries between the regions are shown by dashed lines. The bold solid line indicates the bifurcational amplitude where the metastable state disappears. The shaded region below it indicates the range where the activation energy of escape $R \lesssim D$. The transition between the regions of exponentially strong and nonexponential synchronization occurs for $\omega_F t_r^{(0)} \sim 1$.

scheme is sketched in Fig. 3.5.

The weak-driving region corresponds to the case where the modulation-induced change of the activation energy of escape is small compared to the noise intensity D. In this region the major effect of modulation is weak "heating" of the system, which is quadratic in the modulation amplitude (for underdamped systems, the effective temperature depends on energy [2, 6, 86, 87, 88]). Escape is not synchronized by the modulation. The width of this region along the amplitude axis is $\propto D$ for low frequencies and becomes $\propto \omega_F D^{1/2}$ for large $\Omega_F \sim \omega_F t_r$.

Synchronization emerges once the magnitude of the oscillations of the "instantaneous" activation energy $|s_m|$ becomes much larger than D. There is a broad region

of modulation amplitudes where $|s_{\rm m}| \propto A$ and the logarithm of the period-average escape rate $\overline{W}$ is linear in A, too [92]. This log-linear region in Fig. 3.5 is bounded on the large-A side by the condition $A/A_c \ll 1$, where A_c is the bifurcational value of A. Strong synchronization occurs for small frequencies, $\Omega_F \ll 1$. Here, the escape current has peaks with width much smaller than the modulation period. The prefactor ν in the period-average escape rate scales as $(D/A)^{1/2}$.

Synchronization persists for higher modulation amplitudes. The shape of the peaks of escape current is Gaussian for $\Omega_F^2 s_{\rm m}'' \ll D$, and their width is $\sim (D/s_{\rm m}'')^{1/2}\tau_F$. For higher frequencies, the peaks become strongly asymmetric and non-Gaussian, with width $\sim t_{\rm r}$. In the log-linear region the boundary between the two types of peaks is $\omega_F \propto A^{-1/2}$.

For high modulation frequencies, $|s_{\rm m}|$ becomes small and exponentially strong synchronization of escape disappears. The escape current is still modulated in time, of course, but generally it does not have a shape of sharp narrow peaks even for small noise intensity.

Of special interest is the bifurcation region, because there the dynamics and fluctuations display system-independent features. The region is determined by the condition $|A_c - A| \ll A_c$, as shown in Fig. 3.5. In this region, in the adiabatic approximation the boundary of the range where escape current peaks are Gaussian has the form $\omega_F \propto |A_c - A|^{1/4}$.

Close to A_c, where $(A_c - A)/A_c\Omega_F \sim 1$, the adiabaticity is broken. This condition and the condition $\Omega_F \ll 1$ determine the boundary of the locally nonadiabatic region. Inside this region the escape current has the form of asymmetric narrow peaks. Special scaling is displayed for $(A_c - A)/A_c\Omega_F \ll 1$. Here, the activation energy of escape scales with the distance to the bifurcation amplitude A_c as $(A_c - A)^2$,

whereas the prefactor in the period-average escape rate is $\propto (A_c - A)^{-1}$. Because of the slowing down near the bifurcation point, the locally nonadiabatic behavior and synchronization of escape disappear for small $A_c - A$, which determines the high-A region boundary. This boundary is very close to A_c for small Ω_F, but for higher Ω_F the region of locally nonadiabatic behavior shrinks and ultimately disappears. Outside this region on the high-ω_F side, for A close to A_c the prefactor ν scales as $\nu \propto (A_c - A)^{1/2}$.

In conclusion, we have obtained a general solution of the problem of noise-induced escape in periodically modulated overdamped systems. For small ω_F the pulses of escape current are exponentially sharp and change with increasing ω_F from Gaussian to strongly asymmetric. For large ω_F exponential current modulation disappears. The prefactor ν in the period-average escape rate is a strongly nonmonotonic function of the modulation amplitude A for low frequencies. It first drops with increasing A to $\nu \propto (D/A)^{1/2}$ [92], then varies with A smoothly [54, 93, 112], and then sharply increases, $\nu \propto D^{1/2}/(A_c - A)$ near the bifurcation amplitude A_c. We found three scaling regimes near A_c, where $\nu \propto (A_c - A)^{\zeta}$ with $\zeta = 1/4, -1$, or $1/2$. The widths of the corresponding scaling ranges strongly depend on the modulation frequency.

Chapter 4

Pathways of activated escape in periodically modulated systems

4.1 Introduction

The theory of activated escape should answer two closely related questions: what is the escape rate and how does the system move during escape? Fluctuational trajectories leading to escape or interstate switching are of significant interest and have been extensively studied in recent years using various numerical techniques, see Refs. [119, 120, 121, 122] and papers cited therein. Even though escape is a random event, the probabilities of following different paths are strongly different. Therefore most likely the system follows a certain pathway, i.e., its trajectory is close to the most probable escape path (MPEP), see Ref. [95] and references therein.

The distribution of escape trajectories can be characterized by the prehistory probability distribution (PPD), a quantity accessible to direct experimental measurements. It is obtained by recording trajectories of the system that lead to escape and superimposing the trajectories that, after the system has escaped, pass through a

small vicinity of a point q_f (for a certain modulation phase, in the case of a periodically modulated system). The point q_f is chosen in the phase space sufficiently far behind the boundary of the basin of attraction to the initially occupied metastable state. Formally, the PPD $p_h(q,t|q_f,t_f)$ is the probability density for the system to have passed through a point q at an instant t provided it had been fluctuating about the metastable state for a long time and passed q_f at a later time t_f, $t_f > t$ [80].

The PPD $p_h(q,t|q_f,t_f)$ should peak at q lying on the optimal fluctuational path that leads to q_f. Therefore it "maps out" optimal paths. For stationary systems this has been directly confirmed by extensive simulations [123, 124, 125] and also in laser experiments [81]. In such systems escape can occur at any time, with equal probability, therefore the tube of paths around the optimal escape path is broad.

In this Chapter (see also Ref. [126]) we study escape pathways in periodically modulated systems. Modulation synchronizes escape events. This can be easily understood for escape from a slowly modulated potential well. Here, escape is most likely to occur when the instantaneous potential barrier $\Delta U(t)$ is at its lowest, once per period, cf. Fig. 4.1(a). This corresponds to exponentially strong synchronization. Strong synchronization persists even where the modulation is not slow and the adiabatic picture in which the escape rate is determined by the instantaneous barrier height does not apply [110, 111, 112, 127, 128]. As a result of escape synchronization, there is one most probable escape path per period.

In turn, as we show, the prehistory probability distribution for escape pathways displays a sharp narrow peak, which is centered at the MPEP. Moreover, the PPD may display several narrow peaks in the (q,t) space. For strong escape synchronization and not too low modulation frequencies, the width of the peaks is determined by the typical diffusion length $l_D = (2Dt_r)^{1/2}$, where D is the noise intensity ($D = k_BT$

for thermal noise) and t_r is the relaxation time of the system. This is qualitatively different from the shape of the PPD in stationary systems [81]. Of course, in modulated systems along with the final point q_f through which the system passes one should fix the modulation phase when the passage happens. It is given by the passage time $t_f (\mathrm{mod}\ \tau_F)$, where τ_F is the modulation period.

The occurrence of a narrow peak of the PPD can be understood from the qualitative picture of motion in escape. This picture is sketched in Fig. 4.1 for a system with one dynamical variable q. Escape from a static potential well corresponds to going over the barrier top q_b from the vicinity of the potential minimum q_a, see Fig. 4.1(a). Similarly, a modulated system escapes when it goes over the periodic basin boundary $q_b(t)$ from a periodic metastable state $q_a(t)$, see Fig. 4.1(b) (here and below we assume that the noise correlation time is small; see Ref. [51] for a more general case). Let us suppose that the escaped particle is found at time t_f at a point q_f sufficiently far behind $q_b(t)$. A typical trajectory to this point displays four distinct sections with different types of motion shown schematically by letters A through D.

We discuss the motion backward in time from t_f. Immediately adjacent to q_f is section A of the trajectory in Fig. 4.1. Here, for small noise intensity the system moves close to the noise-free trajectory from the vicinity of $q_b(t)$ to q_f. In the case of a static potential this corresponds to sliding down the potential slope from q_b to q_f. In the diffusion region of width $\sim l_D$ around $q_b(t)$, section B in Fig. 4.1, the motion is mostly diffusion about $q_b(t)$, because noise-free motion with respect to $q_b(t)$ is slow (in the case of a static potential the potential is locally flat at q_b). Section C is the motion from the attractor to the basin boundary. The corresponding trajectory is close to the most probable escape path. This motion is a result of the large fluctuation that has led to escape detected at q_f. For strongly synchronized escape, there is one MPEP

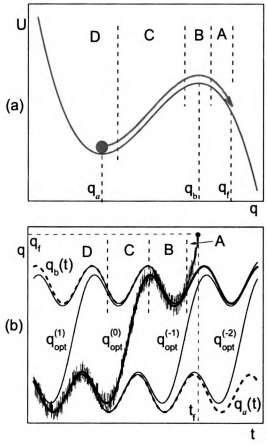

Figure 4.1: Activated motion leading to detection of an escaped particle at point q_f at time t_f (schematically). Panels (a) and (b) illustrate escape from a static and a periodically modulated potential well, respectively. In the latter case $q_a(t)$ and $q_b(t)$ are the periodic stable state and the basin boundary. The trajectories $q_{\rm opt}^{(n)}(t)$ ($n = 1, \ldots, -2$) are the periodically repeated most probable escape paths. The four major stages of motion A, B, C, and D on the way to q_f are discussed in the text.

per modulation period, as shown in Fig. 4.1(b). It approaches $q_b(t)$ asymptotically as $t \to \infty$. If the system was observed behind $q_b(t_f)$ at time t_f, it has most likely arrived to the vicinity of $q_b(t)$ along the MPEP that approached $q_b(t)$ before t_f, but not too much in advance, as shown in Fig. 4.1(b). Finally, well before t_f, in the region D, the system was fluctuating about the attractor.

The above picture suggests that the PPD will display a peak along the trajectory singled out in Fig. 4.1. It also explains why this peak should be narrow: in contrast to stationary systems, which can arrive to the vicinity of q_b at any time, periodically modulated systems approach $q_b(t)$ only once per period. By changing q_f, t_f we can switch between neighboring MPEP's, and therefore there is a possibility for the PPD to have two and potentially even more peaks inside the attraction basin.

As mentioned above, we are interested in the regime where escape events are strongly synchronized by the modulation. It means that the probability density to find the escaped system at a point q_f behind the basin boundary, cf. Fig. 4.1, displays sharp peaks as a function of the observation time t_f. These peaks are periodically repeated in time. They were studied in Ref. [111]. We will choose the time t_f close to the maximum of the peak. This choice is justified, because the corresponding PPD characterizes the most probable escape trajectories. Otherwise the PPD would be formed by trajectories with exponentially smaller probabilities that are very rarely followed in escape.

Interestingly, the condition that the tubes of escape trajectories be narrow in time and space requires that the modulation frequency $\omega_F = 2\pi/\tau_F$ be within a range limited both from below and from above. To understand the lower limit we note that, as mentioned above, for slow modulation escape occurs every period around the time $t_m + k\tau_F$ where the height of the instantaneous potential barrier $\Delta U(t)$ is

at its minimum ($k = 0, \pm 1, \ldots$). The typical width of the time window for escape Δt is given by the condition $|\Delta U(t_{\rm m} \pm \Delta t) - \Delta U(t_{\rm m})| \lesssim D$, which leads to $\Delta t = [D/\Delta \ddot{U}(t_{\rm m})]^{1/2} \sim \omega_F^{-1}[D/\Delta U(t_{\rm m})]^{1/2}$. If $\Delta t \gg t_{\rm r} \ln[\Delta U(t_{\rm m})/D]$, the PPD has the same shape as if the system were escaping out of a stationary potential well of height $\Delta U(t_{\rm m})$. In this case the peak of the PPD inside the attraction basin is broad and asymmetric, its width is independent of the noise intensity [81].

In the opposite limit of high-frequency modulation, $\omega_F t_{\rm r} \gg 1$, escape of an overdamped system is not synchronized. The dynamics is characterized by the coordinates averaged over modulation period. The PPD over such coordinates is described by the theory for stationary systems, and the PPD peak inside the attraction basin is broad.

In the intermediate range of frequencies not only are the PPD peaks narrow but, as mentioned above, the PPD may display several peaks inside the attraction basin. This happens because the motion of the system near the basin boundary is slow. Therefore if the system is observed behind the boundary $q_b(t)$ at a given time t_f, it could have arrived to the boundary along one of a few periodically repeated optimal escape paths, fluctuated about $q_b(t)$ for some time, and then made a transition to (q_f, t_f) over time $\sim t_{\rm r}$.

The multiple-peak structure of the PPD is a specific feature of periodically modulated systems far from equilibrium, i.e. away from both the adiabatic limit of slow modulation and the limit of fast modulation. It is illustrated in Fig. 4.2 for a model system. Two peaks of the PPD inside the attraction basin are clearly resolved in this figure. Their shape is well described by the asymptotic theory developed in this Chapter.

In Sec. 4.2 below we discuss the dynamics of a periodically modulated system and the equations for the most probable escape path. In Sec. 4.3 we obtain a general

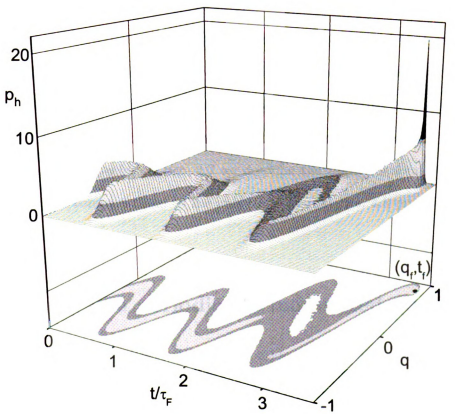

Figure 4.2: The prehistory probability density (PPD) $p_h(q,t|q_f,t_f)$ and its contour plot for a noise-driven overdamped system with equation of motion $\dot{q} = q^2 - 0.25 + A\cos\omega_F t + f(t)$, where $f(t)$ is white noise of intensity D. The parameters are $A = 0.7$, $\omega_F = 2$, $D = 0.01$, $q_f = 0.8$, $t_f = (\tau_F/2)(\mathrm{mod}\,\tau_F)$, where $\tau_F = 2\pi/\omega_F$ is the modulation period. The shadowing (color code on line) corresponds to the 4 regions of the height of the distribution separated by the values $p_h = 0.5, 2, 7$.

expression for the PPD near the basin boundary and relate it to the distribution that describes the quasiperiodic current away from the attraction basin, which gives the escape rate. The PPD is simplified in the adiabatic limit where the modulation period is small compared to the relaxation time. In Sec. 4.4 it is shown that two types of behavior may be displayed near $q_b(t)$ in this case, depending on the ratio of the two small parameters that characterize the dynamics. The analysis is extended to the case of nonadiabatic driving in Sec. 4.5. In Sec. 4.6 we obtain the central result of the Chapter, the PPD inside the attraction basin. We show that it has the shape of a sum of diffusion-broadened Gaussian peaks centered at the periodically repeated most probable escape paths. In Sec. 4.7 we describe the results of simulations of a model system and compare them to the analytical results. Sec. 4.8 provides a brief summary of the results.

4.2 Escape of a periodically modulated system

We investigate the prehistory probability distribution for an overdamped system characterized by one dynamical variable q. The system is in a periodically modulated potential $U(q,t) = U(q,t+\tau_F)$. Fluctuations are induced by an external noise $f(t)$. The motion is described by the Langevin equation

$$\dot{q} = K(q,t) + f(t). \tag{4.1}$$

Here, $K(q,t) \equiv \partial_q U(q,t)$ is the regular periodic force. We consider the simplest case where $f(t)$ is zero-mean white Gaussian noise with correlator $\langle f(t)f(t')\rangle = 2D\delta(t-t')$.

In the absence of noise the system (4.1) has a periodic metastable state (attractor) $q_a(t) = q_a(t+\tau_F)$ and a periodic boundary $q_b(t) = q_b(t+\tau_F)$ of the basin of attraction to $q_a(t)$, see Fig. 4.1(b). The states $q_a(t)$ and $q_b(t)$ are, respectively, the stable and

unstable periodic solutions of the equation $\dot{q} = K(q,t)$. For concreteness we assume that $q_a(t) < q_b(t)$.

The PPD $p_h(q,t|q_f,t_f)$ as defined in the Introduction is the conditional probability density (with respect to q) of passing through a point (q,t) in the coordinate-time space on the way from the attractor to a point (q_f,t_f). It has the form [80]

$$p_h(q,t|q_f,t_f) = \frac{\rho(q_f,t_f|q,t)\rho(q,t|q_{\rm in},t_{\rm in})}{\rho(q_f,t_f|q_{\rm in},t_{\rm in})}, \tag{4.2}$$

where $\rho(q_1,t_1|q_2,t_2)$ is the probability density (with respect to q_1) of a transition from (q_2,t_2) to (q_1,t_1), with $t_1 > t_2$.

We assume that the noise intensity D is small. Then the period-average escape rate is $\overline{W} \propto \exp(-R/D)$, where R is the activation energy of escape, $R \gg D$ [127, 112, 128, 110, 111]. The condition on D is that $\overline{W}^{-1}$ largely exceeds the relaxation time of the system $t_{\rm r}$ and the modulation period τ_F. Eq. (4.2) gives the distribution of escape paths in a broad time range

$$\overline{W}^{-1} \gg t_f - t_{\rm in} > t - t_{\rm in} \gg t_{\rm r}, \tau_F, \tag{4.3}$$

where the population of the attraction basin practically does not change. For $t - t_{\rm in} \gg t_{\rm r}$ the initial state $q_{\rm in}$, which is close to the attractor $q_a(t_{\rm in})$, gets forgotten. Then the right-hand side of Eq. (4.2) becomes independent of $t_{\rm in}$.

The functions $\rho(q,t|q_{\rm in},t_{\rm in}) = \rho(q,t)$ and $\rho(q_f,t_f|q_{\rm in},t_{\rm in}) = \rho(q_f,t_f)$ give the time-periodic probability density to find the system in states q and q_f, respectively. To study escape pathways we calculate the PPD for q_f outside the attraction basin, $q_f > q_b(t_f)$.

The transition probability density $\rho(q,t|q',t')$ is a solution of the Fokker-Planck equation (FPE)

$$\partial_t \rho = -\partial_q[K(q,t)\rho] + D\partial_q^2 \rho, \tag{4.4}$$

with the initial condition $\rho(q,t'|q',t') = \delta(q-q')$. Even for a 1D system, this equation does not have a known explicit solution except for the case of K linear in q. To analyze the PPD we will have to find approximate solutions in different regions and match them.

In the following subsections we discuss the dynamics of the system prior and during escape.

4.2.1 Dynamics near the periodic states

Following Sec. 3.2.1 of Chapter 3, we briefly review the dynamics close to the periodic states $q_i(t)$, $i = a, b$. In the absence of noise it is described by the linear equations $\delta\dot{q} = \mu_i(t)\delta q$ with $\delta q = q - q_i(t)$ and $\mu_i(t)$ given by Eq. (3.2). Time evolution of the deviation δq from $q_i(t)$ is given by Eq. (3.3).

Because of the periodicity of $\mu_i(t)$, the Floquet multipliers M_i ($i = a, b$), Eq. (3.4), are independent of time, with $M_a < 1$ and $M_b > 1$. The relaxation time of the system can be chosen as $t_r = \bar{\mu}_b^{-1} \sim |\bar{\mu}_a|^{-1}$.

Weak noise leads to fluctuations about the attractor, which have Gaussian distribution near the maximum in the time range (4.3). From Eq. (4.4) this distribution has the form of Eq. (3.5), which we rewrite here as

$$\rho_a(q,t) = G\left(q - q_a(t); \sigma_a(t)\right), \tag{4.5}$$

with

$$G(x;\sigma) = (2\pi D\sigma^2)^{-1/2} \exp(-x^2/2D\sigma^2). \tag{4.6}$$

The variance $\sigma_a^2(t)$ is periodic in time. It is given by Eq. (3.6) with $i = a$.

4.2.2 Most probable escape paths

Along with small fluctuations, there also happen occasional large deviations from $q_a(t)$, including escape from the attraction basin. In a broad parameter range escape events are exponentially strongly synchronized with the modulation, see Ref. [111] and papers cited therein. Because large fluctuations have small probabilities, in escape the system closely follows the trajectory that is least improbable among all possible escape trajectories. As mentioned in the Introduction, it is usually called the most probable escape path, $q_{\rm opt}(t)$. Inside the attraction basin, escape trajectories lie within periodically repeated narrow tubes. The tubes have a width $\sim l_D$ and are centered at the MPEP's $q_{\rm opt}^{(n)}(t) \equiv q_{\rm opt}(t + n\tau_F)$, $n = 0, \pm 1, \ldots$.

As discussed in Sec. 3.4, the MPEP's provide a solution to the variational problem of maximizing the probability of a fluctuation in which the system moves from $q_a(t)$ to $q_b(t)$. This problem can be mapped onto the problem of dynamics of an auxiliary Hamiltonian system. The latter is described by the Wentzell-Freidlin Hamiltonian (3.17). Its equations of motion have the form (3.18).

The MPEP's correspond to the minimal action heteroclinic Hamiltonian trajectories $(q_{\rm opt}(t), p_{\rm opt}(t))$ [127, 129]. They start for $t \to -\infty$ at the periodic hyperbolic state $(q_a(t), p = 0)$ of the auxiliary system and for $t \to \infty$ approach its another periodic hyperbolic state, $(q_b(t), p = 0)$.

Well outside the diffusion regions around the periodic states $q_{a,b}(t)$ the motion along the MPEP is fast. It is seen from Eq. (3.18) that the system moves between these regions over time $t_{\rm r}$. Close to $q_b(t)$ the system is slowed down, and in the region $|q - q_b(t)| \lesssim l_D$ the motion is dominated by diffusion. The duration of staying in the vicinity of $q_b(t)$ can be obtained by linearizing the equation of motion (4.1) near q_b and is given by the Suzuki time $t_S \sim \bar{\mu}_b^{-1} \ln(\Delta q / l_D)$ [117, 130], where $\Delta q =$

$\min_t |q_b(t) - q_a(t)|$ is the typical distance between the periodic states.

Periodically modulated systems are advantageous as they allow one to observe, via the prehistory distribution, both the fast motion along the MPEP and the slow motion near the unstable state. As we show below, the peak of the PPD does not display broadening due to diffusion near q_b, as does the PPD in the absence of modulation [81].

4.3 Prehistory Probability Distribution near the basin boundary

We will calculate the PPD in the regime of strong synchronization of escape [110, 111]. In this regime the probability distribution $\rho(q,t)$ of finding a particle behind the basin boundary has the form of sharp periodic pulses as a function of t. It is most interesting to find the PPD for a final point (q_f, t_f) on the (q,t) plane near the center of such a pulse.

We will assume that the point (q_f, t_f) is sufficiently far from the diffusion-dominated layer (region B in Fig. 4.1) around the basin boundary, so that the distance to the boundary is $Q_f = q_f - q_b(t_f) \gg l_D$. This condition is usually realized in experiments, where the position of a particle detector is chosen so as to ensure that the detected particles have practically no chance to return to the attraction basin. At the same time we assume for convenience that the final point is still in the harmonic region, $Q_f \ll \Delta q$, in which case the motion between q_b and q_f can be described by linearizing equation (4.1) in $Q = q - q_b(t)$.

We will start the analysis of the PPD $p_h(q,t|q_f,t_f)$ with the case where not only q_f but also the point (q,t) through which the trajectory of interest has passed is also

in the harmonic region around the basin boundary $q_b(t)$.

4.3.1 Transition probability density

As seen from Eq. (4.2), finding the PPD requires calculating the transition probability density $\rho(q_f, t_f|q, t)$. The Fokker-Planck equation for $\rho(q_f, t_f|q, t)$ can be linearized near $q_b(t)$,

$$\partial_{t_f}\rho = -\mu_b(t_f)\partial_{Q_f}(Q_f\rho) + D\partial^2_{Q_f}\rho, \tag{4.7}$$

where $\rho = \rho(q_f, t_f|q, t)$ and $Q_f = q_f - q_b(t_f)$.

The solution of Eq. (4.7) can be sought in the form of a Gaussian distribution

$$\rho = G\left(Q_f - \tilde{Q}(t_f); \tilde{\sigma}(t_f)\right), \tag{4.8}$$

with $G(x;\sigma)$ given by Eq. (4.6). Substituting Eq. (4.8) into Eq. (4.7) we obtain

$$\frac{d\tilde{\sigma}^2}{dt_f} = 2\mu_b(t_f)\tilde{\sigma}^2 + 2, \quad \frac{d\tilde{Q}}{dt_f} = \mu_b(t_f)\tilde{Q}. \tag{4.9}$$

The initial conditions for these equations follow from the condition $\rho(q_f, t|q, t) = \delta(q_f - q)$. They have the form $\tilde{\sigma}^2(t) = 0$ and $\tilde{Q}(t) = Q = q - q_b(t)$. Then the solution of Eqs. (4.9) is

$$\begin{aligned}\tilde{\sigma}^2(t_f) &= 2\int_t^{t_f} d\tau\kappa_b^2(t_f, \tau),\\ \tilde{Q}(t_f) &= Q\kappa_b(t_f, t).\end{aligned} \tag{4.10}$$

Finally, using the function

$$\sigma_f^2(t_f, t) = \kappa_b^{-2}(t_f, t)\tilde{\sigma}^2(t_f) = 2\int_t^{t_f} d\tau\kappa_b^{-2}(\tau, t), \tag{4.11}$$

we can write the distribution in the form

$$\rho = \kappa_b^{-1}(t_f, t)G\left(Q - Q_f\kappa_b^{-1}(t_f, t); \sigma_f(t_f, t)\right). \tag{4.12}$$

The function $Q_f\kappa_b^{-1}(t_f,t)$ has a simple meaning. Consider the noise-free trajectory that passes through the point Q_f at time t_f. This trajectory should have passed through the point $Q_f\kappa_b^{-1}(t_f,t)$ at time t. As expected, the transition probability (4.12) is maximal for Q coinciding with this point.

The function σ_f^2, Eq. (4.11), is simply related to the function $\sigma_b^2(t)$, Eq. (3.6), introduced earlier,

$$\sigma_b^2(t) - \kappa_b^{-2}(t_f,t)\sigma_b^2(t_f) = \sigma_f^2(t_f,t). \tag{4.13}$$

We will broadly use this relation in what follows.

4.3.2 General expression for the PPD near $q_b(t)$

From Eq. (4.2), the PPD is determined by the product of the transition probability (4.12) and the ratio of the quasiperiodic distributions $\rho(q,t)/\rho(q_f,t_f)$. The distribution $\rho(q,t)$ close to $q_b(t)$ was found in Sec. 3.2.1. It has the form

$$\begin{aligned}
&\rho(q,t) = \int_0^\infty dp\, \rho'(p,Q,t), \qquad Q = q - q_b(t),\\
&\rho'(p,Q,t) = \frac{\mathcal{E}}{\sqrt{D}} \exp\left\{-\frac{1}{D}\left[\frac{p^2\sigma_b^2(t)}{2} + pQ + s(\phi)\right]\right\},\\
&\phi(p,t) = \Omega_F \ln\left[\frac{p\kappa_b(t,t')}{\bar{\mu}_b l_D}\right], \qquad \Omega_F = \omega_F/\bar{\mu}_b.
\end{aligned} \tag{4.14}$$

Here $\mathcal{E}$ and t' are constants, $s(\phi) = s(\phi + 2\pi)$ is a zero-mean 2π-periodic function, and Ω_F is the dimensionless modulation frequency.

The function $s(\phi)$ in Eq. (4.14) plays the role of an instantaneous modulation-induced change of the activation energy. In the regime of strong synchronization of escape the minimal value s_m of $s(\phi)$ satisfies the condition $|s_\mathrm{m}| \gg D$. The minima of $s(\phi)$ lie on the optimal escape paths (see Chapter 3), $p = p_\mathrm{opt}^{(n)}(t) \equiv p_\mathrm{opt}(t + n\tau_F)$. Here $n = 0, \pm 1, \ldots$ enumerates periodically repeated MPEP's, see Fig. 4.1(b); we set

$(q^{(0)}_{\rm opt}(t), p^{(0)}_{\rm opt}(t)) = (q_{\rm opt}(t), p_{\rm opt}(t))$.

Near the basin boundary $q_b(t)$ the optimal paths satisfy the linearized equations (3.18) and evolve in time as

$$p_{\rm opt}(t) = \kappa_b^{-1}(t,t')p_{\rm opt}(t'), \quad Q_{\rm opt}(t) = -\sigma_b^2(t)p_{\rm opt}(t),$$
$$Q_{\rm opt}(t) = q_{\rm opt}(t) - q_b(t), \quad |Q_{\rm opt}| \ll \Delta q. \tag{4.15}$$

Eq. (4.15) describes how a given optimal path approaches $(q_b(t), p = 0)$ for $t \to \infty$. The parameter t' is determined by matching to one of the periodically repeated trajectories (3.18) that start from $(q_a(t), p = 0)$ for $t \to -\infty$.

Expanding the function $s(\phi)$ around its minima at the periodically repeated MPEP's, to second order in $\phi(p,t) - \phi\big(p^{(n)}_{\rm opt}(t), t\big)$ we obtain the probability distribution (4.14) as a sum of contributions from the MPEP's,

$$\rho'(p,Q,t) = \frac{\mathcal{E}e^{-s_{\rm m}/D}}{\sqrt{D}} \sum_n \exp\left[-r^{(n)}(p,Q,t)/D\right],$$
$$r^{(n)} = pQ + \frac{p^2\sigma_b^2(t)}{2} + \frac{\Omega_F^2 s''_{\rm m}}{2} \ln^2\left[\frac{p}{p^{(n)}_{\rm opt}(t)}\right]. \tag{4.16}$$

Here $s''_{\rm m} \equiv (d^2s/d\phi^2)_{\rm m}$ is the curvature of the function s at the minimum. For strong synchronization, where $|s_{\rm m}| \gg D$, we have $s''_{\rm m} \gg D$ as well, which is a consequence of $s(\phi)$ being a zero-mean periodic function. The quantity $s''_{\rm m}$ can be found [110, 111], along with the constant $\mathcal{E}\exp(-s_{\rm m}/D)$, by matching the periodic distribution (4.14) to the distribution well inside the attraction basin.

It follows from Eq. (4.15) that near the basin boundary

$$p^{(n+k)}_{\rm opt}(t) = p^{(n)}_{\rm opt}(t + k\tau_F) = M_b^{-k} p^{(n)}_{\rm opt}(t). \tag{4.17}$$

With account taken of the relation $M_b = \exp(2\pi/\Omega_F)$, this leads to the expression

$$r^{(n+k)} = r^{(n)} + 2\pi k\Omega_F s''_{\rm m} \ln\left[\frac{p}{p^{(n)}_{\rm opt}(t)}\right] + 2\pi^2 k^2 s''_{\rm m}. \tag{4.18}$$

Combining Eqs. (4.12) and (4.16) we obtain for the PPD near the basin boundary,

$$\begin{aligned} & p_{h}(q,t|q_f,t_f) \\ & = \kappa_b^{-1}(t_f,t) G\left(Q - Q_f \kappa_b^{-1}(t_f,t); \sigma_f(t_f,t)\right) \\ & \times \frac{\sum_n \int_0^\infty dp \exp\left[-r^{(n)}(p,Q,t)/D\right]}{\sum_n \int_0^\infty dp \exp\left[-r^{(n)}(p,Q_f,t_f)/D\right]}. \end{aligned} \tag{4.19}$$

This expression gives the general form of the PPD near the basin boundary. We note that, even though the equations of motion near $q_b(t)$ can be linearized, the PPD is generally non-Gaussian. This distortion is an important feature of escape dynamics.

4.4 Adiabatic regime near the basin boundary

We start the analysis with the case of slow modulation, $\Omega_F \ll 1$, where the motion can be described in the adiabatic approximation. As we show below, in the adiabatic regime and for strong synchronization, $s''_{\rm m} \gg D$, only one term contributes to each of the sums in Eq. (4.19). The shape of the PPD in this case is determined by the parameter θ, Eq. (3.36), introduced in Sec. 3.5.

We call θ the distortion parameter. This is because, as shown in Sec. 3.5, for $\theta \ll 1$ the escape current has a form of Gaussian peaks, whereas for larger θ the peaks of the current become non-Gaussian. Formally, θ is equal to the ratio of two small parameters, the squared reduced modulation frequency $\omega_F/\bar{\mu}_b = \Omega_F$ and the reduced noise intensity $D/s''_{\rm m}$.

The physical meaning of θ can be understood in the following way. In the adiabatic picture one usually thinks of escape as occurring in the instantaneous potential $U(q,t)$. Most likely it happens once per period at the time $t_{\rm m}$ when the barrier height $\Delta U(t) = U(q_b(t),t) - U(q_a(t),t)$ is minimal, cf. Fig. 4.1. As explained in

the Introduction, the typical width of the time window for escape Δt is determined by the condition $[d^2\Delta U/dt^2]_{\rm m}(\Delta t)^2 = D$, where the subscript m indicates that the derivative is evaluated for $t = t_{\rm m}$. The parameter $s''_{\rm m}$ in the adiabatic approximation, as given by Eq. (3.33), is

$$s''_{\rm m} = [d^2\Delta U/dt^2]_{\rm m}/\Omega_F^2\mu_b^2(t_{\rm m}) \sim [d^2\Delta U/dt^2]_{\rm m}/\omega_F^2.$$

Therefore the parameter $\theta \sim [(\Delta t)^2\bar{\mu}_b^2]^{-1}$ is the squared ratio of the relaxation time of the system $t_{\rm r} = \bar{\mu}_b^{-1}$ to Δt. It shows whether the system moves fast enough to escape while the barrier remains at its minimum or the barrier noticeably changes during escape leading to a delay of escape with respect to $t_{\rm m}$ and a distortion of the tube of escape trajectories.

Because the PPD evolves over time $\sim t_{\rm r}$, of interest is the time range $|t - t_f| \lesssim t_{\rm r} \ll \tau_F$. Moreover, both t and t_f should be close to $t_{\rm m}$. Then the instantaneous relaxation rate $\mu_b(t)$ can be approximated by its value $\mu_{b\rm m} \equiv \mu_b(t_{\rm m})$. The functions κ_b and σ_f^2 become

$$\begin{aligned}
\kappa_{b\rm m}(t_f, t) &= \exp\left[\mu_{b\rm m}(t_f - t)\right], \\
\sigma_{f\rm m}^2(t_f, t) &= \sigma_{b\rm m}^2\left\{1 - \exp\left[-2\mu_{b\rm m}(t_f - t)\right]\right\},
\end{aligned} \tag{4.20}$$

where

$$\sigma_b^2(t) \approx \sigma_b^2(t_{\rm m}) \equiv \sigma_{b\rm m}^2 = 1/\mu_{b\rm m}.$$

4.4.1 Weak distortion, $\theta \ll 1$

We consider first the limit of weak distortion, $\theta \ll 1$ (more precisely, the weak distortion condition has the form $\theta \ln^2(s''_{\rm m}/D) \ll 1$, see below). In this limit one can think of motion in the fully adiabatic way, assuming that it occurs in a quasistatic

potential $U(q, t_{\rm m})$. The periodic distribution behind the attraction basin $\rho(q_f, t)$, which is proportional to the instantaneous escape rate, has a form of periodic in time Gaussian pulses, with width $\sim (D/s''_{\rm m})^{1/2}\tau_F$ [111].

For small θ expression (4.19) for the PPD can be simplified. We will start with the analysis of the denominator in this expression. If there were no term $\propto \Omega_F^2 s''_{\rm m}/D = \theta$ in $r^{(n)}(p, Q_f, t_f)/D$, the typical values of p contributing to the integral over p would be $\sim D/Q_f$. For such p there may be only one n for which the term $\theta \ln^2[p/p_{\rm opt}^{(n)}(t_f)]$ in $r^{(n)}/D$ is small, whereas for all other n it is $\propto s''_{\rm m}/D$ [cf. Eq. (4.18)], making the integrand exponentially small. A similar argument applies to the numerator in Eq. (4.19), except that, depending on Q, the typical values of p are of order of $(D/\mu_{b\rm m})^{1/2}$, D/Q, or $-\mu_{b\rm m}Q$.

Keeping only the leading term in the sums in the numerator and denominator of Eq. (4.19) and disregarding corrections $\propto \theta$, we obtain

$$p_h(q, t|q_f, t_f) = G\left(Q - Q_f\kappa_{b\rm m}^{-1}(t_f, t); \sigma_{f\rm m}(t_f, t)\right) \times \frac{Q_f\kappa_{b\rm m}^{-1}(t_f, t)}{\sqrt{2D\sigma_{b\rm m}^2}} \exp\left[\frac{Q^2}{2D\sigma_{b\rm m}^2}\right] \operatorname{erfc}\left[\frac{Q}{\sqrt{2D\sigma_{b\rm m}^2}}\right]. \tag{4.21}$$

In deriving this expression we also took into account that the final point q_f is sufficiently far from the diffusion-dominated region behind the basin boundary, $Q_f \gg l_D$, and disregarded corrections $\sim l_D^2/Q_f^2$. We note that the terms $\propto \theta$ in $r^{(n)}$ in the numerator and denominator in Eq. (4.19) have a logarithmic factor. This factor may become large in the weak-noise limit. One can show that for the corrections $\propto \theta$ to be small it is necessary that $\theta \ln^2(s''_{\rm m}/D) \ll 1$. This condition is equivalent to the inequality $\Delta t \gg t_S$, where Δt is the characteristic time window within which the barrier height is practically constant and t_S is the Suzuki, see Eq. (4.22) below.

Equation (4.21) for the PPD is further simplified for such times that the point

$Q_f \kappa_b^{-1}(t_f, t)$ is far behind the basin boundary compared to l_D. This is the point that the noise-free trajectory arriving at Q_f at time t_f passes at time t. For such t, the PPD as a function of Q has the form of a Gaussian peak with variance $D\sigma_f^2(t_f, t)$. This means that the trajectories arriving to the point Q_f are close to the noise-free trajectory. The tube of these trajectories is diffusion-broadened, with width $\propto [D(t_f - t)]^{1/2}$ for small $t_f - t$.

Because for $\theta \ll 1$ escape as a whole occurs in the quasistatic potential $U(q, t_{\rm m})$, the full calculation of the PPD described in Section 4.6 leads to the same result as in the case of escape in a stationary potential studied earlier [81]. With increasing $t_f - t$ the peak of the PPD (4.21) crosses the basin boundary and enters the attraction basin. This is the slowest part of the PPD evolution. Its duration is determined by the Suzuki time

$$t_S = t_{\rm r} \ln(s''_{\rm m}/D). \tag{4.22}$$

The peak is sharply broadened in this region. Deep on the intrawell side, $-Q \gg l_D$, the width of the peak becomes independent of D, i.e. parametrically larger than the diffusion-limited width $\sim l_D$. As $t_f - t$ increases further, the PPD peak approaches the attractor and narrows down, with the width becoming again diffusion-limited. This part of the evolution takes $\sim t_{\rm r}$.

4.4.2 Strong distortion, $\theta \gg 1$

The shape of the PPD near the maximum changes dramatically in the range where the modulation is still dynamically slow, $\Omega_F \ll 1$, but the distortion parameter θ becomes large, $\theta \gg 1$. Here, the shape of the potential barrier for escape changes as the particle crosses the diffusion region around the basin boundary. As a consequence, the pulses of escape current become strongly asymmetric, see Sec. 3.5. This leads to

a strong change of the PPD compared to the picture based on the quasistatic barrier that was discussed before.

For $\theta \gg 1$ in an important range of Q, t and Q_f, t_f the integrands in the numerator and denominator in Eq. (4.19) have sharp extrema as functions of p for $p = p_{\rm opt}^{(n)}$ (a more precise condition is specified below). Integration over p can be done by the steepest descent method. It gives the PPD in the form of a Gaussian distribution over Q with time-dependent center Q_{n_0} and variance $D\sigma_f^2$,

$$p_h(q,t|q_f,t_f) = G\left(Q - Q_{n_0}; \sigma_f(t_f,t)\right), \tag{4.23}$$

where

$$Q_n \equiv Q_n(t|q_f,t_f) = Q_{\rm opt}^{(n)}(t) + \left(Q_f - Q_{\rm opt}^{(n)}(t_f)\right)\kappa_b^{-1}(t_f,t) \tag{4.24}$$

and $n_0 \equiv n_0(q_f,t_f)$. Here we have taken into account that the major contribution to each of the sums in Eq. (4.19) comes from one term, with $n = n_0$.

It is clear from the analysis of the denominator in Eq. (4.19) that the value of n_0 is determined by the condition that $p_{\rm opt}^{(n_0)}(t_f)Q_f/D \sim 1$ for the n_0th optimal path. The very existence of such n_0 follows from the fact that we consider t_f for which the probability density $\rho(q_f,t_f)$ is close to its maximum over t_f; this maximum is reached once per period for $p_{\rm opt}^{(n)}(t_f)Q_f/D = 1$ [110, 111]. The terms with $|n - n_0| \geq 1$ in the denominator in Eq. (4.19) are

$$\propto M_b^{n_0-n}\exp\left(-M_b^{n_0-n}\right) \ll 1$$

where we have used $M_b = \exp(2\pi/\Omega_F) \gg 1$ (this estimate is written for $p_{\rm opt}^{(n_0)}(t_f)Q_f/D = 1$).

A simple qualitative argument shows that the same n_0 gives a major contribution to the sum in the numerator of Eq. (4.19) in the adiabatic regime. Indeed, the terms

with different n correspond to t changing by an integer number of the modulation periods τ_F, whereas in its central part (section C in Fig. 4.1) an optimal escape trajectory lasts for the time small compared to τ_F for adiabatic modulation. Therefore $|t - t_f| \ll \tau_F$. The formal condition for this approximation to be true is that the Suzuki time t_S (4.22) is small compared to the modulation period.

The maximum of the Gaussian PPD peak (4.23) lies at $Q_{n_0}(t|q_f, t_f)$. This function is a sum of the optimal path $Q^{(n)}_{\rm opt}$, which is located inside the attraction basin, and the decaying in time term $\propto Q_f - Q^{(n)}_{\rm opt}(t_f)$, which is determined by the final point (q_f, t_f) and is located outside the attraction basin. Its time dependence is particularly simple in the case where t_f corresponds to the maximum of the distribution $\rho(q_f, t_f)$, i.e., $p^{(n_0)}_{\rm opt}(t_f) = D/Q_f$,

$$Q_{n_0}(t|Q_f, t_f) \approx Q_f e^{-\mu_{\rm bm}(t_f - t)} - \frac{D}{\mu_{\rm bm} Q_f} e^{\mu_{\rm bm}(t_f - t)}. \tag{4.25}$$

The first term in Q_{n_0}, Eq. (4.25), decreases with increasing $t_f - t$, which describes

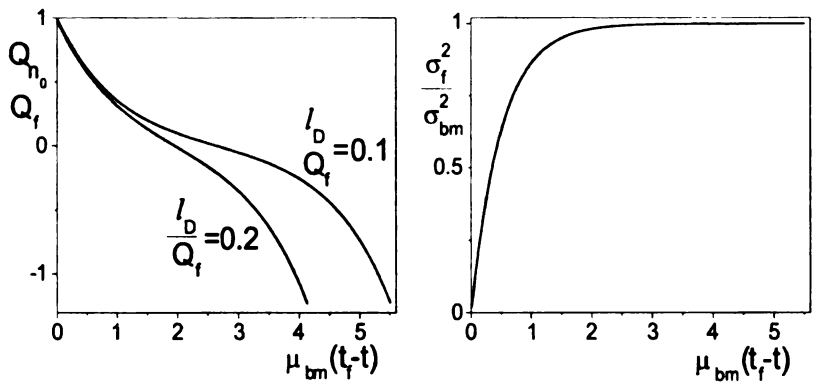

Figure 4.3: The reduced position of the maximum (left) and the reduced width (right) of the PPD (4.23) in the adiabatic regime as a function of the reduced time $\mu_{\rm bm}(t_f - t)$.

approaching the basin boundary backward in time. The second term, on the other hand, increases with $t_f - t$; this term describes the motion, backward in time, from

the boundary to the interior of the attraction basin. The motion at the boundary is initiated by noise, and therefore this term is $\propto D$. For sufficiently long $t_f - t$ the distribution maximum Q_{n_0} approaches the optimal path $Q_{\rm opt}^{(n_0)}(t)$. The overall behavior of Q_{n_0} is shown in Fig. 4.3. It is seen that the motion is slowed down near the basin boundary, and the slowing down strongly depends on the noise intensity, in agreement with Eq. (4.25).

The width of the Gaussian PPD peak (4.23) is diffusion-limited; its time dependence is given by Eq. (4.20) and is also simple. It is shown in the right panel of Fig. 4.3.

The condition that the integrands over p in Eq. (4.19) are maximal for $p_{\rm opt}^{(n_0)}$ imposes a limitation on Q where the explicit expression for the PPD (4.23) applies. For Q close to the maximum of the distribution, $|Q - Q_{n_0}| \lesssim l_D$, this condition takes the form $\theta \gg |Q_{\rm opt}^{(n_0)}(t)/l_D|$. Therefore expression (4.23) describes the distribution not only in the whole range between (Q_f, t_f) and the basin boundary, but also throughout the diffusion region around the basin boundary and a region that goes deeper into the attraction basin.

4.5 Nonadiabatic regime near the basin boundary

The PPD can display a qualitatively different behavior for nonadiabatic modulation, $\Omega_F \sim 1$. With increasing $t_f - t$ the PPD inside the attraction basin can split into several peaks. Such splitting occurs already close to the basin boundary and is described by the general expression (4.19). Formally, the PPD has well-resolved multiple peaks when several terms in the numerator of Eq. (4.19) are of the same order of magnitude.

In the nonadiabatic regime necessarily $\theta \gg 1$. Therefore integration over p in

Eq. (4.19) can be done by the steepest descent method. The integrands are maximal for $p = p_{\rm opt}^{(n)}$. Each term in the numerator gives a Gaussian distribution over Q centered at $Q_n \equiv Q_n(t|q_f, t_f)$, Eq. (4.24), with variance $D\sigma_f^2(t_f, t)$, Eq. (4.11). This is similar to the adiabatic case (4.23), except that now the PPD is a sum of appropriately weighted Gaussian peaks,

$$p_h(q, t|q_f, t_f) = \frac{\sum_n B_n G\left(Q - Q_n; \sigma_f(t_f, t)\right)}{\sum_n B_n}. \tag{4.26}$$

The weighting factors B_n are

$$\begin{aligned} B_n &\equiv B_n(q_f, t_f) = x_n \exp(-x_n), \\ x_n &= x_n(q_f, t_f) = p_{\rm opt}^{(n)}(t_f) Q_f / D. \end{aligned} \tag{4.27}$$

If we keep only one term in the numerator and denominator in Eq. (4.26), with the same $n = n_0$ given by the condition that B_n is maximal for $n = n_0$, Eq. (4.26) goes over into Eq. (4.23). However, in the nonadiabatic case there are regimes where the PPD as a function of (Q, t) may display several peaks. Eq. (4.26) gives their shapes near the maxima.

The number of peaks of p_h depends on Q, t, and Ω_F, as well as the final point (q_f, t_f). As before, we choose the final point so that the probability density behind the basin boundary $\rho(q_f, t_f)$ is close to its maximum over t_f, which occurs for $x_{n_0}(q_f, t_f) \sim 1$. The amplitudes of different peaks are

$$B_{n_0+k} = x_{n_0} M_b^{-k} \exp\left(-x_{n_0} M_b^{-k}\right), \tag{4.28}$$

with $M_b = \exp(2\pi/\Omega_F)$ being the Floquet multiplier, Eq. (3.4). In practice, in the whole range of modulation parameters where escape is strongly synchronized the factor M_b is comparatively large. Therefore for $x_{n_0} \sim 1$ the coefficients B_{n_0+k} rapidly

decay with increasing $|k|$, and only few peaks of the PPD can be simultaneously observed, primarily with non-negative $k = 0, 1, \ldots$.

The other condition for observing several peaks is that the distance between them exceed their width, that is in particular $|Q_{n_0} - Q_{n_0+1}| \gg l_D$. For $Q \approx Q_{n_0} \gg l_D$, i.e., when the PPD maximum is well behind the basin boundary with respect to the attraction basin, we have $|Q_{n_0} - Q_{n_0+1}| \sim |Q_{\rm opt}^{(n_0)}(t)| \sim l_D^2 \kappa_b(t_f, t)/Q_f \ll l_D$, where we have used that $Q_f \gg l_D$ and that $\kappa_b(t_f, t) \sim 1$ when the PPD maximum is behind the boundary. Therefore in this region the PPD has indeed only one peak.

For longer $t_f - t$ when $\kappa_b(t_f, t) \gg 1$ and the peak positions Q_{n_0}, Q_{n_0+1} are well inside the basin of attraction, the distance between them exceeds l_D. In this range the corresponding peaks of p_h can be resolved. The ratio of their amplitudes is given by the factor M_b, as seen from Eq. (4.28). This is in good agreement with the results of numerical simulations for a specific model shown in Fig. 4.2, as will be discussed below.

We note that for $\Omega_F \gg 1$ synchronization of escape by modulation becomes exponentially weak. Although the system is far from the adiabatic limit, dynamics of the period-average coordinate is similar to dynamics in the case of a stationary system. Even though the factor M_b becomes of order 1, of interest is the PPD with respect to the period-averaged coordinate, and this PPD does not display multiple peaks.

4.6 The PPD inside the attraction basin

We assume throughout this Section that escape is strongly synchronized and $\theta \gg 1$. To find the PPD for (q,t) deep inside the attraction basin we will use the equation

$$p_h(q,t|q_f,t_f) = \int dq' p_h(q,t|q',t') p_h(q',t'|q_f,t_f). \tag{4.29}$$

It applies for $t < t' < t_f$, as follows from the definition (4.2), and can be obtained [81] from the Chapman-Kolmogorov equation for the transition probability $\rho(q_f,t_f|q,t)$.

As we show, t' in Eq. (4.29) can be chosen in such a way that only a narrow range of q' contributes to the integral. The corresponding q' are close but not too close to $q_b(t')$. In this range both factors in the integrand, and hence the integral as a whole, can be explicitly calculated. In particular, the function $p_h(q',t'|q_f,t_f)$ is given by Eq. (4.26).

The function $p_h(q,t|q',t')$ is the PPD inside the attraction basin. For a periodically modulated system it was found earlier [131]. Because in escape the system is likely to move close to one of the periodically repeated most probable escape paths $q_{\rm opt}^{(n)}(t)$, we are interested in $p_h(q,t|q',t')$ for both (q,t) and (q',t') lying close to such a path. If both (q,t) and (q',t') are close to an nth path $q_{\rm opt}^{(n)}(t)$, the corresponding PPD $p_h^{(n)}(q,t|q',t')$ is Gaussian [131],

$$p_h^{(n)}(q,t|q',t') = G\big(q - q_n(t|q',t');\sigma_n(t',t)\big) \tag{4.30}$$

Here $q_n(t|q',t')$ is the value of the coordinate at time t on the optimal path that leads to the point (q',t'). This optimal path is described by Eq. (3.18).

The coordinate $q_n(t|q',t')$ as a function of time is close to $q_{\rm opt}^{(n)}(t)$. We can seek it in the form $q_n(t|q',t') = q_{\rm opt}^{(n)}(t) + \delta q_n(t|q',t')$. To the lowest order in the deviation of (q',t') from $q_{\rm opt}^{(n)}(t')$, the function δq_n can be found from linearized equations (3.18).

This gives

$$\delta\ddot{q}_n = V_n(t)\delta q_n, \tag{4.31}$$
$$V_n(t) = \left[\partial_{qt}K + \frac{1}{2}\partial_{qq}(K^2)\right]_{q_{\rm opt}^{(n)}(t)}.$$

The boundary conditions for δq_n are $\delta q_n(t'|q',t') = q' - q_{\rm opt}^{(n)}(t')$ and $\lim_{t\to-\infty}\delta q_n(t|q',t') = 0$; the latter condition simply means that the optimal path approaches the attractor $q_a(t)$ as $t \to -\infty$.

It follows from Eq. (4.31) that function $\beta_n(t) = \delta\dot{q}_n/\delta q_n$ satisfies a first-order (Riccati) equation,

$$\dot{\beta}_n + \beta_n^2 = V_n(t). \tag{4.32}$$

For $q', q_{\rm opt}^{(n)}(t')$ both close to the basin boundary $q_b(t')$, with account taken of the boundary conditions for δq_n the solution of Eq. (4.31) can be written in terms of β_n as

$$\delta q_n(t|q',t') = \left(Q' - Q_{\rm opt}^{(n)}(t')\right)\kappa_n(t,t'), \tag{4.33}$$

where

$$\kappa_n(t,t') = \exp\left[\int_{t'}^{t} d\tau\beta_n(\tau)\right]. \tag{4.34}$$

We now discuss the asymptotic behavior of $\beta_n(t)$. For not too large $t'-t$ the function $V_n(t)$ in Eqs. (4.31), (4.32) should be calculated for $q_{\rm opt}^{(n)}(t) \approx q_b(t)$. For such $V_n(t)$, the solution $\delta q_n(t)$ of Eq. (4.31) can either exponentially increase or decrease with increasing $t'-t$. Of interest to us is the decreasing solution, which will ultimately go to zero for $t'-t \to \infty$. A simple calculation shows that for this solution

$$\beta_n(t) \approx \mu_b(t) \equiv [\partial_q K]_{q_b(t)}, \qquad q_{\rm opt}^{(n)}(t) \approx q_b(t).$$

For much larger $t'-t$ the optimal path $q_{\rm opt}^{(n)}(t)$ approaches the attractor $q_a(t)$, and then the function $V_n(t)$ in Eqs. (4.31), (4.32) should be calculated for $q_{\rm opt}^{(n)}(t) \approx q_a(t)$.

One can show that the solution $\delta q_n(t) \to 0$ for $t \to -\infty$ corresponds to

$$\beta_n(t) \approx \mu_a(t) + 2\sigma_a^{-2}(t), \qquad q_{\rm opt}^{(n)}(t) \approx q_a(t),$$

where $\sigma_a^2(t)$ is the variance of the periodic distribution about the attractor given by Eq. (3.6).

To the lowest order in $q' - q_{\rm opt}^{(n)}(t')$, the variance of the prehistory probability distribution (4.30) is also expressed in terms of the function β_n [131],

$$\sigma_n^2(t', t) = 2\int_t^{t'} d\tau \kappa_n^{-2}(\tau, t). \tag{4.35}$$

Using Eqs. (4.32), (4.34), and (4.35) one can show that $\sigma_n^2(t', t \to -\infty) = \sigma_a^2(t)$. For $t \to -\infty$ the distribution $p_h^{(n)}(q, t|q', t')$ goes over into the periodic Gaussian distribution $\rho_a(q, t)$, Eq. (4.5), centered at the periodic attractor.

It follows from Eqs. (4.30)-(4.33) that, for q close to $q_{\rm opt}^{(n)}(t)$, the PPD $p_h^{(n)}(q, t|q', t')$ displays a diffusion-broadened Gaussian peak as a function of q' with maximum close to $q_{\rm opt}^{(n)}(t')$. The displacement of the maximum over q' from $q_{\rm opt}^{(n)}(t')$ is $\propto [q - q_{\rm opt}^{(n)}(t)]$. On the other hand, the function $p_h(q', t'|q_f, t_f)$ as given by Eq. (4.26) is a sum of Gaussian distributions centered at the optimal escape paths. Therefore integration over q' in Eq. (4.29) can be done by the steepest descent method. The extreme values of q' are also close to the optimal escape paths.

Different peaks of the PPD $p_h(q', t'|q_f, t_f)$, Eq. (4.26), correspond to the MPEP's shifted by an integer number of modulation periods. For each of these peaks one should use in Eq. (4.29) the PPD $p_h(q, t|q't')$ given by $p_h^{(n)}$ with the appropriate n.

The result of integration over q' describes the peaks of the PPD $p_h(q, t|q_f, t_f)$ for q close to $q_{\rm opt}^{(n)}(t)$ with appropriate n. These peaks are Gaussian near the maxima,

$$p_h(q, t|q_f, t_f) = \frac{1}{\sum_n B_n} \sum_n B_n G\left(q - q_{\rm opt}^{(n)}(t) - \left(Q_f - Q_{\rm opt}^{(n)}(t_f)\right) \kappa_n^{-1}(t_f, t); \sigma_n(t_f, t)\right). \tag{4.36}$$

[Here $B_n \equiv B_n(q_f, t_f)$ are given by Eq. (4.27).] In obtaining this equation we used the relations

$$\kappa_b(t_f, t')\kappa_n(t', t) = \kappa_n(t_f, t),$$
$$\sigma_n^2(t', t) + \sigma_f^2(t_f, t')\kappa_n^{-2}(t', t) = \sigma_n^2(t_f, t),$$

which in turn follow from the relation $\beta_n(t) \approx \mu_b(t)$ in the harmonic region near the basin boundary. As a consequence, the result of integration over q' in Eq. (4.29) is independent of the matching time t'.

Equation (4.36) is the central result of this Chapter. It gives, in the explicit form, the PPD of finding the system at a position q inside the attraction basin at a moment t, provided the system has been observed at a point q_f outside the attraction basin at a time $t_f > t$. It shows that, in the regime of strong synchronization, the peaks are Gaussian. They are centered at the most probable escape paths and are diffusion broadened throughout the attraction basin. This is in dramatic contrast with the PPD in the absence of synchronization, where the PPD peak inside the attraction basin is strongly asymmetric and its width is independent of the noise intensity D [81].

It follows from Eq. (4.36) that the PPD may have multiple peaks inside the attraction basin. They can be observed only for strongly nonadiabatic modulation, where the Suzuki time is $t_S \gtrsim \tau_F$. In this case the system stays in the diffusion layer around the basin boundary $q_b(t)$ long enough to accumulate influxes from several periodically repeated most probable escape paths $q_{\rm opt}^{(n)}(t)$. On the other hand, the modulation period τ_F should not be too short, because the exponential synchronization of escape would be lost. Since synchronization loss occurs for $t_{\rm r} \gg \tau_F$, the PPD displays well resolved multiple peaks only in a limited parameter range. The limitation is more re-

strictive to the considered case where the final point (q_f, t_f) is close to the maximum of the distribution behind the barrier. If this condition is not imposed, the peaks are well resolved in a broader range, but measuring the PPD becomes more complicated on the whole. An example is discussed in the next Section.

An important feature of the distribution (4.36) is weak dependence of the shape of the Gaussian peaks inside the attraction basin on the final point (q_f, t_f), which is a consequence of the smallness of the factor $\kappa_n^{-1}(t_f, t)$. This shows that the PPD reveals the actual structure of the tubes of the paths followed in escape inside the attraction basin. In contrast, the relative amplitudes of the PPD peaks B_n are sensitive to the choice of the point (q_f, t_f).

4.7 Results for a model system

In this section, we present the results of numerical simulations of the PPD for a simple model system and compare them with the analytical predictions. We consider a Brownian particle in a sinusoidally modulated potential of the form of a cubic parabola. The Langevin equation of motion has the form of Eq. (4.1) with

$$K(q,t) = q^2 - \frac{1}{4} + A\cos(\omega_F t). \tag{4.37}$$

The dynamics was simulated using the second-order integration scheme for stochastic differential equations [107]. The system was initially prepared in the vicinity of the metastable state $q_a(t)$. The final point (q_f, t_f) was chosen behind the basin boundary $q_b(t)$. The PPD was calculated as a normalized probability distribution of paths $q(t)$ arriving at the point q_f for a particular modulation phase $\phi_f = \omega_F t_f (\mathrm{mod}\, 2\pi)$.

An example of the full PPD is shown in Fig. 4.2. The point (q_f, t_f) is chosen

so that in escape the system is likely to pass near it (t_f is determined mod τ_F), that is the quasistationary distribution $\rho(q_f, t_f)$ is close to its maximum over t_f for a given q_f behind the basin boundary [the parameter $p_{\rm opt}^{(n_0)}(t_f)[q_f - q_b(t_f)]/D$ is equal to 1.2, whereas the maximum of $\rho(q_f, t_f)$ is expected where this parameter is equal to 1, [111]]. For the chosen modulation parameters and noise intensity the calculated activation energy of escape is $R \approx 0.0910$ and $R/D \approx 9.1$; the ratio of the modulation frequency to the relaxation rate $\Omega_F \approx 2.24$. We accumulated $\sim 10^5$ escape trajectories that arrive into a small area centered at (q_f, t_f), with width $\delta q = 0.02, \delta t = 0.02\tau_F$.

It is seen from Fig. 4.2 that, in the regime of strong synchronization and for strongly non-Gaussian pulses of escape current, the peaks of the PPD are narrow both behind the basin boundary and inside the attraction basin. Moreover, for the chosen parameter values two distinct peaks of the PPD are well resolved inside the attraction basin. They correspond to the two paths the system is most likely to follow in escape.

The positions of the PPD peaks on (q, t) plane are shown in Fig. 4.4 with full squares where there is one peak, and with crosses where two peaks are well resolved. They are compared with the periodically repeated optimal escape paths calculated by solving numerically the variational equations (3.18) for the model (4.1), (4.37). Such paths start from the periodic attractor $q_a(t)$ for $t \to -\infty$ and approach the basin boundary $q_b(t)$ for $t \to \infty$, which are also shown in the figure. It is seen that, as expected from our analysis, the PPD maxima lie nearly on top of the most probable escape paths. The small deviation is due to diffusion broadening and associated small asymmetry of the PPD peaks for the noise intensity used in the simulations. Fig. 4.4 demonstrates that studying the PPD provides a direct way of observing most probable

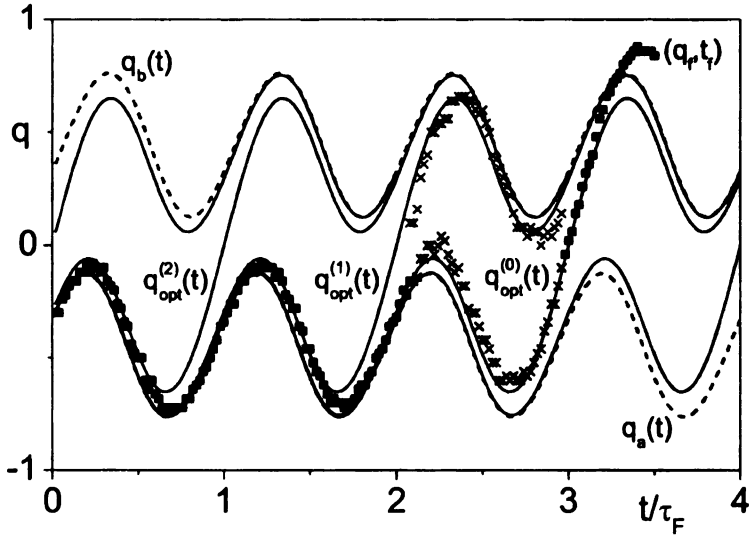

Figure 4.4: The positions of the maxima of the PPD $p_h(q,t|q_f,t_f)$ in Fig. 4.2, which show the most probable paths followed by the system in escape. The data of simulations are shown by full squares where the PPD has one peak and by crosses where two peaks are well resolved. Solid lines show periodically repeated most probable escape paths $q^{(n)}_{\rm opt}(t)$ for the model (4.1), (4.37). Dashed lines show the basin boundary $q_b(t)$ and the attractor $q_a(t)$.

escape paths.

The observed shape of the PPD peaks is compared with the theory in Fig. 4.5, which shows the cross-sections of the PPD at several instants of time counted off from the final time t_f. For small $t_f - t$ the system is behind the basin boundary and moves close to the noise-free trajectory leading to (q_f, t_f) . The top left panel refers to the case where the system is localized close to the boundary. Here and for smaller $t_f - t$ the PPD has a single sharp peak.

For earlier time (larger $t_f - t$) the system could either be moving towards the basin boundary along the most probable escape path or could have been fluctuating about the basin boundary after it had arrived to its vicinity along the previous MPEP (shifted by τ_F). As we showed analytically, the probability of staying near

the boundary is smaller, but the PPD may still display two peaks. This is seen in the right top panel. The main peak corresponds to motion along the MPEP, which is close to $q_b(t)$ for the chosen time. The higher-q shoulder corresponds to the poorly resolved (for the chosen time) peak for fluctuations about the basin boundary.

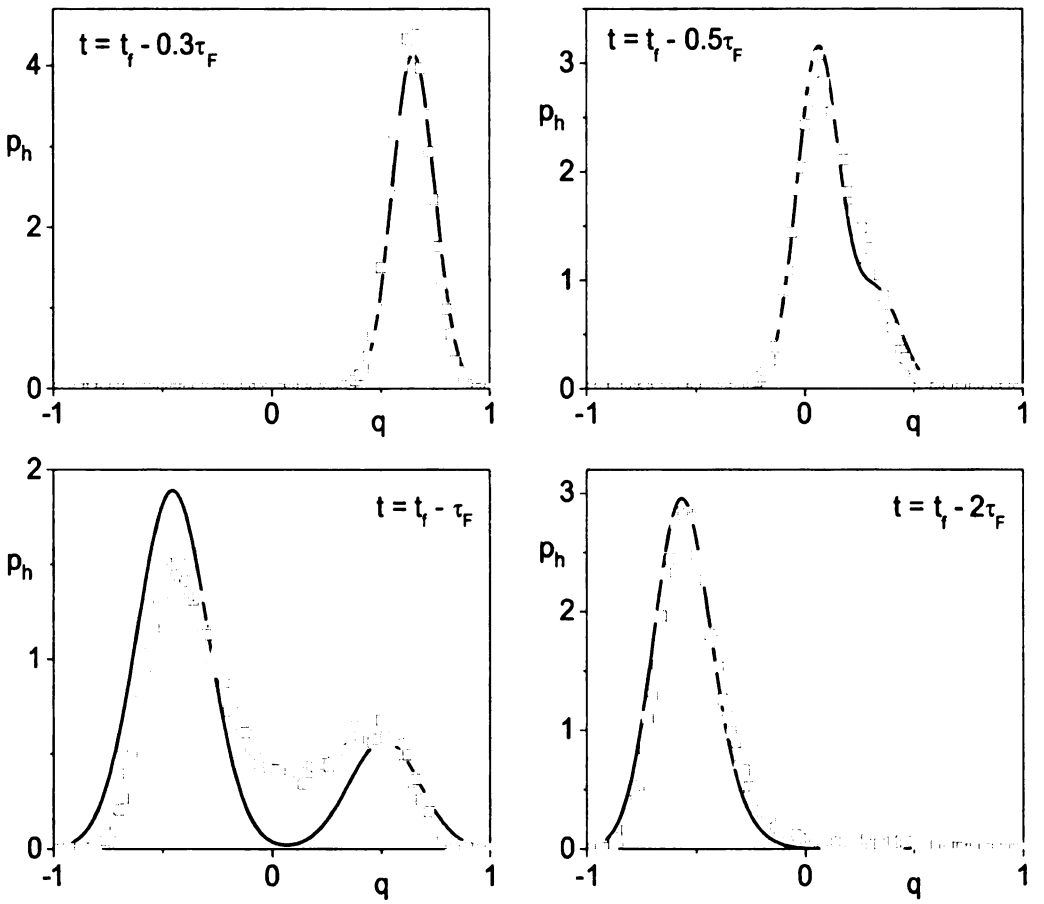

Figure 4.5: Cross-sections of the PPD $p_h(q,t|q_f,t_f)$ shown in Fig. 4.2 as functions of the coordinate q for the time $t_f - t = 0.3\tau_F, 0.5\tau_F, \tau_F, 2\tau_F$. The results refer to the model system (4.1), (4.37) with $A = 0.7$, $\omega_F = 2$, $D = 0.01$, $q_f = 0.8$, $t_f = 0.5\tau_F$. The point (q_f, t_f) is close to the expected maximum of the distribution behind the basin boundary. Solid lines show the expression (4.36). Squares show the results of simulations.

For still larger but not too large $t_f - t$ the escaping system should have been

moving towards the basin boundary. In the present case it most likely followed one of the two periodically repeated MPEPs, with different probabilities. Well-resolved peaks of the PPD in this range are seen in the left lower panel of Fig. 4.5. For large $t_f - t$ compared to the relaxation time and τ_F, the system should have been fluctuating about the attractor $q_a(t)$. The PPD in this case should have a single peak, which is seen in the right lower panel.

It is seen from Fig. 4.5 that the results of simulations agree with the analytical results. Not surprisingly, the observed peaks are broader than the asymptotic theory predicts. This is a consequence of the relatively large noise intensity used in the simulations.

4.8 Conclusions

In this Chapter we have studied the prehistory probability distribution for activated escape in periodically modulated systems. We have shown that the PPD can display one or several narrow peaks within the basin of attraction to the metastable state. The peaks are located at the periodically repeated most probable escape paths. They are Gaussian near the maxima and are diffusion broadened, see Eq. (4.36).

The number of peaks that can be observed depends on the parameters of the system. The multipeak structure is best resolved in a limited parameter range. On the one hand, the modulation should not be too slow, so that the system does not follow it adiabatically. On the other hand, it should not be too fast, so that escape events are strongly synchronized and the system dynamics is not described by period-averaged coordinates.

Most of the results refer to the case where the final point (q_f, t_f) is chosen so

that the escaped system has a high probability density of passing through this point. Such choice simplifies the experimental observation of the PPD. For the corresponding (q_f, t_f) the amplitudes of different peaks of the PPD differ from each other significantly, as seen from Eq. (4.28). These amplitudes are sensitive to the choice of (q_f, t_f). In contrast, the positions and shapes of the PPD peaks very weakly depend on (q_f, t_f). This shows that the PPD provides a means for studying the distribution of trajectories leading to escape.

We have performed extensive numerical simulations of escape of a Brownian particle from a model modulated metastable potential. The simulations confirmed the possibility to clearly observe most probable escape paths. They are in a good qualitative and quantitative agreement with the analytical theory.

Observing most probable escape paths is interesting from several points of view. First, periodically modulated systems are far from thermal equilibrium. In contrast to the case of systems in equilibrium, most probable escape paths in nonequilibrium systems have no immediate relation to dynamical trajectories in the absence of noise and display interesting and often counterintuitive behavior [132]. Therefore observing escape paths has broad implications. Second, understanding the dynamics of a system in escape enables efficient control of this dynamics and the escape probability by applying a control field in the right place and at the right time.

In conclusion, the results of this Chapter suggest a way of direct observation of most probable escape paths, in space and time. They also describe, qualitatively and quantitatively, the distribution of the trajectories followed in escape.

Chapter 5

Conclusions

While it is generally understood how escape happens in equilibrium, it is still largely an open question for systems away from equilibrium, such as those modulated by time-dependent fields. In this thesis we have established previously unknown universal features of activated escape in nonequilibrium systems. In particular we investigated scaling of the activation energy and the pre-exponential factor of the escape rate near a bifurcation point, time dependence of the escape current, and dynamics of escape pathways in periodically modulated systems.

In equilibrium systems, the rate of noise-induced activated escape from a metastable state is $W \propto \exp(-R/D)$, where R is the activation energy, and D is the noise intensity. For thermal fluctuations $D = k_B T$ and the activation energy R is given by the height of the free energy barrier. When the system approaches a saddle-node bifurcation point (spinodal point) where the energy barrier disappears, the activation energy scales as $R \propto |A - A_c|^{\xi}$, with $\xi = 3/2$. Here A is the control parameter, e.g. the strength of the applied DC field, and A_c is the critical value of A. This scaling is related to the universality of critical dynamics near the bifurcation point, where the effective potential becomes locally cubic.

In periodically modulated systems, the period-averaged escape rate has a similar form, $\overline{W} \propto \exp(-R/D)$, but the activation energy R is not equal to the barrier height. The most interesting and unexpected scaling behavior is displayed for sufficiently slow modulation, where dynamics away from the critical point can be well described in the adiabatic approximation. Due to the critical slowing down, the adiabatic approximation necessarily breaks down close to $A = A_c$. As we have shown, this breakdown of adiabaticity occurs in a universal way. Sufficiently far from A_c the adiabatic scaling with $\xi = 3/2$ is observed. For smaller $|A_c - A|$ there emerges a new dynamical time scale and a new, locally nonadiabatic scaling of the activation energy with $\xi = 2$. For even smaller $|A_c - A|$ the exponent goes back to $\xi = 3/2$. Thus, scaling of the activation energy in periodically modulated systems involves crossovers between three scaling exponents $\xi = 3/2, 2, 3/2$ instead of a single exponent $\xi = 3/2$ in the equilibrium case. The widths of the three regions with different scaling depend on the modulation frequency. The new dynamical scaling with $\xi = 2$ is a consequence of nonadiabatic retardation effects and has no analogue in equilibrium systems.

The full escape rate in equilibrium is independent of time and has the form $W = \nu \exp(-R/D)$, where the prefactor ν is given by the generalized "attempt frequency" in the metastable potential well. In periodically modulated systems escape rate $W(t)$ is a periodic function of time. It is given by the current $j(q,t)$ away from the metastable state, which also depends on the position q where it is measured. It is physically meaningful to measure the current sufficiently far behind the boundary of the basin of attraction to the metastable state.

We calculate the escape current using the eikonal approximation and methods of nonlinear Hamiltonian dynamics and matched expansions. We identify a single parameter θ that determines the shape of the periodic pulses of the escape current

as functions of time. It depends on both the strength and the frequency of the modulation and is given by the ratio of two small parameters, the scaled modulation frequency and the scaled noise intensity. In the limit of adiabatically slow modulation or small $|A-A_c|$ we have $\theta \ll 1$, and the current pulses have Gaussian shape with the width much smaller than the modulation period. For $\theta \gg 1$ the pulses are strongly non-Gaussian and asymmetric.

The method developed for the analysis of the instantaneous escape rate made it possible to find the prefactor ν of the period-averaged escape rate and analyze it close to the bifurcation point $A = A_c$ where the periodic metastable state disappears. We have found that the prefactor displays three regions of system-independent scaling corresponding to the scaling regions of the activation energy, with $\nu \propto |A - A_c|^{\zeta}$. The scaling exponents are $\zeta = 1/4, -1, 1/2$. The exponent $\zeta = 1/4$ can be observed for sufficiently slow modulation not too close to the bifurcation point. The negative exponent $\zeta = -1$ is a consequence of the onset of local nonadiabaticity, which leads to the exponent $\xi = 2$ for the activation energy. The exponent $\zeta = 1/2$ can be observed for fast modulation or very close to the bifurcation point.

One of important questions regarding fluctuating systems is how a fluctuation evolves in time. For instance, if we find a system at a phase-space point far away from equilibrium it might be of interest to know how the system was moving on the way to this point. This knowledge gives one the power to control fluctuations in the system, e.g. to increase or suppress the probability to visit certain areas of the phase space by applying external fields. Control of infrequent events such as escape from a metastable state is facilitated by the fact that, in fluctuations leading to such events the system is most likely to follow a certain dynamical path. Fluctuational trajectories form a narrow tube centered at this path. We have developed a formalism

for studying these tubes in periodically modulated systems. We found, and confirmed by detailed simulations that, in contrast to stationary systems, periodically modulated systems can exhibit several tubes of trajectories leading to escape at a given time. The tubes have specific shapes and intensities, which we have described analytically. The spatial and temporal localization of the trajectories suggests the ways of optimal and selective control of escape events.

APPENDICES

Appendix A

Variational equations for the escape problem

We will consider here the optimal trajectory that the system is most likely to follow in escape, $\mathbf{q}_{\rm opt}(t)$, and the random force $\mathbf{f}_{\rm opt}(t)$ that drives the system during this motion. The trajectories $\mathbf{q}_{\rm opt}(t), \mathbf{f}_{\rm opt}(t)$ provide the absolute minimum to the functional $\mathcal{R}[\mathbf{q}, \mathbf{f}]$ (2.9). The variational equations have the form

$$\int dt' \hat{\mathcal{F}}(t-t')\,\mathbf{f}(t') - \boldsymbol{\lambda}(t) = \mathbf{0}, \tag{A.1}$$

$$\dot{\boldsymbol{\lambda}} = -\boldsymbol{\nabla}(\boldsymbol{\lambda}\cdot\mathbf{K}), \tag{A.2}$$

$$\dot{\mathbf{q}} - \mathbf{K}(\mathbf{q}; A, t) - \mathbf{f}(t) = \mathbf{0} \tag{A.3}$$

(here and below we use the hat to indicate a matrix; $\boldsymbol{\nabla} \equiv \partial/\partial\mathbf{q}$).

From Eqs. (2.7) and (A.1) it follows that the optimal noise realization is expressed in terms of the Lagrange multiplier $\boldsymbol{\lambda}$ and the matrix of the noise correlation functions $\hat{\varphi}$ (2.3) as

$$\mathbf{f}_{\rm opt} = D^{-1} \int dt' \hat{\varphi}(t-t')\,\boldsymbol{\lambda}(t'). \tag{A.4}$$

Therefore, for the optimal path, the activation energy functional (2.6) is

$$\mathcal{R} = \frac{1}{2} D^{-1} \iint dt dt' \boldsymbol{\lambda}(t) \cdot \hat{\varphi}(t - t') \boldsymbol{\lambda}(t') \tag{A.5}$$

(note that the noise intensity D drops out from $\mathcal{R}$, because the correlation functions $\varphi_{ij}(t)$ are proportional to the noise intensity themselves).

From the structure of the functional (A.5) (integration over time goes from $-\infty$ to ∞ and the integral is nonnegative) and from the fact that the system is initially in the vicinity of a stable state one immediately derives the boundary condition (2.8) for $t \to -\infty$. The arguments generalize to periodically driven systems the analysis of Ref. [51] for stationary systems.

Close to a periodic stable state $\mathbf{q}_a(t)$ time evolution of $\boldsymbol{\lambda}(t)$ can be described using the matrix $\hat{\mu}_a(t) = \left(\partial K_i / \partial q_j\right)_a$, where the derivatives are evaluated for the state $\mathbf{q}_a(t)$. Because of the periodicity of $\mathbf{q}_a(t)$, the matrix $\hat{\mu}_a(t)$ is also periodic in time. It determines the monodromy matrix

$$\hat{M}_a(t) = T_t \exp\left[\int_t^{t+\tau_F} dt_1 \, \hat{\mu}_a(t_1)\right],$$

where T_t is the operator of chronological ordering (cf. Appendix C). The matrix $\hat{M}_a$ shows how the distance between a point $\mathbf{q}$ and the cycle $\mathbf{q}_a(t)$ varies over the modulation period in the absence of noise for small $|\mathbf{q} - \mathbf{q}_a(t)|$:

$$\mathbf{q}(t + \tau_F) - \mathbf{q}_a(t) = \hat{M}_a(t)[\mathbf{q}(t) - \mathbf{q}_a(t)]$$

From the condition that $\mathbf{q}_a(t)$ is a stable state, the eigenvalues of the matrix $\hat{M}_a$ are all less then 1 in absolute value: in this case the distance between $\mathbf{q}$ and $\mathbf{q}_a(t)$ decreases with increasing time.

It is seen from Eq. (A.2) that the monodromy matrix for $\boldsymbol{\lambda}$ is the inverse transposed of $\hat{M}_a$. Therefore its eigenvalues are all larger than 1 in absolute value. Hence, if the

system is in the stable state $\mathbf{q}_a(t)$ for $t \to -\infty$, then $\boldsymbol{\lambda}(t) \to \mathbf{0}$ for $t \to -\infty$, and from (A.1) $\mathbf{f}(t) \to \mathbf{0}$, too.

For the periodic saddle $\mathbf{q}_b(t)$ on the boundary of the attraction basin, one of the eigenvalues of the corresponding monodromy matrix exceeds 1 in absolute value. It is such a saddle-type boundary that can merge with an attractor at a saddle-node bifurcation we are interested in. Respectively, one eigenvalue of the matrix that describes time evolution of $\boldsymbol{\lambda}$ is < 1. If $\boldsymbol{\lambda}$ is pointing along the corresponding eigenvector, it will decay as $t \to \infty$. Then $\mathbf{f}(t)$ will decay, too, from Eq. (A.1). This means that the system may asymptotically approach a saddle-type state. Note that there are no optimal paths that would go from one stable state to another, because the condition $\boldsymbol{\lambda} \to \mathbf{0}$ for $t \to \infty$ is not satisfied there. This explains the boundary condition (2.8) for $t \to \infty$.

Because the function $\mathbf{K}$ is periodic in time, Eqs. (A.1)–(A.3) with boundary conditions (2.8) have a periodic set of solutions. If $\mathbf{q}(t), \mathbf{f}(t), \boldsymbol{\lambda}(t)$ is a solution, then $\mathbf{q}(t + \tau_F), \mathbf{f}(t + \tau_F), \boldsymbol{\lambda}(t + \tau_F)$ is a solution, too. These solutions are heteroclinic orbits: they connect the states $\mathbf{q}_a(t), \mathbf{f} = \boldsymbol{\lambda} = \mathbf{0}$ and $\mathbf{q}_b(t), \mathbf{f} = \boldsymbol{\lambda} = \mathbf{0}$, which are also solutions of Eqs. (A.1)–(A.3). Generally, only one heteroclinic orbit per period provides the minimum to the functional $\mathcal{R}$ (2.9).

A.1 Escape in systems with a slow variable

Eqs. (A.1)–(A.3) are largely simplified if one of the motions in the system is slow and all other variables follow this motion adiabatically, i.e., their relaxation time $t_{\mathrm{r}}^{(0)}$ is much smaller than the relaxation time of the slow variable t_{r}, at least for a part of the modulation period near a bifurcation point. We will assume that slow motion

is described by q_1; the variable q_1 itself may be a periodic function modulated by a slowly varying factor Q_1, as in the case discussed in Sec. 2.3.3. In this case we will be interested primarily in the factor Q_1.

Over a time $\sim t_r^{(0)}$, the variables $q_{i>1}$ reach their equilibrium values $q'_i(q_1, t)$ for given Q_1, t. They are determined by the equations

$$\dot{q}'_i = K_i(q_1, q'_{i>1}; A, t) + f_i \quad (i > 1) \tag{A.6}$$

In the absence of noise, $f_i = 0$, the solutions of these equations are periodic for given Q_1. As we will see below, the terms f_i here are small and give small corrections.

It is important that the periodic solutions $q'_{i>1}$ with $f_{i>1} = 0$ be stable. From this condition and Eq. (A.2) it follows immediately that $\lambda_{i>1} = 0$, otherwise the components $\lambda_{i>1}$ would exponentially grow in time, leading to the onset of a large force that would drive the system away from the state (A.6) with given Q_1.

The nonzero component of the Lagrange multiplier λ_1 is determined by the component of the optimal force f_1. The latter should overcome the restoring force on the slow variable Q_1 and drive it from the stable to the unstable state. But the slowness of Q_1 means that the restoring force is small, and therefore the force f_1 should be small, too. It is smaller than the force that would be needed to overcome the restoring force for the fast variables by at least a factor $\sim t_r^{(0)}/t_r$. Therefore λ_1 is small as well.

For given $\lambda_1(t)$ we can find all components $f_{i>1}$ from Eq. (A.4). They are all $\propto 1/t_r$, and therefore to lowest order in $t_r^{(0)}/t_r$ they can be disregarded in the solution of Eq. (A.6) for $q_{i>1}$.

The problem of escape is therefore reduced to a one-dimensional problem for the variable q_1, the force f_1, and the Lagrange multiplier λ_1. In Eq. (A.3) for q_1, the functions $q_{i>1}$ should be replaced by $q'_{i>1}$ calculated for $f_i = 0$.

Further simplification occurs if the noise spectrum is smooth. The analysis here is different for the cases of slow and fast modulation, i.e. whether $\omega_F t_r$ is small or large. The case $\omega_F t_r \gg 1$ is discussed in Appendix C. Here and in Appendix B we consider the case $\omega_F t_r \ll 1$. The major effect of noise on the slow variable q_1 comes from the noise spectral components at frequencies $\omega \lesssim 1/t_r$. If the noise spectrum is flat for such frequencies, the noise can be assumed to be white on the "slow" time scale. In other words, the correlation function $\varphi_{11}(t)$ can be replaced by $2D\delta(t)$ [in this situation it is convenient to choose D from this condition rather than to define it by Eq. (2.4)]. Then $\mathcal{F}_{11}(t) = \frac{1}{2}\delta(t)$.

For a 1D system driven by white noise of intensity D, Eqs. (A.1)–(A.3) have a solution

$$f_1(t) = 2\lambda_1(t) = \dot{q}_1 - K_1, \tag{A.7}$$
$$\mathcal{R} = \frac{1}{4}\int dt\ (\dot{q}_1 - K_1)^2$$

This reduces the variational problem of finding the optimal path to the known formulation for white-noise driven systems [55].

Appendix B

Reduced equation of motion for slow driving

In this Appendix we derive simplified equations of motion for the case of slow driving where the relaxation time $t_r \ll \tau_F$ and the motion can be described in the adiabatic approximation. We will consider the vicinity of the adiabatic bifurcation point $\mathbf{q} = \mathbf{0}, t = 0, A = A_c^{\rm ad}$. A convenient basis for $\mathbf{q}$ is provided by the set of the right eigenvectors of the matrix $\hat{\mu} = (\partial K_i/\partial q_j)$, where the derivatives are evaluated at the adiabatic bifurcation point. In this basis the equation of motion (2.1) has the form

$$\begin{aligned} \dot{q}_i &\approx \mu_i q_i + \frac{1}{2}\sum\nolimits_{j,k} K_{i;jk} q_j q_k + K_{i;A}\delta A^{\rm ad} + K_{i;t} t \\ &+ \frac{1}{2} K_{i;tt} t^2 + \sum\nolimits_j K_{i;jt} q_j t + f_i(t). \end{aligned} \tag{B.1}$$

Here $K_{i;jk} = \partial^2 K_i/\partial q_j \partial q_k$, $K_{i;A} = \partial K_i/\partial A$, etc, with all derivatives calculated at the adiabatic bifurcation point, and $\delta A^{\rm ad} = A - A_c^{\rm ad}$. Since the function $\mathbf{K}$ depends on t only in terms of the modulation phase $\phi = \omega_F t$, we have $K_{i;t} \propto \omega_F$. The expansion in t in (B.1) is, in fact, an expansion in $\omega_F t$.

Because the eigenvalue μ_1 is equal to zero, for small $|\mathbf{q}|$ relaxation of q_1 is much

slower than relaxation of $q_{i>1}$. In the absence of noise, over the relaxation time $t_{\rm r}^{(0)}$ the variables $q_{i>1}$ approach their quasistationary values for given q_1 and $\phi = \omega_F t$. They can be obtained from the equations of motion (B.1) for $q_{i>1}$ in which $\dot{q}_i$ and $f_i(t)$ are disregarded,

$$q_i \approx -\mu_i^{-1}\left[K_{i;t}t + K_{i;11}q_1^2 + K_{i;A}\delta A^{\rm ad} + \ldots\right] \quad (i>1). \tag{B.2}$$

Here, the major term is linear in $\omega_F t$. The full expression is a series in $q_1, \omega_F t$, and δA, and the omitted terms are of higher order in these variables. Because of the noise, $q_{i>1}$ will additionally perform small fluctuations with amplitude $\propto D^{1/2}$.

The dynamics of the slow variable q_1 on times exceeding $t_{\rm r}^{(0)}$ is given by Eq. (B.1) with $i=1$, in which $q_{i>1}$ are replaced with their quasistationary values. To lowest order in q_1, $\delta A^{\rm ad}$, and $\omega_F t$ only the linear in t term should be kept in Eq. (B.2). This gives

$$\dot{q}_1 = \alpha q_1^2 + \beta\,\delta A^{\rm ad} - \alpha\gamma^2(\omega_F t)^2 + f_1(t), \tag{B.3}$$

$$\alpha = \tfrac{1}{2}K_{1;11},\ \beta = K_{1;A},$$

with

$$\gamma^2 = -K_{1;11}^{-1}\omega_F^{-2}\left(K_{1;tt} + \sum\nolimits_{i,j>1}\mu_i^{-1}\mu_j^{-1}K_{1;ij}K_{i;t}K_{j;t} - 2\sum\nolimits_{j>1}\mu_j^{-1}K_{1;jt}K_{j;t}\right). \tag{B.4}$$

Note that the coefficient γ is independent of ω_F.

Eq. (B.3) reduces the multi-dimensional problem of random motion near a bifurcation point to a one-dimensional problem. In the case of a one-dimensional overdamped system driven by an additive periodic force it was derived earlier in Refs. [133, 134]. Besides the noise term, it differs from the equation of motion for stationary systems in the vicinity of a saddle-node bifurcation point [84] in that it has a term $\propto (\omega_F t)^2$.

Depending on the sign of $\delta A^{\rm ad}$, Eq. (B.3) has either two adiabatic solutions

$$(q_1)^{\rm ad}_{a,b} = \mp {\rm sgn}(\alpha)[-(\beta/\alpha)\delta A^{\rm ad} + (\gamma\omega_F t)^2]^{1/2} \tag{B.5}$$

or none. For concreteness, we assume that the adiabatic solutions exist for $\delta A^{\rm ad} < 0$, i.e. $\alpha\beta > 0$. The solutions are even functions of time. They touch each other at $t = 0$ for $\delta A^{\rm ad} = 0$. We assume that the periodic adiabatic states $\mathbf{q}^{\rm ad}_{a,b}(t)$ exist for all times provided $\delta A^{\rm ad} < 0$.

The term $K_{1;t}t$ in Eq. (B.1) has to be equal to zero, otherwise the bifurcation point will be far from $\delta A^{\rm ad} = t = 0$. On the other hand, the equation of motion (B.3) may contain the term $Cq_1\omega_F t$, where C is a sum of $K_{1;1t}$ and appropriately weighted products $K_{1;1i}K_{i;t}$. This term can be eliminated by a linear transformation $q_1 \to q_1 + C\omega_F t/2\alpha$ and renormalizations $\delta A^{\rm ad} \to \delta A^{\rm ad} + C\omega_F/2\alpha\beta$, $\gamma^2 \to \gamma^2 + (C/2\alpha)^2$. The renormalized γ^2 should be positive, if the stable and unstable adiabatic periodic states touch each other only for $\delta A^{\rm ad} = t = 0$ and only once per period.

The term $\propto q_1\omega_F t$ does not arise in the important case where the modulation is performed by an additive periodic force $\mathbf{F}(t)$, see Eq. (2.2). Here, the adiabatic states $\mathbf{q}^{\rm ad}_{a,b}(t)$ correspond to the minimum and maximum of the potential $U_0(\mathbf{q}) - \mathbf{F}(t)\cdot\mathbf{q}$, cf. Fig. 2.1 (a). They merge first with increasing modulation amplitude A when the field component $|F_1|$ is at its maximum over t. This means that $\partial_t\mathbf{K} = \partial^2_{\mathbf{q}t}\mathbf{K} = \mathbf{0}$ at the bifurcation point.

As explained in Sec. 2.3, the typical relaxation time near the bifurcation point does not exceed $t_l = (\alpha\gamma\omega_F)^{-1/2}$. If the correlation time of the noise $f_1(t)$ is much less than $t_l, t^{\rm ad}_{\rm r}$ and the power spectrum of the noise does not have singular features for high frequencies, then the dimensionless noise

$$\tilde{f}(\tau) \equiv (\gamma\omega_F)^{-1} f_1(t) \quad (\tau = t/t_l) \tag{B.6}$$

is effectively δ-correlated as a function of the "slow" time τ, with $\langle \tilde{f}(\tau)\tilde{f}(0)\rangle = 2\tilde{D}\delta(\tau)$. From Eqs. (2.3), (B.6) the effective noise intensity is

$$\tilde{D} = |\alpha/4|^{1/2}(\gamma\omega_F)^{-3/2}\int_{-\infty}^{\infty} dt\,\varphi_{11}(t). \tag{B.7}$$

Appendix C

Reduced equation of motion for fast driving

In this Section we consider the case where modulation near the bifurcation point is effectively fast, so that $\omega_F t_r \gg 1$. Here, throughout the modulation cycle the stable and unstable states $\mathbf{q}_{a,b}(t)$ stay close to each other and to the critical cycle $\mathbf{q}_c(t)$ into which they merge at the bifurcation point $A = A_c$. Therefore the equation of motion (2.1) can be expanded in $\delta\mathbf{q} = \mathbf{q} - \mathbf{q}_c(t)$, $A - A_c$, leading to Eq. (2.22). The expansion coefficients are periodic in time.

It is convenient to start the analysis by simplifying the part of Eq. (2.22)

$$\delta\dot{\mathbf{q}} = \hat{\mu}\,\delta\mathbf{q}, \quad \hat{\mu} = \hat{\mu}(t + \tau_F),$$

that describes motion in the linear approximation in $\delta\mathbf{q}$. We introduce the matrix $\hat{\kappa}(t, t_i)$ such that

$$\hat{\kappa}(t, t_i) = T_t \exp\left(\int_{t_i}^{t} dt_1 \hat{\mu}(t_1)\right), \tag{C.1}$$

where T_t is the operator of chronological ordering. This matrix satisfies the equation

$\partial\hat{\kappa}(t,t_\mathrm{i})/\partial t = \hat{\mu}(t)\hat{\kappa}(t,t_\mathrm{i})$ and gives the monodromy matrix $\hat{M}$,

$$\hat{M}(t) \equiv \hat{M}(t+\tau_F) = \hat{\kappa}(t+\tau_F, t).$$

The eigenvalues M_ν of the matrix $\hat{M}$ determine the evolution of $\delta\mathbf{q}(t)$ in linear approximation. Over the period τ_F, the coefficients of the expansion of $\delta\mathbf{q}(t)$ in the right eigenvectors $\mathbf{e}_\nu(t)$ of $\hat{M}$ change in M_ν times (we use Greek letters to enumerate eigenvalues and eigenvectors; they should be distinguished from the vector components, like q_i). The eigenvalues M_ν are independent of time because of periodicity of $\hat{M}(t), \hat{\mu}(t)$. They are simply related to the Floquet exponents for the periodic state $\mathbf{q}_c(t)$.

At the saddle-node bifurcation, where stable and saddle-type states coalesce, one of the eigenvalues (for example, M_1) becomes equal to 1, whereas $|M_{\nu>1}| < 1$. This means that the system is attracted to $\mathbf{q}_c(t)$ in all directions except for the critical direction $\mathbf{e}_1(t)$; the distance from $\mathbf{q}_c(t)$ along $\mathbf{e}_1(t)$ does not change over the period, in linear approximation. In what follows we choose $\mathbf{e}_1$ to be real.

For small δA of an appropriate sign, the state $\mathbf{q}_c(t)$ splits along $\mathbf{e}_1(t)$ into a stable and an unstable state. The system approaches the vicinity of these states along the directions $\mathbf{e}_{\nu>1}$ over a short time $\tau_F \max\left[1/\left|\ln|M_{\nu>1}|\right|\right] \sim t_\mathrm{r}^{(0)}$. In contrast, the motion along $\mathbf{e}_1$ is slow.

The $\mathbf{e}_1$-component of $\delta\mathbf{q}$ is the soft mode. We are interested in its dynamics on times long compared to $t_\mathrm{r}^{(0)}, \tau_F$. The analysis is simplified by the fact that, for $t - t_\mathrm{i} \gg \left|\tau_F/\ln|M_{\nu>1}|\right|$, the matrix $\hat{\kappa}(t,t_\mathrm{i})$ projects any vector $\delta\mathbf{q}(t_\mathrm{i})$ on the vector $\mathbf{e}_1(t)$. In particular,

$$\hat{\kappa}(t,t_\mathrm{i})\mathbf{e}_1(t_\mathrm{i}) \approx \kappa_{11}(t,t_\mathrm{i})\mathbf{e}_1(t). \tag{C.2}$$

This is a consequence of the transitive property $\hat{\kappa}(t,t_\mathrm{i}) = \hat{\kappa}(t,t')\hat{\kappa}(t',t_\mathrm{i})$ and the fact

that, for an arbitrary vector $\delta\mathbf{q}$, we have $\hat{M}^n(t)\,\delta\mathbf{q} \to C\mathbf{e}_1(t)$ for $n \to \infty$. The function κ_{11} in Eq. (C.2) is given by the expression

$$\kappa_{11}(t,t_\mathrm{i}) = \bar{\mathbf{e}}_1(t)\cdot\hat{\kappa}(t,t_\mathrm{i})\mathbf{e}_1(t_\mathrm{i}).$$

Here, $\bar{\mathbf{e}}_1$ is the left eigenvector of the matrix $\hat{M}$, which corresponds to the eigenvalue $M_1 = 1$, and we use normalization $\bar{\mathbf{e}}_1(t)\cdot\mathbf{e}_1(t) = 1$. The matrix element $\kappa_{11}(t,t_\mathrm{i})$ is periodic, $\kappa_{11}(t+\tau_F,t_\mathrm{i}) = \kappa_{11}(t,t_\mathrm{i})$.

Equation of motion for $\kappa_{11}(t,t_\mathrm{i})$ for large $t-t_\mathrm{i}$ follows from Eq. (C.1),

$$\begin{aligned}\frac{\partial}{\partial t}\left[\kappa_{11}(t,t_\mathrm{i})\mathbf{e}_1(t)\right] &= \mu_{11}(t)\kappa_{11}(t,t_\mathrm{i})\mathbf{e}_1(t),\\ \mu_{11}(t) &= \bar{\mathbf{e}}_1(t)\cdot\hat{\mu}(t)\mathbf{e}_1(t).\end{aligned} \tag{C.3}$$

Close to the bifurcation point, the component of $\delta\mathbf{q}$ along the vector $\mathbf{e}_1(t)$ has a slowly varying factor. In contrast, the components of $\delta\mathbf{q}$ along the vectors $\mathbf{e}_{\nu>1}$ are "fast". Over time $\gtrsim t_\mathrm{r}^{(0)}$ they reach quasiperiodic values for a given value of the slow component, and then fluctuate with amplitude $\propto D^{1/2}$. From (2.22), the quasiperiodic values are quadratic in the slow component and therefore small. As a consequence, the slow motion is indeed one-dimensional,

$$\delta\mathbf{q}(t) \approx Q_1(t)\kappa_{11}(t,t_\mathrm{i})\mathbf{e}_1(t). \tag{C.4}$$

The instant t_i here is arbitrary; $Q_1(t)$ contains a multiplicative factor that depends on t_i (but $\delta\mathbf{q}(t)$ is independent of t_i). The time t_i drops out of all final expressions, see Sec. IV.

The equation for $Q_1(t)$ is obtained by substituting Eq. (C.4) into Eq. (2.22) and then multiplying Eq. (2.22) by the vector $\bar{\mathbf{e}}_1(t)$ from the left. This gives

$$\kappa_{11}(t,t_\mathrm{i})\dot{Q}_1 = \mathcal{K}(Q_1,t) + \bar{\mathbf{e}}_1(t)\cdot\mathbf{f}(t), \tag{C.5}$$

$$\mathcal{K}(Q_1,t) = \tfrac{1}{2}\kappa_{11}^2(t,t_\mathrm{i})Q_1^2\left(\mathbf{e}_1(t)\cdot\boldsymbol{\nabla}\right)^2 K_1 + \delta A\,(\partial_A K_1),$$

where $K_1 = \bar{\mathbf{e}}_1 \cdot \mathbf{K}$.

In the absence of noise, the solution of Eq. (C.5) is a sum of smooth and oscillating parts, $Q_1(t) = Q^{\rm sm}(t) + Q^{\rm osc}$. The term $Q^{\rm sm}$ remains nearly constant on the time scale τ_F, whereas $\dot{Q}^{\rm osc} \sim \omega_F Q^{\rm osc}$. It is seen from Eq. (C.5) that $Q^{\rm osc} \propto \delta A$. The term $Q^{\rm sm}$ is much larger. An equation for $Q^{\rm sm}$ can be obtained by averaging Eq. (C.5) over time. It has the form

$$\dot{Q}^{\rm sm} = \alpha'(Q^{\rm sm})^2 + \beta'\,\delta A + f'(t). \tag{C.6}$$

The coefficients α', β' in Eq. (C.6) are given by the expressions

$$\begin{aligned} \alpha' &= \frac{1}{2}\big\langle \kappa_{11}(t,t_{\rm i})\big(\mathbf{e}_1(t)\cdot\boldsymbol{\nabla}\big)^2 K_1\big\rangle_t, \\ \beta' &= \big\langle \kappa_{11}^{-1}(t,t_{\rm i})\partial K_1/\partial A\big\rangle_t, \end{aligned} \tag{C.7}$$

where $\langle\cdot\rangle_t$ means period-average centered at time t,

$$\big\langle \mathcal{G}\big\rangle_t = \tau_F^{-1}\int_{t-\tau_F/2}^{t+\tau_F/2} dt'\; \mathcal{G}(t',t_{\rm i}). \tag{C.8}$$

The result of the averaging (C.8) is independent of t for time-periodic $\mathcal{G}$, as in the case of the coefficients α', β', and therefore α', β' are independent of t.

The function $f'(t)$ in Eq. (C.6) is a random force,

$$f'(t) = \kappa_{11}^{-1}(t,t_{\rm i})\bar{\mathbf{e}}_1(t)\cdot\mathbf{f}(t). \tag{C.9}$$

Eq. (C.6) has the same form as the equation for the soft mode in the adiabatic limit (2.12) in the absence of the term $\propto (\omega_F t)^2$. For $\alpha'\beta'\,\delta A < 0$ the system has a stable and an unstable stationary solution $Q^{\rm sm}_{a,b}$. These solutions are given by an equation similar to Eq. (2.19),

$$Q^{\rm sm}_{a,b} = \mp{\rm sgn}(\alpha')(-\beta'\,\delta A/\alpha')^{1/2} \tag{C.10}$$

(in what follows without lost of generality we set $\alpha' > 0$).

Typical values of $Q^{\rm sm}$ are $\propto |\delta A|^{1/2}$, as seen from Eq. (C.10). They largely exceed the amplitude of the fast variables in $\delta\mathbf{q}$, which are all $\propto \delta A$, in the neglect of noise. The relaxation time of $Q^{\rm sm}$ is $t_{\rm r} = |2\alpha Q_a^{\rm sm}|^{-1} \propto |\delta A|^{-1/2}$. It is much larger than τ_F close to the bifurcation point. The condition $\omega_F t_{\rm r} \gg 1$ was the major approximation made in the derivation of Eqs. (C.5), (C.6), besides the condition of the weak noise.

A transformation from $Q^{\rm sm}, t$ to reduced variables

$$Q = \alpha'^{1/2} Q^{\rm sm}, \qquad \tau = \alpha'^{1/2} t \tag{C.11}$$

allows us to write Eq. (C.6) in the compact form (2.23). The random force $\tilde{f}(\tau) = f'(\alpha'^{1/2}t)$ is effectively δ-correlated. From Eqs. (2.3), (C.9), its intensity is

$$\begin{aligned} \tilde{D} = \quad & |\alpha'/4|^{1/2} \int_{-\infty}^{\infty} dt_1 \left\langle \kappa_{11}^{-1}(t+t_1, t_{\rm i}) \kappa_{11}^{-1}(t+t_2, t_{\rm i}) \right. \\ & \left. \times \bar{\mathbf{e}}_1(t+t_1) \cdot \hat{\varphi}(t_1 - t_2) \bar{\mathbf{e}}_1(t+t_2) \right\rangle_t . \end{aligned} \tag{C.12}$$

Here, $\hat{\varphi}$ is the matrix of the noise correlation functions (2.3).

As a result of the period-averaging over t, in Eq. (C.12) the integrand becomes a function of $t_1 - t_2$, and therefore the integral over t_1 is independent of t_2. Still, it depends on $t_{\rm i}$, but this dependence will drop out of the final expressions for observable quantities, in particular the activation energy of escape.

Appendix D

Distribution matching for dynamically weak modulation

In this Appendix we study, using our general approach, the case of moderately weak modulation and compare the results to the previous work [92]. Following Ref. [92] we assume that the force $K(q,t) = -U_{0q} + F(t)$, where $U_0(q)$ is the metastable potential in the absence of modulation [in this Appendix we use the notation $f_q \equiv \partial_q f$]. The force $F(t+\tau_F) = F(t)$ is dynamically weak. This means that it weakly disturbs the motion in the absence of fluctuations. Yet it may strongly change the escape rate, because there it is compared with the small noise intensity.

The distribution ρ inside the attraction basin can be found by calculating the action $S(q,t)$ in Eq. (3.15) to the first order in F. From Eqs. (3.16), (3.17), S can be written in a standard way as an integral of the Lagrangian L,

$$S(q,t) = \int_{-\infty}^{t} d\tau L\left(q,\dot{q};\tau\right), \quad L = \frac{1}{4}\left[\dot{q} - K(q,t)\right]^2. \tag{D.1}$$

The linear in F correction to S can be obtained by integrating the term $\propto F$ along the optimal escape path $q_0(t)$ in the absence of driving, $\dot{q}_0 = p_0 = U_{0q}(q_0)$. This

gives

$$S(q,t) = U_0(q) - U_0(q_{a0}) + s(q,t),$$
$$s(q,t) = -\int_{-\infty}^{t} d\tau \dot{q}_0(\tau) F(\tau), \tag{D.2}$$

where the optimal path is chosen so that $q_0(t) = q$, and q_{a0} is the stable state $q_a(t)$ in the limit $F = 0$, with $U_{0q}(q_{a0}) = 0$; similarly, we use below q_{b0} as the basin boundary for $F = 0$, with $U_{0q}(q_{b0}) = 0$. The quantity $\chi(t) = -\dot{q}_0(t)$ determines the field-induced change of the logarithm of the escape rate, and therefore was called logarithmic susceptibility.

Eq. (D.2) allows one to match the intrawell distribution $\rho(q,t) = |\mu_{a0}/2\pi D|^{1/2} \exp[-S(q,t)/D]$ to the boundary-layer distribution (3.7)-(3.9) for

$$-Q = q_{b0} - q \gg |s(q,t)/\mu_{b0}|^{1/2},\ l_D \tag{D.3}$$

[here $\mu_{i0} \equiv -U_{0qq}(q_{i0})$ with $i = a, b$]. In the range (D.3) the integral over p (3.7) can be evaluated by the steepest descent, giving $\rho(q,t) \approx \mathcal{E}(2\pi\mu_{b0})^{1/2} \exp[-s(\phi)/D]$, with $\phi = (\omega_F/\mu_{b0}) \ln(-Q/l_D) + \omega_F(t - t')$. The exponent of this boundary-layer distribution coincides with $-s(q,t)/D$ in the range (D.3) if we set [92]

$$s(\phi) = \sum_n \tilde{\chi}(n\omega_F) F_n e^{in\phi},$$
$$\tilde{\chi}(\omega) = -\int_{-\infty}^{+\infty} dt \dot{q}_0(t) e^{i\omega t}. \tag{D.4}$$

Here F_n are Fourier components of $F(t)$. Matching the prefactors in the intrawell and boundary-layer distributions gives

$$\mathcal{E} = \frac{1}{2\pi} |\mu_{a0}\mu_{b0}|^{1/2} \exp[-\Delta U_0/D]. \tag{D.5}$$

We emphasize that the matching has been done not only far from the diffusion region, but also in the range (D.3), that is, much further away from the boundary than diffusion length l_D, in the regime of strong synchronization, $|s_m| \gg D$.

We will show now that the alternative approach of Section 3.4 gives the same result in the case of strong synchronization, $|s_{\rm m}| \gg D$. To do this we have to solve the equation for the prefactor (3.22) to the first order in F, which in turn requires finding the first-order corrections to the optimal path q_1, p_1. Linearizing the first of Eqs. (3.18), one obtains

$$\dot{q}_1 = K_{0q} q_1 + F(t) + 2p_1. \tag{D.6}$$

Here $K_{0q}(q) \equiv -U_{0qq}(q)$, and the derivative is evaluated for the zeroth-order optimal path, $q = q_0(t)$. The correction to the momentum, $p_1 \equiv \partial S/\partial q - p_0$, from Eq. (D.2) is

$$p_1 = -K_{0q} q_1 - F(t) + \frac{1}{\dot{q}_0(t)} \int_{-\infty}^{t} d\tau \dot{q}_0(\tau) \dot{F}(\tau). \tag{D.7}$$

To obtain Eq. (D.7), we used the fact that $q_0(t) = q$, and therefore $\partial q_0(\tau)/\partial q = \dot{q}_0(\tau)/\dot{q}_0(t)$. We also took into account that $p_1(t) \to 0$ for $t \to -\infty$.

In the absence of driving the prefactor is constant, and the function $z(t)$ from Eq. (3.22) is determined by the initial condition (3.23), $z = z_0 = 2\pi D/|\mu_{a0}|$. Let $z = z_0 + z_1$, where z_1 is a correction $\propto F$. The linearized Eq. (3.22) is

$$\ddot{z}_1 - 2K_{0q}\dot{z}_1 = 2z_0 K_{0qq}(\dot{q}_1 - p_1). \tag{D.8}$$

From Eqs. (D.6)-(D.8),

$$\dot{z}_1 = \frac{2z_0}{\dot{q}_0^2(t)} \int_{-\infty}^{t} d\tau\, \dot{q}_0(\tau) \dot{F}(\tau) [K_{0q}(q_0(t)) - K_{0q}(q_0(\tau))]. \tag{D.9}$$

To find the parameters $s_{\rm m}''$ and $\mathcal{E}$ of the boundary-layer distribution (3.26), (3.27) we need to find z_1 close to q_{b0}, i.e. for $t \to \infty$. It follows from the results of Sec. 3.5 that, for strong modulation, in this range

$$\dot{z} \approx 2\mu_{b0} D \mathcal{Z}_2 \dot{q}_0^{-2}(t), \tag{D.10}$$

where we used that $p_0 = \dot{q}_0$, $\dot{p}_0 = -\mu_{b0} p_0$. Before we compare this expression with Eq. (D.9) we note that the condition that s, as given by Eq. (D.4), is minimal for $\phi = \phi_{\rm m}$ corresponds to

$$\int_{-\infty}^{\infty} dt \dot{q}_0(t) \dot{F}(t) = 0.$$

This condition describes synchronization of the most probable escape path by the modulation. In the absence of modulation $q_0(t - t_c)$ is an MPEP for any t_c. Modulation lifts the time degeneracy, only one MPEP per period provides a minimum to s. As a consequence, the first integral in Eq. (D.9) goes to zero for $t \to \infty$. Then from Eqs. (D.9), (D.10) we obtain, taking into account that $\dot{q}_0 = -K_0$,

$$\mathcal{Z}_2 = -\frac{2\pi}{|\mu_{a0}\mu_{b0}|} \int_{-\infty}^{\infty} dt\, \dot{q}_0(t) \ddot{F}(t). \tag{D.11}$$

It follows from Eq. (D.4) that $\mathcal{Z}_2 = 2\pi\omega_F^2 s_{\rm m}''/|\mu_{a0}\mu_{b0}|$. Taking into account Eqs. (3.29), (3.27), we obtain the same result for the prefactor in the boundary-layer distribution as Eq. (D.5). We note that this result refers to the case of comparatively strong modulation, $|s_{\rm m}| \gg D$, and is obtained by matching the intrawell and boundary-layer distributions not in the region (D.3) [92], but closer to the basin boundary, where $|s_{\rm m}| \gg \mu_b Q^2$.

Appendix E

Nonadiabatic corrections for slow modulation

In this Appendix we show an alternative approach to the analysis of adiabatically slow modulation. By treating time variation of the modulation as a perturbation, we find the most probable escape path (MPEP) and also solve Eq. (3.22) for the auxiliary function z and obtain the constant $\mathcal{Z}_2$, cf. Eq. (3.24). This provides an alternative way of finding the parameters of the boundary-layer distribution and also gives an insight into the actual dynamics of escape for slow modulation.

The small parameter of the slow-modulation theory is the reduced frequency, $\omega_F t_{\rm r} \ll 1$. The typical duration of escape is the relaxation time $\sim t_{\rm r}$, it is much smaller than the modulation period $\tau_F = 2\pi/\omega_F$. Escape is most likely to happen once per period, for the modulation phase $\phi_{\rm m} = \omega_F t_{\rm m}$ (which, as we show, corresponds to the minimal barrier height; $t_{\rm r}$ is the adiabatic relaxation time for $t = t_{\rm m}$). For t close to $t_{\rm m}$ we can expand the force in the form

$$K(q,t) = K_0(q) + F_1(q,t) + F_2(q,t), \tag{E.1}$$

where $K_0(q) \equiv K(q, t_{\rm m})$, $F_1(q,t) \equiv K_t(q, t_{\rm m})(t - t_{\rm m})$, $F_2(q,t) \equiv (1/2)K_{tt}(q, t_{\rm m})(t - t_{\rm m})^2$ (here and below $f_t \equiv \partial_t f$, $f_q \equiv \partial_q f$). Thus, K_0 represents a stationary force, F_1 and F_2 are the time-dependent corrections of first and second order in $\omega_F t_{\rm r}$.

To zeroth order in $\omega_F t_{\rm r}$, the positions of the stable state q_a and basin boundary q_b of the system are the solutions q_{a0} and q_{b0} of the adiabatic equation $K_0(q) = 0$ with $\mu_{a0} < 0$ and $\mu_{b0} > 0$, respectively, where $\mu_{i0} = K_{0q}(q_{i0})$ $(i = a, b)$. The parameters μ_{i0} characterize the relaxation rate of the system. We emphasize that, in contrast to Appendix D where K_0 referred to the system in the absence of modulation, here K_0 and the parameters $q_{a,b}, \mu_{a,b}$ are calculated for strong modulation but at a specific instant of time $t_{\rm m}$.

Because of the time-dependent terms in K, the positions q_i $(i = a, b)$ acquire corrections $q_{i1,2}$ of the first and second order in $\omega_F t_{\rm r}$, so that $q_i = q_{i0} + q_{i1} + q_{i2}$. They can be found from the equation $\dot{q}_i = K(q_i, t)$ and have the form

$$q_{i1} = -\left[\frac{F_{1t}}{\mu_{i0}^2} + \frac{F_1}{\mu_{i0}}\right]_{q_{i0}}, \quad i = a, b, \tag{E.2}$$

and

$$\begin{aligned} q_{i2} = \Bigg[& -\frac{5}{2}\frac{K_{0qq}F_{1t}^2}{\mu_{i0}^5} + \frac{3F_{1t}F_{1qt}}{\mu_{i0}^4} - \frac{F_{2tt}}{\mu_{i0}^3} \\ & - \frac{2K_{0qq}F_{1t}F_1}{\mu_{i0}^4} + \frac{3F_{1qt}F_1}{\mu_{i0}^3} - \frac{F_{2t}}{\mu_{i0}^2} \\ & - \frac{1}{2}\frac{K_{0qq}F_1^2}{\mu_{i0}^3} + \frac{F_{1q}F_1}{\mu_{i0}^2} - \frac{F_2}{\mu_{i0}} \Bigg]_{q_{i0}}, \qquad i = a, b. \end{aligned} \tag{E.3}$$

We now consider corrections to the MPEP. For K given by Eq. (E.1) it is natural to seek the solution of Eqs. (3.18) in the form $q = q_0 + q_1 + q_2$, $p = p_0 + p_1 + p_2$. To zeroth order in ω_F the MPEP is given by the equation

$$\dot{q}_0 = p_0 = -K_0(q_0).$$

The first-order corrections q_1, p_1 satisfy Eq. (D.6) with $F = F_1$ and with the boundary conditions $q_1 \to q_{a1}$ at $t \to -\infty$ and $q_1 \to q_{b1}$ at $t \to \infty$. In the second order

$$\dot{q}_2 = K_{0q}q_2 + \frac{1}{2}K_{0qq}q_1^2 + F_{1q}q_1 + F_2 + 2p_2 \tag{E.4}$$

with $q_2 \to q_{a2}$ at $t \to -\infty$ and $q_2 \to q_{b2}$ at $t \to \infty$. Here and below the functions $K_0, F_{1,2}$ and their derivatives are calculated along the zeroth-order MPEP $q_0(t)$.

From the expression for the action (D.1) with the force (E.1) we obtain, similar to Eq. (D.7),

$$p_1 = -K_{0q}q_1 - F_1 + \frac{1}{\dot{q}_0(t)}\int_{-\infty}^{t} d\tau \dot{q}_0 F_{1\tau}.$$

Using this expression and Eq. (3.18), we further obtain

$$\dot{q}_1 - p_1 = \frac{1}{\dot{q}_0(t)}\int_{-\infty}^{t} d\tau \dot{q}_0 F_{1\tau}. \tag{E.5}$$

The momentum $p_1 \to 0$ at $t \to \pm\infty$, therefore Eq. (E.5) requires that

$$\frac{1}{\dot{q}_0(t)}\int_{-\infty}^{t} d\tau \dot{q}_0 F_{1\tau} \to \begin{cases} \dot{q}_{a1}, & t \to -\infty, \\ \dot{q}_{b1}, & t \to \infty \end{cases} \tag{E.6}$$

where $\dot{q}_{a1,b1}$ are given by Eq. (E.2).

For $t \to -\infty$ the condition (E.6) is met, hence the choice of the lower limit of integration. To consider the $t \to +\infty$ limit we write the left-hand side of Eq. (E.6) as

$$\frac{1}{\dot{q}_0(t)}\int_{-\infty}^{\infty} d\tau \dot{q}_0 F_{1\tau} - \frac{1}{\dot{q}_0(t)}\int_{t}^{\infty} d\tau \dot{q}_0 F_{1\tau}.$$

For $t \to \infty$ the second term goes to $\dot{q}_{b1}$. Therefore to satisfy the condition (E.6) we must have

$$\int_{-\infty}^{\infty} d\tau \dot{q}_0 F_{1\tau} = \int_{q_{a0}}^{q_{b0}} dq F_{1\tau}(q) = 0. \tag{E.7}$$

In changing the integration variable we used that F_{1t} does not depend on t explicitly.

The condition (E.7) is equivalent to the requirement that the adiabatic barrier height

$$\Delta U(t) = \int_{q_a(t)}^{q_b(t)} dq[K_0(q) + F_1(q,t) + F_2(q,t)] \tag{E.8}$$

be minimal, $d\Delta U/dt = 0$, to the first order in ω_F.

We note that the condition (E.7) is invariant with respect to time shift of the MPEP $q_0(t) \to q_0(t - t_c)$, with an arbitrary t_c. However, it does specify the modulation phase $\phi_{\rm m} = \omega_F t_{\rm m}$ when escape is most likely to occur.

The term in the action of second order in $\omega_F t_{\rm r}$ has the form

$$S_2(q,t) = \frac{1}{4}\int_{-\infty}^{t} d\tau(\dot{q}_1 - K_{0q}q_1 - F_1)^2$$
$$+ \int_{-\infty}^{t} d\tau \dot{q}_0(\dot{q}_2 - K_{0q}q_2 - \frac{1}{2}K_{0qq}q_1^2 - F_{1q}q_1 - F_2).$$

Using this equation to calculate $p_2 = \partial_q S_2$, we obtain from Eq. (E.4)

$$\dot{q}_2 - p_2 = \frac{1}{\dot{q}_0(t)}\int_{-\infty}^{t} d\tau\, \dot{q}_0 u(\tau), \tag{E.9}$$
$$u(t) = F_{1qt}q_1 + F_{2t} + (\dot{q}_1 - p_1)(K_{0qq}q_1 + F_{1q}).$$

Using Eq. (E.3), one can check that (E.9) satisfies the boundary condition $q_2 \to q_{a2}$, $p_2 \to 0$ for $t \to -\infty$. To satisfy the boundary condition at $t \to +\infty$ we must require that

$$\int_{-\infty}^{\infty} d\tau \dot{q}_0 u(\tau) = 0. \tag{E.10}$$

The integral (E.10) depends on the position t_c of the "center" of the MPEP $q_0(t - t_c)$ and thus specifies this position. Eqs. (E.7) and (E.10) fully determine both the phase of the modulation where escape is most likely to occur and the MPEP as a function of time.

We are now in a position to develop a perturbation theory for the function $z(t)$, which should be calculated along the MPEP from Eq. (3.22). The parameter of

interest $\mathcal{Z}_2$ is determined by the asymptotic behavior of z for $t \to \infty$: this is the coefficient at the diverging term $Dp_0^{-2}(t)$ in $z(t)$, cf. Eq. (3.24). As we will see, $\mathcal{Z}_2 \propto \omega_F^2$, and therefore we need to find z to second order in $\omega_F t_r$. Respectively, we seek z in the form $z = z_0 + z_1 + z_2$, with $z_j \propto [\omega_F t_r]^j$ $(j = 0, 1, 2)$.

The initial conditions for z_j follow from Eq. (3.23). The function $\sigma_a^2(t)$ in Eq. (3.23) is a periodic solution of the equation $\dot{\sigma}_a^2 = 2\mu_a\sigma_a^2 + 2$, which can be easily solved by perturbation theory in $\omega_F t_r$. To zeroth order $(\sigma_a^2)_0 = 1/|\mu_{a0}|$, and $z_0 = 2\pi D/|\mu_{a0}|$.

From Eq. (3.22), the equation for z_1 has the form

$$\ddot{z}_1 - 2K_{0q}\dot{z}_1 = 2z_0[K_{0qq}(\dot{q}_1 - p_1) + F_{1qt}].$$

This equation differs from Eq. (D.8) by the term F_{1qt}, which allows for q-dependence of the perturbation force. The left-hand side can be written as $(1/\dot{q}_0^2)d(\dot{z}_1\dot{q}_0^2)/dt$, which immediately gives

$$\begin{aligned} \dot{z}_1\dot{q}_0^2 &= 2z_0\int_{-\infty}^{t} d\tau \dot{q}_0^2[K_{0qq}(\dot{q}_1 - p_1) + F_{1q\tau}] \\ &= 2z_0\dot{q}_0[K_{0q}(\dot{q}_1 - p_1) + F_{1t}]. \end{aligned} \tag{E.11}$$

Here we have taken into account the initial condition for z_1 for $t \to -\infty$ and also used the relation

$$\frac{d}{dt}(\dot{q}_1 - p_1) = K_{0q}(\dot{q}_1 - p_1) + F_{1t}, \tag{E.12}$$

which follows from Eq. (E.5). Taking into account that $\dot{q}_1, p_1, F_{1t}$ do not diverge for $t \to \infty$, we see from Eq. (E.11) that $\dot{z}_1(t)\dot{q}_0^2 \to 0$ as $t \to +\infty$. Therefore z_1 does not contain a term $\propto \exp(2\mu_{b0}t) \propto p_0^{-2}(t)$ for $t \to \infty$, and as a consequence it does not contribute to $\mathcal{Z}_2$.

In the second order, from Eq. (3.22) we have

$$\ddot{z}_2 - 2K_{0q}\dot{z}_2 = v(t), \tag{E.13}$$

where

$$v(t) = 2z_0[K_{0qq}(\dot{q}_2 - p_2) + (K_{0qqq}q_1 + F_{1qq})(\dot{q}_1 - p_1)$$
$$+F_{1qqt}q_1 + F_{2qt}] + 2\dot{z}_1(K_{0qq}q_1 + F_{1q})$$
$$+2z_1[K_{0qq}(\dot{q}_1 - p_1) + F_{1qt}]. \tag{E.14}$$

The left-hand side of Eq. (E.13) is $(1/\dot{q}_0^2)d(\dot{z}_2\dot{q}_0^2)/dt$, and therefore

$$\dot{z}_2(t)\dot{q}_0^2(t) = \int_{-\infty}^{t} d\tau \dot{q}_0^2 v(\tau). \tag{E.15}$$

A cumbersome calculation, which involves integration by parts using conditions (E.7), (E.10) and Eqs. (E.2), (E.4), (E.5), (E.9), shows that, as $t \to +\infty$, the integral in the right hand side of Eq. (E.15) tends to a constant

$$C = 2z_0 \left[-\int_{-\infty}^{\infty} d\tau \dot{q}_0 F_{2tt} + \frac{[F_{1t}(q_{b0})]^2}{\mu_{b0}} - \frac{[F_{1t}(q_{a0})]^2}{\mu_{a0}} \right]. \tag{E.16}$$

Eq. (E.16) is the central result of this Appendix. It follows from this equation and the fact that the singular part of z behaves as $\exp(2\mu_{b0}t)$ for $t \to \infty$ that

$$\mathcal{Z}_2 = D^{-1} \lim_{t\to\infty} z(t)p_0^2(t) = \frac{C}{2\mu_{b0}D}.$$

On the other hand, from Eqs. (E.8), (E.16) we obtain

$$\Delta\ddot{U}(t_{\rm m}) = \frac{C}{2z_0} = \frac{C|\mu_{a0}|}{4\pi D}.$$

Therefore

$$\mathcal{Z}_2 = 2\pi\Delta\ddot{U}(t_{\rm m})/|\mu_{a0}\mu_{b0}|,$$

which coincides with the result of Eqs. (3.29), (3.33).

Bibliography

Bibliography

[1] A. Einstein, Annal. Phys. **33**(16), 1275 (1910).

[2] M. H. Devoret, D. Esteve, J. M. Martinis, A. Cleland, and J. Clarke, Phys. Rev. B **36**(1), 58 (1987).

[3] J. M. Martinis and R. L. Kautz, Phys. Rev. Lett. **63**(14), 1507 (1989).

[4] V. Lefevre-Seguin, E. Turlot, C. Urbina, D. Esteve, and M. Devoret, Phys. Rev. B **46**(9) (1992).

[5] R. L. Kautz, Rep. Prog. Phys. **59**(8), 935 (1996).

[6] E. Turlot, S. Linkwitz, D. Esteve, C. Urbina, M. H. Devoret, and H. Grabert, Chem. Phys. **235**(1-3), 47 (1998).

[7] I. Siddiqi, R. Vijay, F. Pierre, C. M. Wilson, M. Metcalfe, C. Rigetti, L. Frunzio, and M. H. Devoret, Phys. Rev. Lett. **93**(20), 207002 (2004).

[8] F. J. Albert, N. C. Emley, E. B. Myers, D. C. Ralph, and R. A. Buhrman, Phys. Rev. Lett. **89**(22), 226802 (2002).

[9] I. N. Krivorotov, N. C. Emley, A. G. F. Garcia, J. C. Sankey, S. I. Kiselev, D. C. Ralph, and R. A. Buhrman, Phys. Rev. Lett. **93**(16), 166603 (2004).

[10] S. Urazhdin, N. O. Birge, W. P. Pratt, and J. Bass, J. Appl. Phys. **95**(11), 7429 (2004).

[11] M. B. Willemsen, A. S. van de Nes, M. P. van Exter, J. P. Woerdman, M. Brunner, and R. Hovel, Appl. Phys. Lett. **77**(22), 3514 (2000).

[12] B. Nagler, M. Peeters, J. Albert, G. Verschaffelt, K. Panajotov, H. Thienpont, I. Veretennicoff, J. Danckaert, S. Barbay, G. Giacomelli, and F. Marin, Phys. Rev. A **68**(1), 013813 (2003).

[13] M. Sondermann, T. Ackemann, S. Balle, J. Mulet, and K. Panajotov, Opt. Commun. **235**(4-6), 421 (2004).

[14] R. Landauer, J. Appl. Phys. **33**(7), 2209 (1962).

[15] V. J. Goldman, D. C. Tsui, and J. E. Cunningham, Phys. Rev. Lett. **58**(12), 1256 (1987).

[16] G. Pilling, D. H. Cobden, P. L. McEuen, C. I. Duruoz, and J. S. Harris, Jr., Surface Science **361-362**, 652 (1996).

[17] M. Rogozia, S. W. Teitsworth, H. T. Grahn, and K. H. Ploog, Phys. Rev. B **65**(20), 205303 (2002).

[18] J. A. Bonetti, D. S. Caplan, D. J. Van Harlingen, and M. B. Weissman, Phys. Rev. Lett. **93**(8), 087002 (2004).

[19] N. Birge and B. Golding, Tunneling of defects in metals, in: *Mesoscopic Quantum Phenomena*, (Nova Press, New York, 2002).

[20] X. M. H. Huang, C. A. Zorman, M. Mehregany, and M. L. Roukes, Nature **421**(6922), 496 (2003).

[21] J. S. Aldridge and A. N. Cleland, Phys. Rev. Lett. **94**(15), 156403 (2005).

[22] R. L. Badzey, G. Zolfagharkhani, A. Gaidarzhy, and P. Mohanty, Appl. Phys. Lett. **86**(2), 023106 (2005).

[23] M. Blencowe, Phys. Rep. **395**(3), 159 (2004).

[24] L. I. McCann, M. Dykman, and B. Golding, Nature **402**(6763), 785 (1999).

[25] A. Simon and A. Libchaber, Phys. Rev. Lett. **68**(23), 3375 (1992).

[26] P. T. Korda, M. B. Taylor, and D. G. Grier, Phys. Rev. Lett. **89**(12), 128301 (2002).

[27] S. H. Lee and D. G. Grier, Phys. Rev. E **71**(6), 060102 (2005).

[28] *Focus issue: unsolved problems of noise and fluctuations*, Chaos, Vol. 11, no. 3 (2001).

[29] H. Kramers, Physica (Utrecht) **7**, 284 (1940).

[30] J. Kurkijärvi, Phys. Rev. B **6**, 832 (1972).

[31] R. Victora, Phys. Rev. Lett. **63**, 457 (1989).

[32] C. B. Muratov and E. Vanden-Eijnden, J. Stat. Phys. **114**(3-4), 605 (2004).

[33] A. Garg, Phys. Rev. B **51**(21), 15161 (1995).

[34] T. Fulton and L. Dunkelberge, Phys. Rev. B **9**, 4760 (1974).

[35] J. Martinis, M. Devoret, and J. Clarke, Phys. Rev. B **35**, 4682 (1987).

[36] F. Sharifi, J. L. Gavilano, and D. J. V. Harlingen, Phys. Rev. Lett. **61**, 742 (1988).

[37] S. Han, J. Lapointe, and J. E. Lukens, Phys. Rev. Lett. **63**, 1712 (1989).

[38] S.-X. Li, Y. Yu, Y. Zhang, W. Qiu, S. Han, and Z. Wang, Phys. Rev. Lett. **89**, 098301 (2002).

[39] W. Wernsdorfer, K. Hasselbach, A. Benoit, B. Barbara, B. Doudin, J. Meier, J. P. Ansermet, and D. Mailly, Phys. Rev. B **55**(17), 11552 (1997).

[40] W. Wernsdorfer, E. Bonet Orozco, K. Hasselbach, A. Benoit, B. Barbara, N. Demoncy, A. Loiseau, H. Pascard, and D. Mailly, Phys. Rev. Lett. **78**(1791), (1997).

[41] R. Koch, G. Grinstein, G. Keefe, Y. Lu, P. Trouilloud, and W. Gallagher, Phys. Rev. Lett. **84**, 5419 (2000).

[42] S. Ingvarsson, G. Xiao, S. S. P. Parkin, W. J. Gallagher, G. Grinstein, and R. H. Koch, Phys. Rev. Lett. **85**(15), 3289 (2000).

[43] W. Wernsdorfer, Adv. Chem. Phys., Vol 118 **118**, 99 (2001).

[44] A. D. Ventcel' and M. I. Freidlin, Uspehi Mat. Nauk **25**(1 (151)), 3 (1970).

[45] M. I. Dykman and M. A. Krivoglaz, Zh. Eksper. Teor. Fiz. **77**(1), 60 (1979).

[46] R. Graham, Phys. Lett. A **80**(5-6), 351 (1980).

[47] R. Graham, Phys. Lett. A **103**(5), 255 (1984).

[48] J. Luciani and A. Verga, Europhys. Lett. **4**(3), 255 (1987).

[49] A. J. Bray and A. J. McKane, Phys. Rev. Lett. **62**(5), 493 (1989).

[50] A. J. McKane, H. C. Luckock, and A. J. Bray, Phys. Rev. A **41**(2), 644 (1990).

[51] M. I. Dykman, Phys. Rev. A **42**(4), 2020 (1990).

[52] R. S. Maier and D. L. Stein, Phys. Rev. E **48**(2), 931 (1993).

[53] M. I. Dykman, D. G. Luchinsky, R. Manella, P. V. E. McClintock, H. E. Short, N. D. Stein, and N. G. Stocks, Phys. Lett. A **193**(1), 61 (1994).

[54] R. S. Maier and D. L. Stein, Phys. Rev. Lett. **87**(27), 270601 (2001).

[55] M. I. Freidlin and A. D. Wentzell, *Random perturbations of dynamical systems* (Springer-Verlag, 1998).

[56] O. A. Tretiakov, T. Gramespacher, and K. A. Matveev, Phys. Rev. B **67**, 073303 (2003).

[57] M. I. Dykman and M. A. Krivoglaz, Physica A **104**(3), 480 (1980).

[58] E. Knobloch and K. A. Wiesenfeld, J. Stat. Phys. **33**(3), 611 (1983).

[59] A. P. Dmitriev and M. I. Dyakonov, JETP Lett. **44**(2), 84 (1986).

[60] B. Golding and J. R. Kruse, unpublished work.

[61] R. Graham, Europhys. Lett. **3**(3), 259 (1987).

[62] M. I. Dykman, B. Golding, and D. Ryvkine, Phys. Rev. Lett. **92**(8), 080602 (2004).

[63] M. I. Dykman, I. B. Schwartz, and M. Shapiro, Phys. Rev. E **72**(2), 021102 (2005).

[64] I. Siddiqi, R. Vijay, F. Pierre, C. M. Wilson, L. Frunzio, M. Metcalfe, C. Rigetti, and M. H. Devoret, cond-mat/0507248 (2005).

[65] C. Stambaugh and H. B. Chan, Phys. Rev. B **73**, 172302 (2006).

[66] K. Kim, M. Heo, K. Lee, H. Ha, K. Jang, H. Noh, and W. Jhe, Phys. Rev. A **72**, 053402 (2005).

[67] A. Förster and A. Mikhailov, Phys. Lett. A **126**, 459 (1988).

[68] L. Onsager and S. Machlup, Phys. Rev. **91**(6), 1505 (1953).

[69] D. G. Luchinsky, J. Phys. A **30**(16), L577 (1997).

[70] J. L. Lebowitz and H. Spohn, J. Stat. Phys. **95**(1 - 2), 333 (1999).

[71] G. Gallavotti and E. G. D. Cohen, J. Stat. Phys. **80**(5-6), 931 (1995).

[72] J. Kurchan, J. Phys. A: Math. and General **31**(16), 3719 (1998).

[73] G. E. Crooks, Phys. Rev. E **60**(3), 2721 (1999).

[74] D. J. Evans and D. J. Searles, Adv. Phys. **51**(7), 1529 (2002), ISSN 0001-8732.

[75] R. van Zon and E. Cohen, Phys. Rev. E **69**(51), 056121 (2004).

[76] M. I. Dykman, M. M. Millonas, and V. N. Smelyanskiy, Phys. Lett. A **195**(1), 53 (1994).

[77] R. Graham, D. Roekaerts, and T. Tel, Phys. Rev. A **31**(5), 3364 (1985).

[78] H. R. Jauslin, Physica A **144**(1), 179 (1987).

[79] R. S. Maier and D. L. Stein, Phys. Rev. Lett. **85**(7), 1358 (2000).

[80] M. I. Dykman, P. V. E. McClintock, V. N. Smelyanski, N. D. Stein, and N. G. Stocks, Phys. Rev. Lett. **68**(18), 2718 (1992).

[81] J. Hales, A. Zhukov, R. Roy, and M. I. Dykman, Phys. Rev. Lett. **85**(1), 78 (2000).

[82] E. B. Myers, F. J. Albert, J. C. Sankey, E. Bonet, R. A. Buhrman, and D. C. Ralph, Phys. Rev. Lett. **89**, 196801 (2002).

[83] L. Landau and E. Lifshitz, *Statistical Physics Part I. 3rd edition revised by E.M. Lifshitz and L.P. Pitaevskii* (Pergamon, Oxford, 1980).

[84] J. Guckenheimer and P. Holmes, *Nonlinear Oscillators, Dynamical Systems and Bifurcations of Vector Fields* (Springer-Verlag, New York, 1987).

[85] D. Ryvkine, M. I. Dykman, and B. Golding, Phys. Rev. E **69**(6), 061102 (2004).

[86] A. Larkin and Y. Ovchinnikov, J. Low Temp. Phys. **63**, 317 (1986).

[87] B. Ivlev and V. Mel'nikov, Phys. Lett. A **116**, 427 (1986).

[88] S. Linkwitz and H. Grabert, Phys. Rev. B **44**(21), 11901 (1991).

[89] I. Dayan, M. Gitterman, and G. Weiss, Phys. Rev. A **46**, 757 (1992).

[90] R. Mantegna and B. Spagnolo, Phys. Rev. Lett. **76**, 563 (1996).

[91] M. Bier, Phys. Rev. E **59**, 6422 (1999).

[92] V. N. Smelyanskiy, M. I. Dykman, and B. Golding, Phys. Rev. Lett. **82**(16), 3193 (1999).

[93] J. Lehmann, P. Reimann, and P. Hanggi, Phys. Rev. E **62**(5), 6282 (2000).

[94] M. I. Dykman, B. Golding, L. I. McCann, V. N. Smelyanskiy, D. G. Luchinsky, R. Mannella, and P. V. E. McClintock, Chaos **11**(3), 587 (2001).

[95] S. M. Soskin, R. Mannella, and P. V. E. McClintock, Phys. Rep. **373**, 247 (2003).

[96] M. V. Fistul, A. E. Miroshnichenko, and S. Flach, Phys. Rev. B **68**(15), 153107 (2003).

[97] M. I. Dykman, D. G. Luchinsky, R. Mannella, P. V. E. McClintock, N. D. Stein, and N. G. Stocks, Nuovo Cimento **17**(7-8), 661 (1995).

[98] K. Wiesenfeld and F. Jaramillo, Chaos 1998 **8**, 539 (1998).

[99] F. Julicher, A. Ajdari, and J. Prost, Rev. Mod. Phys. **69**, 1269 (1997).

[100] P. Reimann, Phys. Rep. **361**, 57 (2002).

[101] R. P. Feynman and A. R. Hibbs, *Quantum Mechanics and Path Integrals* (McGraw-Hill, New-York, 1965).

[102] J. S. Langer, Ann. Phys. **41**, 108 (1967).

[103] S. Coleman, Phys. Rev. D **15**, 2929 (1977).

[104] E. Benoit, ed., *Dynamic Bifurcations*, vol. 1493 of *Lecture Notes on Mathematics* (Springer-Verlag, Berlin, Luminy, 1990).

[105] P. Mandel and T. Erneux, Opt. Commun. **44**, 55 (1982).

[106] L. Landau and E. Lifshitz, *Mechanics* (Pergamon, London, 1976).

[107] R. Mannella, Intl. J. Mod. Phys. C **13**, 1177 (2002).

[108] C. R. Doering and J. C. Gadoua, Phys. Rev. Lett. **69**(16), 2318 (1992).

[109] M. Bier, Phys. Rev. E **71**, 011108 (2005).

[110] M. I. Dykman and D. Ryvkine, Phys. Rev. Lett. **94**(7), 070602 (2005).

[111] D. Ryvkine and M. I. Dykman, Phys. Rev. E **72**(1), 011110 (pages 15) (2005).

[112] J. Lehmann, P. Reimann, and P. Hanggi, Phys. Rev. Lett. **84**(8), 1639 (2000).

[113] R. Graham and T. Tel, J. Stat. Phys. **35**(5-6), 729 (1984).

[114] M. Berry, Adv. Phys. **25** (1976).

[115] D. Ludwig, SIAM Rev. **17**, 605 (1975).

[116] D. Ryter and P. Jordan, Phys. Rev. Lett. **104A**, 193 (1984).

[117] M. Suzuki, J. Stat. Phys. **16**(6), 477 (1977).

[118] V. N. Smelyanskiy, M. I. Dykman, H. Rabitz, B. E. Vugmeister, S. L. Bernasek, and A. B. Bocarsly, J. Chem. Phys. **110**(23), 11488 (1999).

[119] I. B. Schwartz, L. Billings, and E. M. Bollt, Phys. Rev. E **70**(4), 046220 (2004).

[120] D. Moroni, T. S. van Erp, and P. G. Bolhuis, Physica A **340**(1-3), 395 (2004).

[121] D. M. Zuckerman, J. Phys. Chem. B **108**(16), 5127 (2004).

[122] W. N. E, W. Q. Ren, and E. Vanden-Eijnden, Phys. Rev. B **66**(5), 052301 (2002).

[123] D. G. Luchinsky and P. V. E. McClintock, Nature **389**(6650), 463 (1997).

[124] M. Morillo, J. M. Casado, and J. Gomez-Ordonez, Phys. Rev. E **55**(2), 1521 (1997).

[125] M. Arrayas, J. M. Casado, J. G. Ordonez, P. V. E. McClintock, M. Morillo, and N. D. Stein, Phys. Rev. Lett. **80**(11), 2273 (1998).

[126] D. Ryvkine and M. I. Dykman, Phys. Rev. E **73**, 061109 (2006).

[127] V. N. Smelyanskiy, M. I. Dykman, H. Rabitz, and B. E. Vugmeister, Phys. Rev. Lett. **79**(17), 3113 (1997).

[128] R. S. Maier and D. L. Stein, Phys. Rev. Lett. **86**(18), 3942 (2001).

[129] R. Graham and T. Tel, Phys. Rev. Lett. **52**(1), 9 (1984).

[130] M. Suzuki, J. Stat. Phys. **16**(1), 11 (1977).

[131] M. I. Dykman, D. G. Luchinsky, P. V. E. McClintock, and V. N. Smelyanskiy, Phys. Rev. Lett. **77**(26), 5229 (1996).

[132] R. S. Maier and D. L. Stein, Phys. Rev. Lett. **71**(12), 1783 (1993).

[133] N. Berglund and B. Gentz, J. Phys. A **35**, 2057 (2002).

[134] M. Dykman, B. Golding, J. Kruse, L. McCann, and D. Ryvkine, cond-mat/0204621 (2002).